ISSN 0110-3326

RESEARCH REPORT

Foundation Loads Due to Lateral Spreading at the Landing Road Bridge, Whakatane

Richard P. Keenan

May 1996

96/10

Department of Civil Engineering

University of Canterbury
Christchurch New Zealand

ISSN 0110-3326

FOUNDATION LOADS DUE TO LATERAL SPREADING AT THE LANDING ROAD BRIDGE, WHAKATANE

by

Richard P. KEENAN

This report is identical to a project report of the same name submitted to the University of Canterbury in partial fulfilment of the requirements for a Master of Engineering degree.

Research Report 96/10 May 1996

Department of Civil Engineering
University of Canterbury
Christchurch
NEW ZEALAND

Abstract

This report investigated liquefaction-induced lateral spreading loads with a case study of the Landing Road Bridge site in Whakatane, where about 1.5 m of horizontal surface displacement occurred following the 1987 Edgecumbe Earthquake. Soil mounded behind the piers on the true left bank of the Whakatane River in an apparent passive failure. Preliminary estimates based on CPT data show a passive load of about 500 kN per pier, which is of the same order as the collapse load of the raked-pile foundation. Thus, extensive site investigation, laboratory testing and analysis was undertaken to make an improved estimate of the lateral loads.

Trenching at Piers C and E showed clear evidence of failure surfaces consistent with passive failure and observation of the absence of cracking at the top of the piles confirms the bounds on soil loads obtained from analysis of the structural strength of the foundation. Strength testing of intact block samples of the backfill used around the piers could not be achieved due to the presence of large woodchips and other rubbish. Thus, testing of reconstituted specimens was undertaken to estimate the strength of the backfill and total passive load exerted by the lateral spreading soil. Calculations showed a wide range in possible passive soil loads and appeared to be no better than initial estimates.

Simple approaches to analyse lateral spreading loads are presented with possible design methods to minimise potential structural damage.

Acknowledgements

The New Zealand Earthquake Commission is gratefully acknowledged for providing financial assistance to enable this project to be undertaken. Works Consultancy Services are thanked for giving permission to carry out this work.

Dr John Berrill is thanked for his supervision of the project work. None of this work would have been possible without John's ideas and his experience, guidance, insight and recommendations throughout this research have made for a fulfilling and enjoyable Masters. He is also a great man to have on the hand auger.

The staff at Environment Bay of Plenty were most helpful and provided resources enabling the site investigation to undertaken. Trenching work at the site was completed with the help of Dr Jarg Pettinga, whose experience and direction was invaluable. Mr Siale Pasa is thanked for his assistance with organisation of equipment used in the field, site investigation and laboratory testing. The excavation skills and general assistance on site from Mr Mark Laugesen was greatly appreciated.

Staff and students in the Civil Engineering Department at the University of Canterbury are thanked for all of their help during my time at university. I would also like to thank my friends for putting up with me for the past four years, especially Grant Higgins, Nathan Barrett, Justin Smith, Chris Murphy, Andrew Milburn, Robert Bruce, Mike Osbourne, Andrew Landells and *The Saxons*.

Finally, I would like to acknowledge the support of my close relatives and immediate family; Jan, Mike, Matthew, Daniel, Brendon and Sarah who have always been there for me.

Contents

Chapter 5 Laboratory Testing 55

Chapter 1

Introduction

Liquefaction of cohesionless soils induced by strong earthquake ground motion is a common occurrence around the world. It has been the cause of many geotechnical failures and is an important consideration in the design of engineering structures where the potential for liquefaction is high.

One important aspect of liquefaction is the lateral spreading of near surface soil layers. When structural elements such as piles and lifelines are present in a moving liquefied soil, they may be subjected to large drag forces as they resist the motion. Cracking, yielding and ultimate failure of these structural elements is possible as they are deformed within the lateral spreading soil.

Lateral spreading as a result of liquefaction is common along the banks of canals, streams and rivers where deposits of young, loose, fine grained, saturated sand are present. Gentle sloping topography aids the lateral movement of liquefied soil, but lateral spreading may occur on level ground adjacent to waterways, where unequal horizontal end pressures on the soil mass force the banks to converge. Cracks may appear in cohesive soil overlying the liquefied layer resulting in the ejection of sand to the ground surface, commonly known as sand boils. Lateral movement will continue until excess pore water pressures generated by earthquake shaking dissipate. The liquefied soil will gradually regain strength and eventually lateral spreading movement will cease.

This report focuses on the problem of lateral spreading and its effects on foundations. First, the literature of lateral spreading is reviewed; then the case of Landing Road Bridge, Whakatane, which suffered lateral spreading damage in the 1987 Edgecumbe earthquake, is examined. Loads imposed on the structure by the unliquefied silt crust are estimated, together with the collapse load on the pile foundations. By subtracting these two loads, and noting that the foundations did not collapse gives an upper bound to the drag forces imposed on the piles by the liquefied soil. We see that these are not large compared with the forces imposed by the unliquefied crust.

Trenching beneath the bridge where soil had mounded behind Piers C and E revealed passive failures in the cohesive soil crust. Soil samples were taken and strength parameters were estimated to give an indication of the horizontal passive force applied to the substructure.

Where the possibility of lateral spreading is high it is important for designers to consider soil loads on the foundations as an important load mechanism. A simple approach to estimating these loads is proposed together with some methods to reduce possible structural damage caused by lateral spreading.

Figure 1.1 shows the location of Landing Road Bridge in relation to the epicentre of the 1987 Edgecumbe Earthquake. A map of Whakatane is shown in Figure 1.2. and an oblique view of the bridge looking upstream, taken soon after the Edgecumbe Earthquake, is shown in Figure 1.3.

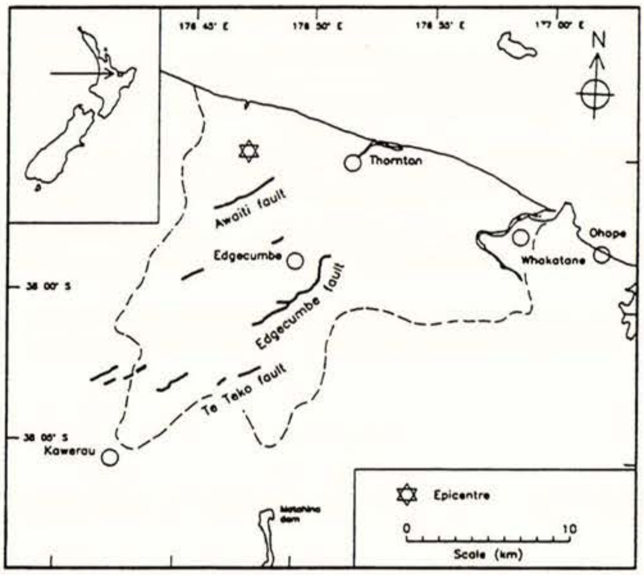

Figure 1.1 Bay of Plenty Region with the Rangitaiki Plains (dashed line), 1987 Edgecumbe Earthquake epicentre (star) and the location of Landing Road Bridge (from Crook and Hannah 1989)

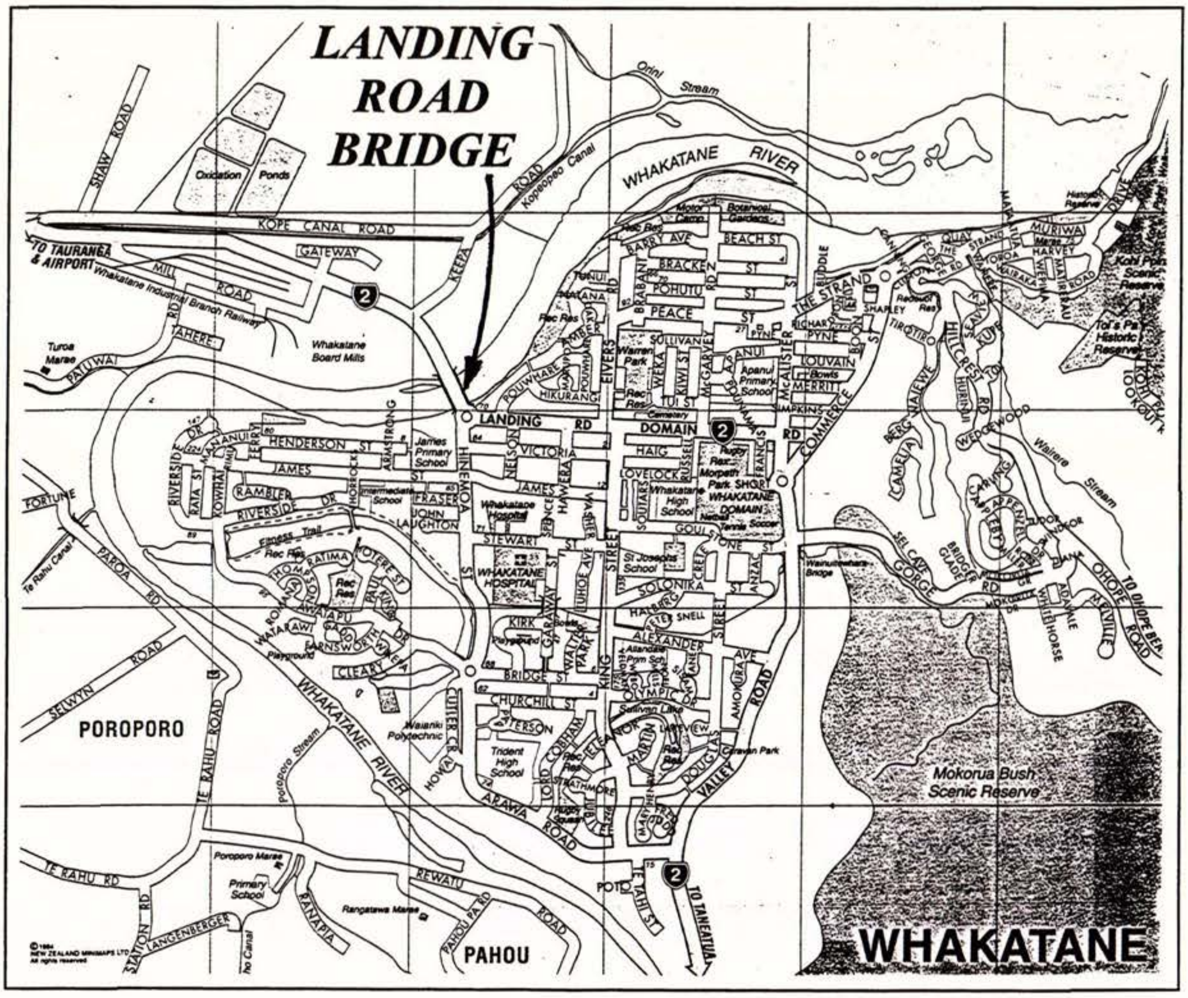

Figure 1.2 Location of Landing Road Bridge in Whakatane (courtesy of New Zealand Minimaps Ltd, © 1994)

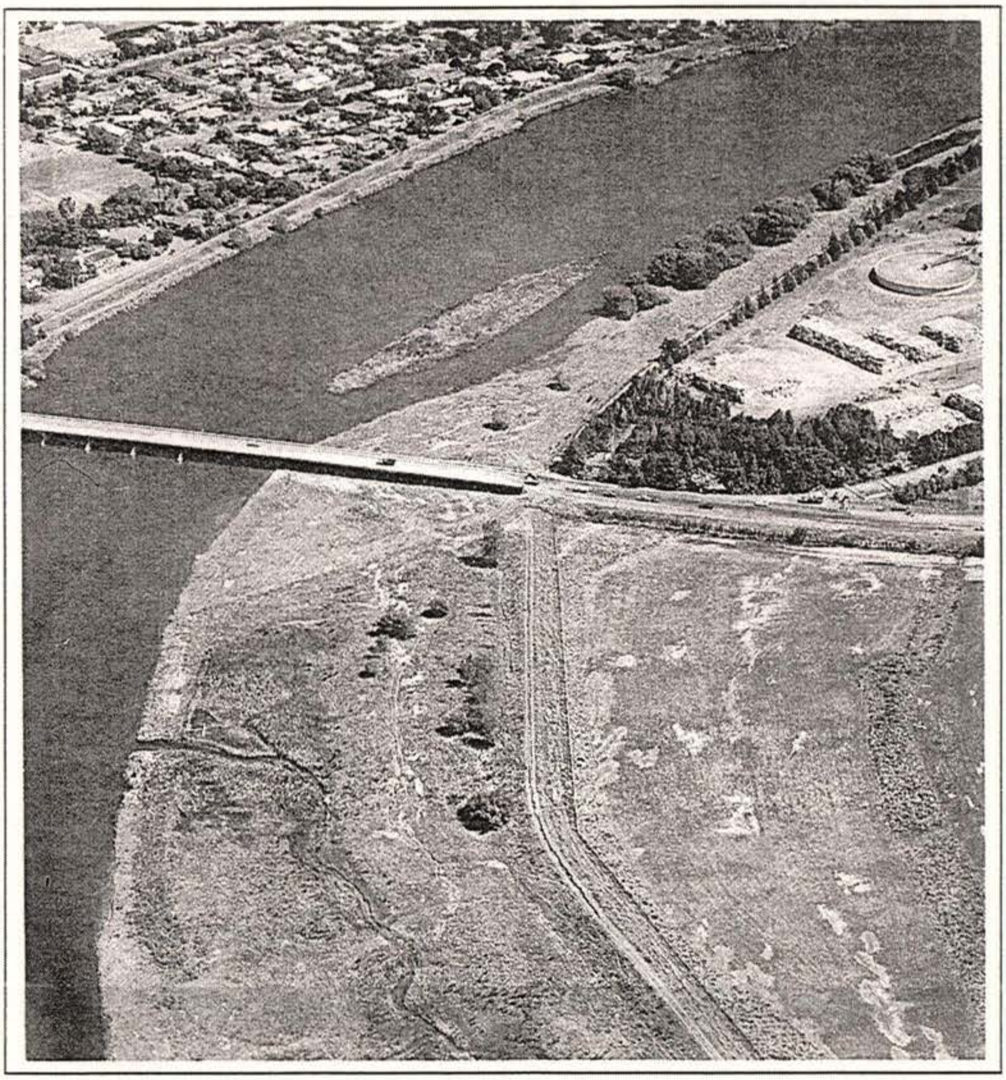

Figure 1.3 Oblique view of Landing Road Bridge looking south west. Sand boils on the true left bank from the Edgecumbe Earthquake can be seen in the foreground (courtesy of D. L. Homer)

Chapter 2

Literature Review

A literature survey was undertaken to review lateral spreading in general. There are many well documented accounts of liquefaction induced lateral spreading including the 1964 Niiagata and Alaskan Earthquakes, the 1989 Loma Prieta Earthquake (Hamada and O'Rourke 1992). More recent earthquakes such as the 1994 Northridge and 1995 Hyogoken-Nanbu (Kobe) Earthquake will provide important case histories for the future.

Many model tests have been undertaken to investigate the mechanism of liquefaction, of which some gave interesting results. Numerical and analytical models have been used in conjunction with model tests. Very little work has considered lateral spreading loads imposed on foundations and more research is needed in this area.

2.1 LATERAL SPREADING

The most prominent type of liquefaction induced ground failure is lateral spreading. Blocks of crustal soil overlying the liquefied layer form, which are mostly intact and move towards a free face or down a slope. The resulting ground displacement causes extensional fissures in the crustal soil and sometimes sand may be ejected by excess pore water pressures. On gentle slopes with gradients up to 5 percent, total displacements may vary from a few centimetres to several metres.

The main factors influencing liquefaction and horizontal ground movement can be grouped into three categories, as identified by O'Rourke and Hamada (1992):

1. Seismic Factors.
    - Earthquake magnitude.
    - Distance to nearest fault rupture or seismic source.
    - Maximum horizontal ground acceleration.
    - Duration of ground motion.

2. Geological and Topographical Factors.
    - Mode of deposition.
    - Total thickness of unconsolidated sediment.
    - Depth to groundwater.
    - Ground slope.
    - Proximity to and height of free face.

3. Soil Factors.
    - Age of sediment, degree of consolidation and cementation.
    - Grain size distribution of particles.
    - Mean grain size of particles (D_{50}).
    - Silt content.
    - Clay content.
    - Density state of granular layers and residual shear strength of liquefied soil.
    - Thickness, continuity and depth of liquefied zone.

2.2 EMPIRICAL PREDICTION OF LATERAL SPREAD

Hamada, Yasuda and Isoyama (1987) used data from the 1964 Niiagata Earthquake on liquefaction induced lateral spreading to develop the following empirical equation for permanent horizontal displacement:

$$D = 0.75H^{0.5}\theta^{0.33} \tag{2.1}$$

where D_H = magnitude of permanent horizontal ground displacement (m)

H = thickness of the liquefied layer (m)

θ = the greater gradient of the ground surface or the lower boundary of the liquefied layer (%)

Large scatter in the data meant that using this equation could give answers that vary by 50 to 200 % of the true result (see Figure 2.1). In the case of Landing Road Bridge, we have θ = zero at the ground surface which means that this model can not be applied.

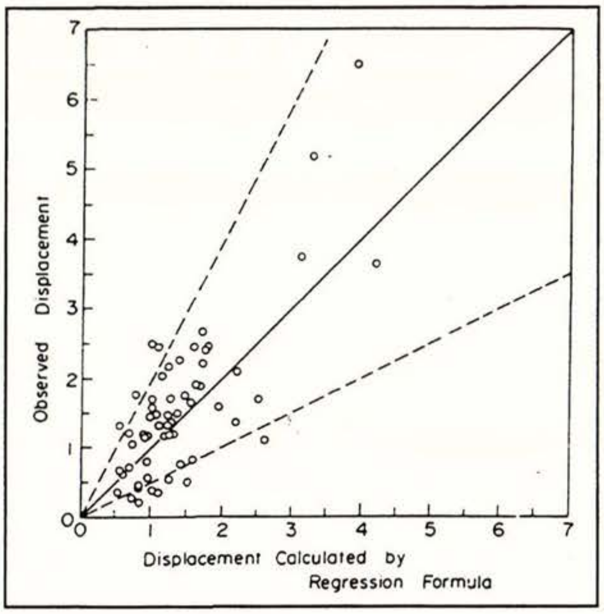

Figure 2.1 Observed versus predicted displacement (from Hamada et al 1987)

Based on data for various localities affected by liquefaction during earthquakes in the western United States and Alaska, Youd and Perkins (1987) defined the Liquefaction Severity Index or LSI as a function of two parameters:

$$\log_{10}LSI = -3.49 - 1.86 \log_{10}R + 0.98 M_w \qquad (2.2)$$

where LSI = maximum expected permanent horizontal ground displacement (in)

R = shortest horizontal distance measured from the surface projection of the seismic energy source or fault rupture to the site of interest (km)

M_w = moment magnitude of the earthquake

The LSI data was evaluated from the displacement of lateral spreads on gentle sloping, late Holocene, fluvial and beach deposits. The maximum permanent lateral displacement of the ground at Landing Road Bridge is not predicted well using this model. Displacements up to 1.5 m were observed there whereas this model predicts only 0.1 m. The large discrepancy may be due to the fact that there are other important factors that need to be considered when estimating lateral displacements.

Bartlett and Youd (1995) developed an empirical model for predicting the magnitude of lateral displacement induced by liquefied soil. It is based on the analysis of past earthquakes in Japan and the United States, using multiple linear regression techniques. They considered lateral displacements to be a function of earthquake, topographical, geological and soil factors. Two equations were developed; one for a free face such as beside a river channel, and the second for the case of free field lateral spreading on sloping ground (see Figure 2.2).

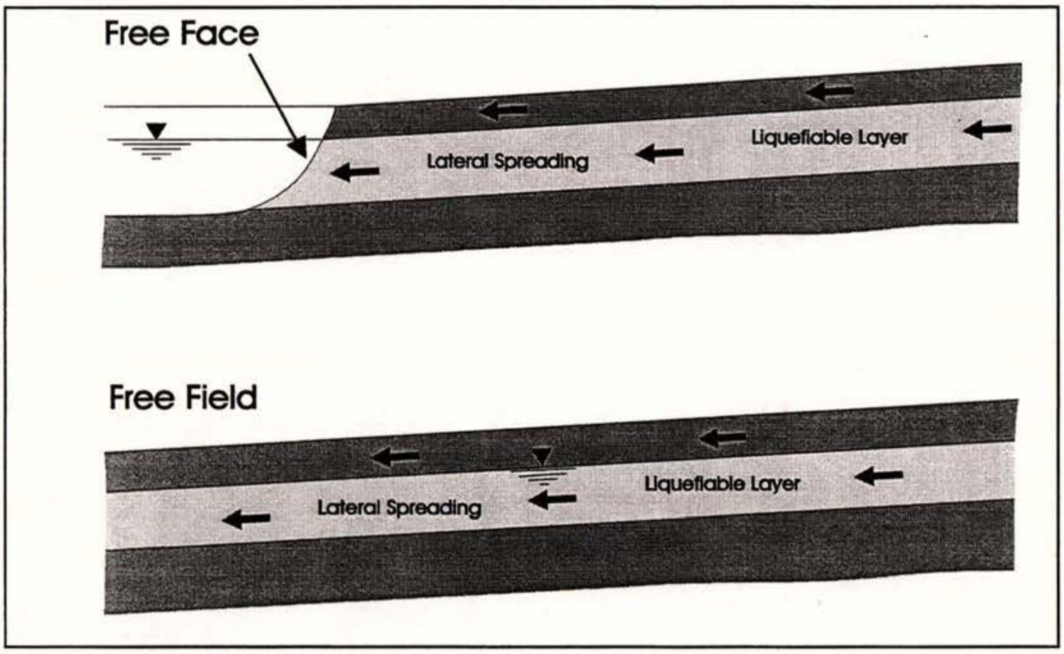

Figure 2.2 Free face and free field lateral spreading

- Free Face: $\log(D_H) = -16.366 + 1.178M - 0.927\log R - 0.013R + 0.657\log W + 0.348\log T_{15} + 4.527\log(100\text{-}F_{15}) - 0.922(D_{50})_{15}$ (2.3)

- Free Field: $\log(D_H) = -15.787 + 1.178M - 0.927\log R - 0.013R + 0.429\log S + 0.348\log T_{15} + 4.527\log(100\text{-}F_{15}) - 0.922(D_{50})_{15}$ (2.4)

where D_H = displacement (m)

$M = M_w$, moment magnitude of the earthquake

R = horizontal distance of site from epicentre (km)

W = 100(H/L) (%)

where H = height of the free face or depth of channel (m)

L = horizontal distance from the channel (m)

S = ground slope (%)

T_{15} = cumulative thickness of saturated cohesionless sediments with SPT $(N_1)_{60}$ values less than or equal to 15 (m)

F_{15} = average fines content for the T_{15} layers (%)

$(D_{50})_{15}$ = mean grain size for the T_{15} layers (mm)

These equations gave a correlation coefficient of 83% and all of the coefficients are significant at the 99.9 % level. They are generally valid for earthquakes with $6 \leq M_w \leq 8$ in sandy to silty sand soils where liquefiable sediments lie within 10 m of the ground surface.

When this model is applied to the case of Landing Road Bridge, the outcome is significantly more accurate than the previous two methods. The free face model was used because of the presence of the Whakatane River. Table 2.1 shows the results for three positions on the true left bank.

POSITION	*Free Face D_H (m)*
L = 300 m, which is about the farthest back that lateral spreading occurred at this site	0.06
L = 90 m, which is approximately the distance from the river channel to abutment A	0.14
L = 3 m, right near the river channel	1.06

Table 2.1 Lateral spreading displacement prediction at Landing Road Bridge (after Youd and Perkins 1995)

2.3 MODEL TESTS

The liquefaction phenomenon has been investigated extensively by many authors through the use of experimental model tests. Centrifuge tests have been employed, where the centrifuge is used to induce a similar stress field due to self weight in a small scale model, as in the prototype. The length ratio between model to prototype is proportional to the acceleration ratio; hence with 50 to 100g centrifuges, quite large soil masses can be modelled and prototype behaviour inferred.

In another class of experiment, large scale models, which are placed on shaking tables, have been subjected to ground motion records of historic earthquakes and sinusoidal motions. Often model piles and pipes are placed in these models to determine how they are affected by liquefaction.

Testing which examined liquefaction induced lateral spreading and drag forces imposed on buried objects was focussed on in the literature survey.

2.3.1 Centrifuge Tests

This method of testing requires the creation of curved models which represent level ground or slope conditions. In the case of modelling a flat ground surface, the distance from the centre of rotation to the model ground surface must be kept constant so that the vertical accelerations are uniform for that surface. Modelling a sloping ground surface requires accurate shaping of the model, which can be difficult.

The main principle in scaling laws for conversion to prototype conditions are outlined by Fiegel and Kutter (1994a). A $1/S$ scale model subject to a gravitational acceleration of Sg will feel the same stresses as the prototype. A known conflict exists between the time scale factors for dynamic shaking, $1/S$, and pore water pressure dissipation, $1/S^2$. This problem can be solved by changing the pore fluid viscosity or by understanding that the model soils actually simulate prototype soils with an absolute permeability S times greater. Scaling the soil permeability, k, allows for $1/S$ scaling of time during both dynamic shaking and pore water pressure dissipation.

Fiegel and Kutter (1994b) conducted two dynamic centrifuge tests with different model configurations (see Figure 2.3) to investigate lateral spreading. The first test used a single layer of liquefiable sand and the second consisted of sand overlaid with a non-liquefiable silt, both at slope of 2.6°. In these tests, sand with a mean particle size (D_{50})

of 0.13 mm, was placed by dry pluviation to give a relative density (D_R) of about 60% and initial void ratio of $e_0 = 0.67$.

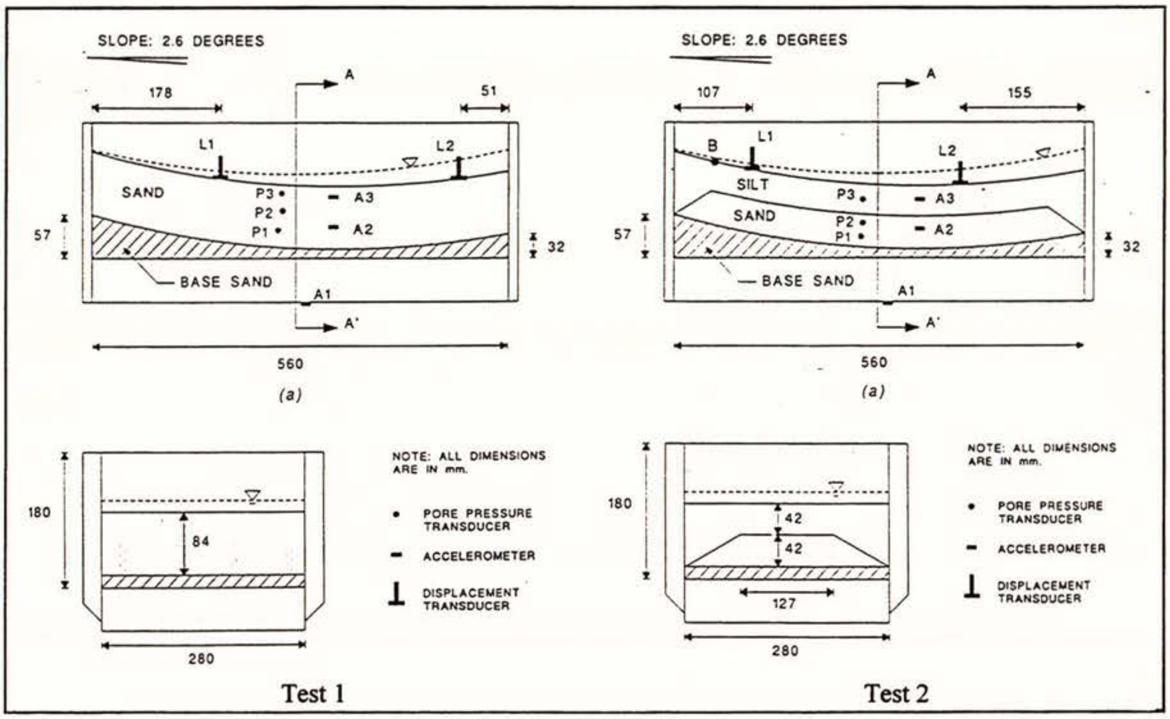

Test 1 Test 2

Figure 2.3 Model configurations for tests 1 and 2 (elevation (a) and section (b)) (from Fiegel and Kutter 1994b)

The models were subjected to peak accelerations of 0.7g (prototype value) using a scaled version of the 1940 El Centro earthquake. Each test was configured to approximate free field lateral spreading in the soil.

In the case of the second test, their results give an insight to the mechanism of lateral spreading of a cohesive crustal soil. Excess pore water pressure within a liquefied soil increases with depth, giving a vertical hydraulic gradient which causes the upward flow of water. The presence of an overlying less permeable layer can restrict this flow of water, resulting in an accumulation of water at the interface between the two layers. Solidification of the liquefied sand proceeds from the bottom of the layer toward the surface. Thus the surface of the layer stays liquefied for the longest time. This resulted in a dramatic reduction of sliding resistance at the interface and most of the lateral displacement was found to be confined to this zone in this experiment. The sand at the interface loosened and a redistribution of voids occurred. Almost all of the lateral movement occurred during the shaking which suggests that inertial forces in the silt layer can be an important driving mechanism for lateral spreading in certain situations.

2.3.2 Large Scale Model Tests

Sasaki, Tokida, Matsumoto and Saya (1991) investigated lateral flow of soils induced by liquefaction with eight model tests. A rectangular box of dimensions 6 m long, 0.8 m wide and 1 m high was used to test seven different model configurations. Each test consisted of variations in thicknesses and slopes with liquefiable and non-liquefiable layers. The last test used a semi-circular tank with a radius of 2 m (see Figure 2.4). The liquefiable soil used in each test was Sengen-Yama sand with solid density ρ_s of 2.66 t/m^3, $D_{50} = 0.27$ mm, $e_{max} = 0.976$, $e_{min} = 0.596$, $\gamma = 18\text{-}19$ kN/m^3 above the water table and 14-15 kN/m^3 below.

Each model was constructed on a shake table and subjected to a sinusoidal acceleration of 2 Hz for 20 seconds. Peak horizontal accelerations of approximately 0.6 - 1.90 m/s^2 were used. In every test, instrumentation was used to monitor pore water pressures, displacements and accelerations.

A brief outline of their test results is presented. From the rectangular box tests, it was found that the magnitude of lateral spreading was affected severely by the slope of the ground surface. The slope of the lower boundary of the liquefiable layer had much less influence on deformations. The greatest displacements were achieved when both the ground surface and the bottom of the liquefiable layer were inclined together.

The lateral ground flow at the ground surface (D in m) could be expressed as a function of three variables:

- θ = slope of the ground surface (%)
- H = thickness of the liquefied layer (m)
- T = duration of excitation after the onset of complete liquefaction (sec)

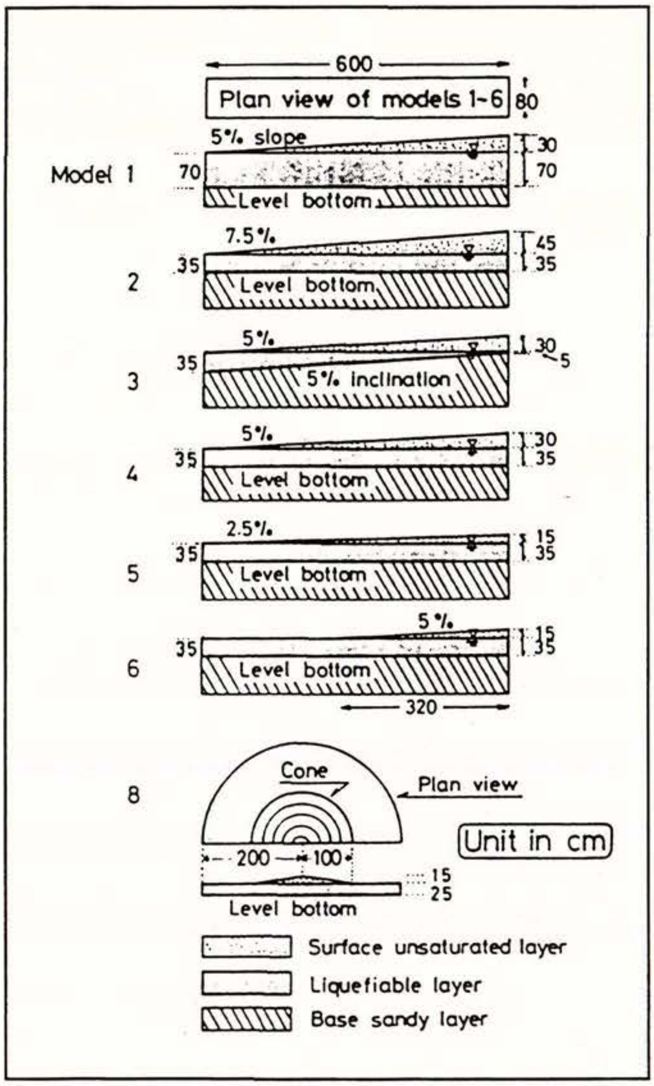

Figure 2.4 Model configurations for large scale shake table tests (from Sasaki <u>et al</u> 1992)

A graph of the parameter D/(TH) plotted against θ for each test is shown in Figure 2.5. All of the test results fit within a band indicated by the dotted lines showing that there is some relationship between the two parameters, but also some significant scatter in the results. This verifies the scatter in data shown by Hamada (1987), which comes from measurements in the field.

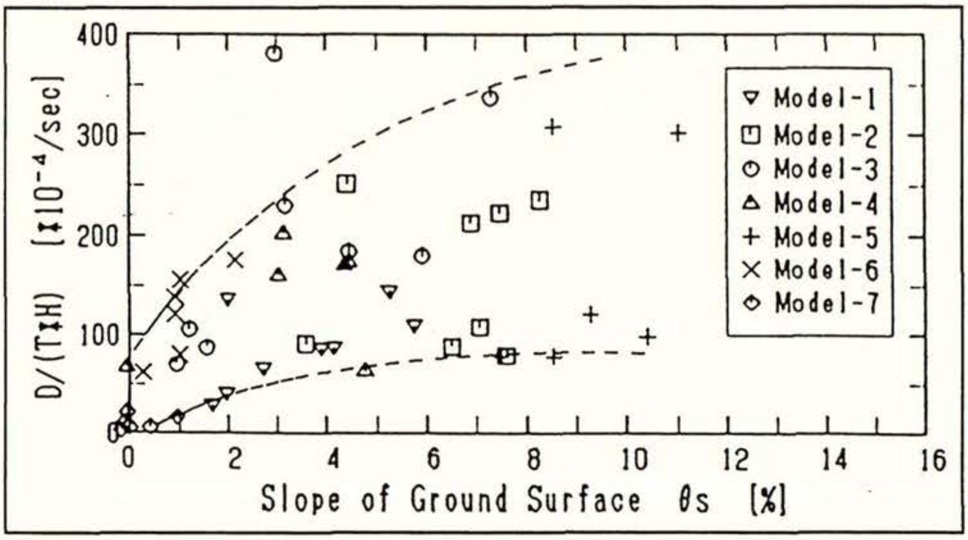

Figure 2.5 Test results for models 1-7 (from Sasaki et al 1991)

In the semi-circular test, the tank was subjected to excitation in one plane only. This test was performed to see if the direction of excitation had any significant affect on the direction of lateral spreading. The results of movement vectors surveyed from the surface of the model are shown in Figure 2.6.

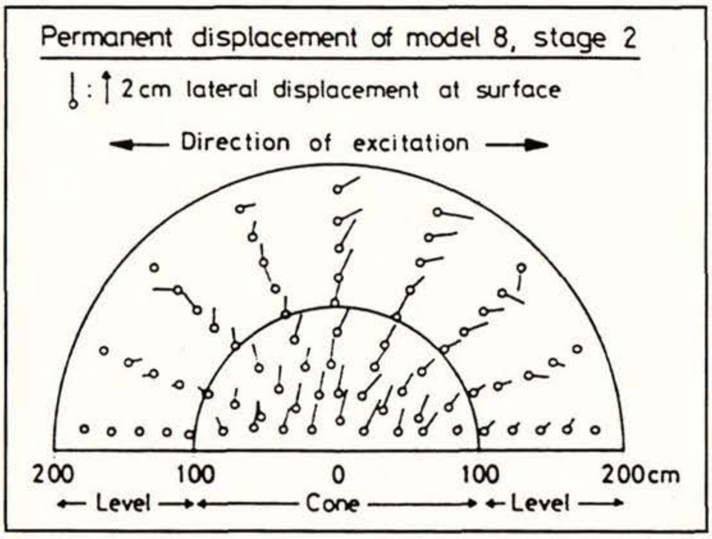

Figure 2.6 Horizontal surface displacement in the semi-circular model (from Sasaki et al 1992)

Excluding the vectors affected by side friction from the walls of the tank, the movements are oriented radially. Some of the movements are directed back towards the centre which may have been caused by local inverse inclination at the ground surface.

They concluded that the direction of permanent lateral displacement is independent of the direction of the seismic inertia force. It is governed by the direction of initial shear stress in the liquefiable layer before excitation which is due to gravity. The influence of seismic inertia is indirect, controlling the extent of soil liquefaction and possibly the rate of development of the lateral soil movement.

Tokida, Iwasaki, Matsumoto and Hamada (1993) performed some large scale model tests to investigate the dynamic behaviour of a pile model set in flowing soils induced by liquefaction. The first test used an 8 metre long by 1 m wide container constructed on a shake table to hold a sloping fill of saturated sand. A model pile was placed in the container, fixed at the base and free to move at the top. A sloping liquefiable soil was created around it with a denser, non-liquefiable base soil (see Figure 2.7). Both layers consisted of Sengen-Yama sands with a D_{50} of 0.25 mm.

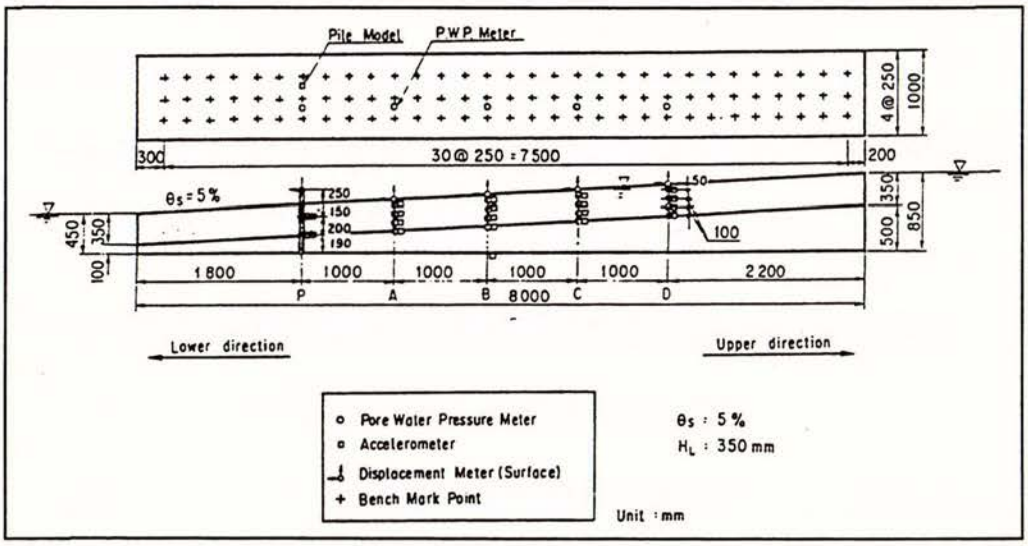

Figure 2.7 Test configuration for lateral spreading model
(from Tokida <u>et al</u> 1993)

The container was subjected to a sinusoidal shaking motion with pore water pressure meters, accelerometers, displacement meters and strain gauge meters installed to monitor the time history of the model behaviour. The peak driving stress on the pile from the liquefiable sand occurred about one fifth of the depth of the liquefiable sand from the top of the pile. It was found to be 27 kPa and it occurred when the sand was fully liquefied and moving down slope. The peak resisting stress on the pile in the soil occurred at the interface between the liquefiable and non-liquefiable layers and was approximately 72 kPa. Figure 2.8 shows how the horizontal lateral loads varied over the length of the model pile at different time intervals.

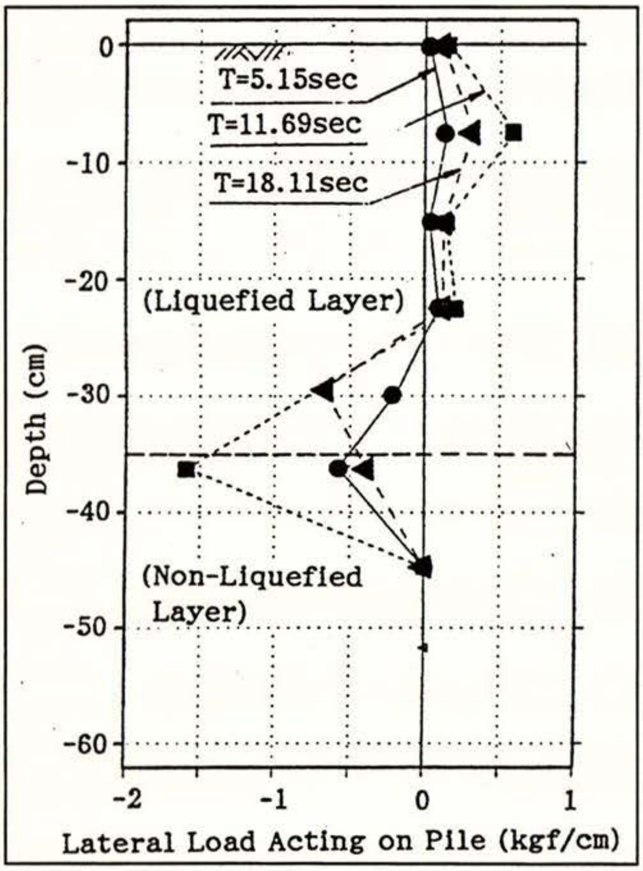

Figure 2.8 Horizontal stresses on pile at different times during the test (from Tokida et al 1993)

A second series of tests involved dragging various pile group configurations through liquefied sand in the container whilst monitoring the pile and sand behaviour. High excess pore water pressures were found to remain longer nearer the surface which is consistent with Fiegel and Kutter's (1994b) results. As the excess pore water pressure increased the total load imposed on the piles by the liquefied soil decreased. The total load on the piles was dependent on the number of piles perpendicular to the direction of motion of the soil. As the sliding velocity of the piles is increased in the liquefied soil, the total load increases correspondingly. When soil liquefaction did not occur the drag velocity of the piles in the soil had no effect on the total load resistance of the soil. When partial soil liquefaction occurred the total load on the piles was proportional to the sliding velocity.

These results are important when considering the Landing Road Bridge site because significant lateral spreading has occurred there with the moving liquefied soil exerting lateral loads on the piles, and the overlying crustal soil loading the pile cap and pier in a passive nature. One could expect a similar drag forces of around 30 kPa to occur on the piles as they resist the liquefied sand motion.

Vargas and Towhata (1995) conducted shake table tests to examine the fluid behaviour of liquefied sand and determine its viscosity. A hollow steel pipe, 300 mm in length with a diameter of 30 mm, was placed on guide rods in a container with load transducers to determine drag forces. Very loose sandy ground, which could flow under low confining stresses, was placed in the container, located on the shake table. Toyoura sand was placed in the container using wet tamping methods. The properties of this sand are ρ_s = 2.65 t/m^3, D_{50} = 0.17 mm, e_{max} = 0.974, e_{min} = 0.605 and the range of relative densities (D_R) measured during the experiments was -30 to +10%. To simulate lateral flow in level ground, the pipe was moved horizontally after liquefaction had occurred. Figure 2.9 shows the layout of the sand container and instrumentation.

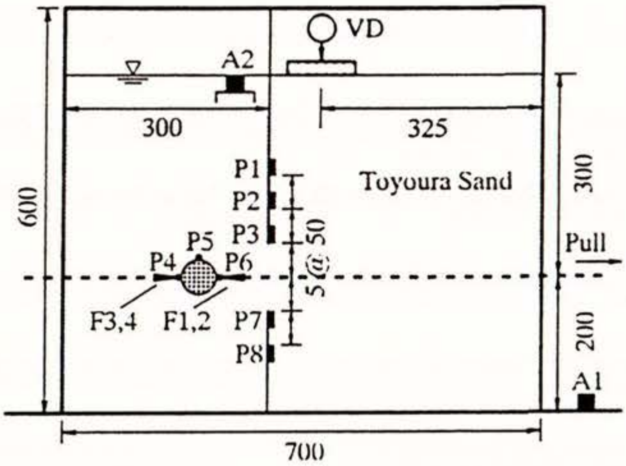

A = accelerometer, F = load cell, P = piezometer
VD = vertical displacement meter. All dimensions in mm.

Figure 2.9 Test configuration for drag force experiments (from Vargas and Towhata 1995)

Three types of test were performed and they produced some interesting results. The first test series considered monotonic displacement of the pipe after the end of shaking when high excess pore water pressures remain and start to slowly dissipate. Velocities up to 19 mm/sec were used and this was considered to be analogous to probable velocities of flow in prototype slopes. With the level ground model that was used, there was no initial static shear stress caused by gravity (the component of weight parallel to a slope) and the duration of liquefaction is short in a small container. These two factors caused difficulties in the measurement of the drag immediately after shaking had stopped since the excess pore water pressures dissipate quickly and the liquefied sand regains strength.

The measured drag increases steadily during the pore water pressure dissipation from an initially small value at complete liquefaction. The initial drag force at the beginning of pipe movement was small compared with that at the end of movement as shown in Figure 2.10. Close examination of the transducer force plots allowed the determination of this small initial drag force.

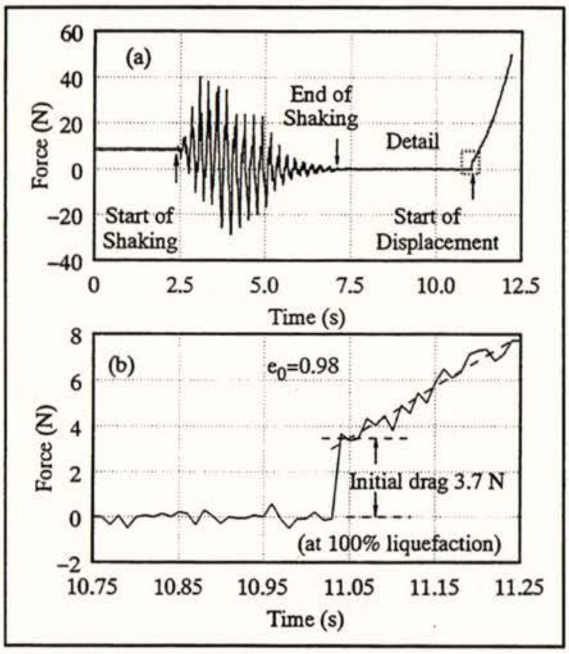

Figure 2.10 Measurement of initial drag (from Vargas and Towhata 1995)

Results from these tests were plotted with that of previous work, within the range of velocities studied, showing that the drag exerted by liquefied sand was approximately proportional to the pipe velocity. It became almost constant as the void ratio of the sand increased. As the viscosity of the liquefied sand increased, the corresponding drag force (at the same velocity) increased.

The second series of tests investigated drag forces during monotonic displacement of the pile under continuous, constant amplitude shaking. When shaking was applied in the same direction as that of the pipe displacement, the drag fluctuated with a constant amplitude and overall slowly increased with further displacement. Total drag forces were almost constant when the direction of shaking was perpendicular to that of the pipes movement and similar magnitudes to those in the first series of tests were found for the same density and velocity.

The pipe was moved cyclically under continuous, constant amplitude shaking for the third group of tests. The drag during cyclic motion was taken as half the difference between the average values obtained in two consecutive half cycles. These results were comparable with those obtained when the pipe underwent monotonic displacement.

Based on the measurements of drag, the viscosity of the liquefied sand was computed using a fluid mechanics relationship. The calculated viscosities for the sand used in these tests varied between 0.2 and 1.5 kPa.sec. Vargas and Towhata noted that previous studies have shown the range in viscosities for similar conditions to be between 0.1 and 10 kPa.sec.

The drag forces imposed on the piles at Landing Road Bridge by lateral spreading during the Edgecumbe earthquake were estimated by Berrill et al (1995) to be no more than 30 kPa or 50 percent of the total overburden stress.

2.4 LATERAL LOADS ON PILE FOUNDATIONS

The behaviour of piles embedded in the ground when exposed to lateral actions and accompanying bending moments, shear forces and displacements is extremely difficult to predict with great accuracy. Lateral forces may result from the inertia of the structure above during seismic excitation, traffic, wind loads and loads imposed by the soil surrounding them.

Two areas were investigated in particular. Firstly, loads which are caused by the inertial forces of the structure above and secondly, those which are due to liquefaction. Pender (1993) gives a good summary of current methods for the aseismic design and analysis of pile foundations. Case histories are presented along with techniques for modelling lateral pile stiffness, pile groups, soil properties, non-linear effects and ultimate horizontal pile capacities. Liquefaction effects on piles were not discussed in the report. Poulos and Davis (1980) and Elson (1984) discuss the analysis and design of laterally loaded piles, some of which Pender (1993) considers.

Inertia loads are usually the result of earthquake ground motions which cause the ground beneath a structure to move and the structure itself tries to resist the movement. Piled foundations are subjected to bending, shear and axial loads which are transmitted into the surrounding soil as the structure above responds to the ground movement. Many observations of pile damage caused by earthquakes have been reported. Pender (1993) discusses case histories of piles in sand, silts and cohesive soils, raked piles, end bearing piles and gapping effects in large diameter piles.

Horizontal loads on piles caused by liquefaction of cohesionless soils surrounding them can only occur if the soil itself moves and the piles resist the movement. Some form of lateral restraint must be present in order for the loads to develop. In some situations the piles may move freely with the soil and the loads imposed on them will be small. But usually with large deformations there are more important consequences such as buildings tilting and bridge decks falling from their supports.

Miura, Stewart and O'Rourke (1991) used analytical techniques to estimate the maximum bending moments induced in piles subjected to lateral ground displacement. The pile was assumed to be embedded in a non-liquefiable base soil with a liquefiable layer above and a non-liquefiable surface layer (see Figure 2.11).

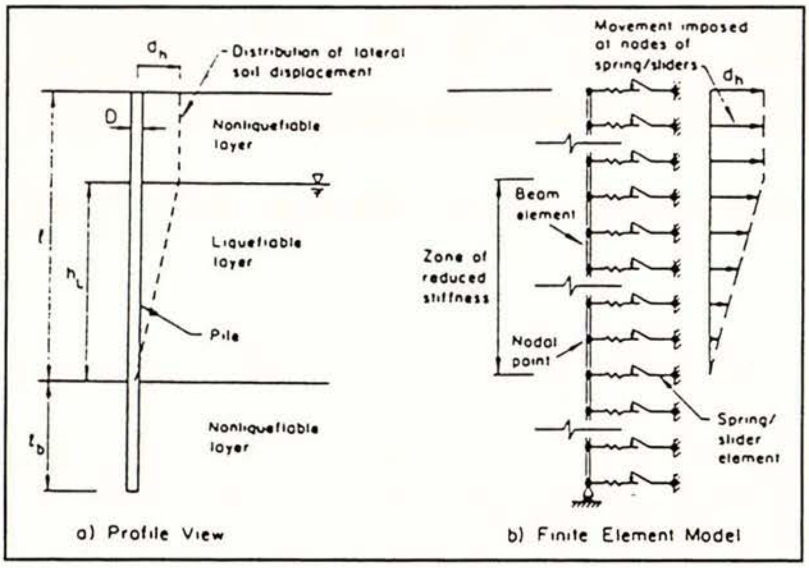

a) Profile View

b) Finite Element Model

Figure 2.11 Pile and soil-structure interaction model (from Miura et al 1991)

Fixed and free end conditions, base embedment effects and pile cap connectivity effects were investigated with both linear and non linear analyses. Soil stiffness was represented by springs and the pile by a series of beam elements. Their results showed that for a free head pile (no rotational stiffness at the top of the pile) the positions of maximum bending moment occur at the interface between non-liquefiable layers and liquefiable layers. When pile caps are embedded in the crustal non-liquefiable layer that moves over top of a liquefiable layer, the maximum bending moment in the pile usually occurs at the connection between the pile and pile cap.

Their analyses revealed that the existence of a non-liquefiable layer at the ground surface can significantly affect the maximum bending moment in the pile. When a relatively thick non-liquefiable layer exists above a liquefiable layer, neither the material nonlinearity of the soil nor the loss of soil stiffness within the liquefiable layer significantly affect the maximum bending moment in the pile. When no intact soil or a very thin non-liquefiable layer at the ground surface is expected, the estimation of maximum bending moments is not simple and substantially reduced bending moments are possible. The soil stiffness of the liquefiable layer must be chosen carefully for a reliable analysis as it significantly affects the pile response.

2.5 DESIGN METHODS FOR LATERAL SPREADING INDUCED LOADS ON PILES

There is no easy way for the bridge designer to design a pile or group of piles for lateral spreading of the soil above and around them. It is an issue that has not been examined extensively in the past. In New Zealand, some of the bridges on major routes are very likely to be sited in potentially liquefiable deposits that may be subjected to lateral spreading of the soil, which could cause foundation damage.

A simple approach to analysing lateral spreading loads on piles could consider two possible components of loading. Firstly loads from the unliquefied passive failure of the soil around the pile and secondly drag forces created by the motion of liquefied soil. This is discussed in detail in Chapters 6 and 7.

2.5.1 The New Zealand Loadings Code NZS4203:1992

The loadings code gives no real direction for the design of foundation elements for an engineering structure. Horizontal loads such as wind and earthquake actions are given for the design of the structure above ground but all of these loads must follow a load path to the foundations. The loads induced on the foundations due to these actions can be calculated simply. The foundation design itself is a much more difficult problem as both the soil and foundation structure properties are difficult to model accurately.

Pile foundations are used primarily for the axial capacity they can provide, but they may also be subjected to bending moments and shear forces from the structure above. Raked pile groups have a much higher resistance to horizontal loading because a large proportion of the horizontal component of load is carried axially by the piles. Lateral forces from the soil surrounding piles may occur, as seen in many lateral spreading situations. For vertical piles, this type of load is resisted by flexure in the piles. In the case of raked piles, flexure will occur with additional resistance given by side friction and end bearing.

Soil-structure interaction is difficult to predict. Estimates of structural behaviour may be in error by several orders of magnitude from the true result. In reality soil is a very complex, non-linear material that poses great problems for the designer. It is difficult to assign one set of parameters to a particular soil as often significant temporal and spatial variability is encountered.

Chapter 3

Landing Road Bridge

3.1 HISTORY OF THE LANDING ROAD BRIDGE SITE

Christensen (1994) detailed the history of the bridge site, considering the river channel movement, soil deposition and bridge construction. A brief summary only will be given. The Landing Road Bridge is located over the Whakatane River west of the town centre. It is the main transport link for Whakatane with State Highway 2 crossing the river. Figure 3.1 shows a view of the bridge taken from the true left bank looking south.

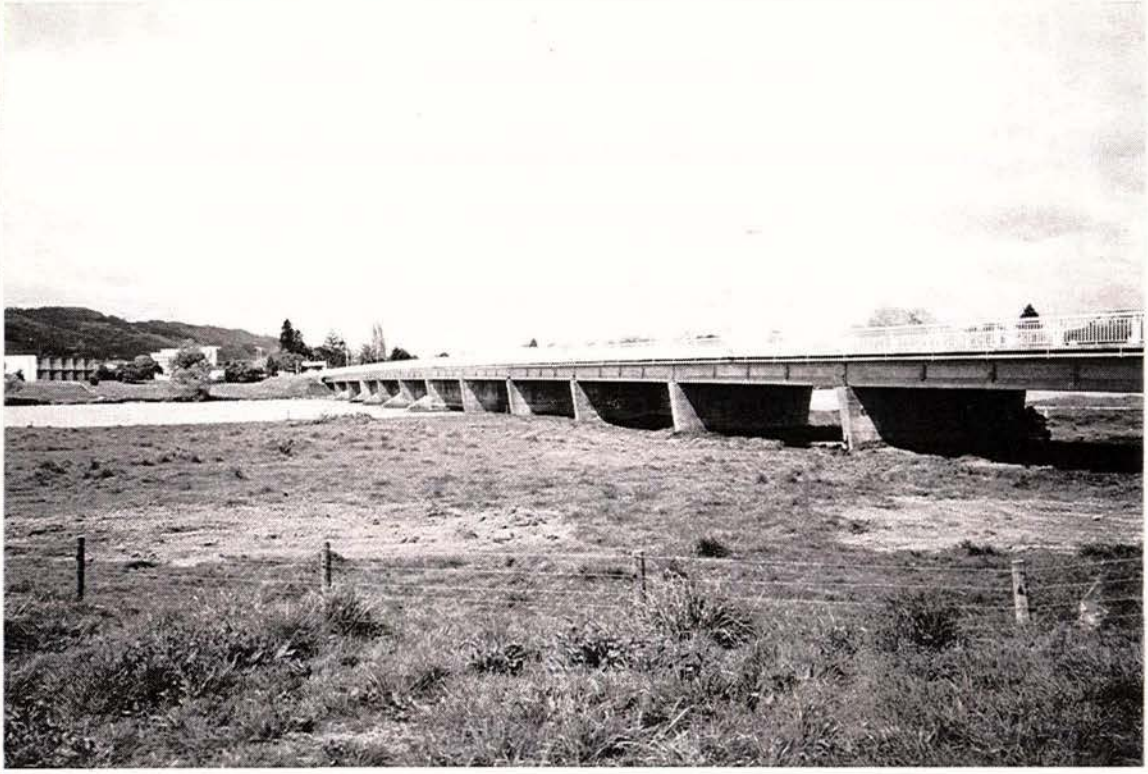

Figure 3.1 Landing Road Bridge, Whakatane

The north-west abutment and Piers B through F (at the right hand end of the bridge as seen in Figure 1.3, which looks upstream), are situated in relatively young sediments due to the active movement of the river channel towards the east in the last few hundred years. Typically the soil at the site consists of 1 to 1.5 m of sandy silt overlying medium to coarse pumiceous sands. The top 4 m of sand is loose and becomes immediately denser below this. Presumably it is this upper 5 to 6 m of soil that was layed down recently as the river channel migrated to the south east. The river channel piers and south-east abutment are situated in much older material.

Bridge construction commenced in 1962 using a standard design common throughout New Zealand. The superstructure is made up of 13 simply supported spans of 18.3 m length carrying a two lane concrete deck and two footpaths. The deck is supported by five post tensioned concrete I beams and diaphragms. At the beam ends the diaphragms are joined by linkage bolts over the piers and they rest on 16 mm rubber pads. The substructure consists of tapered concrete slab piers connected to a pile cap with 8 precast pretensioned 406 mm square raked piles (raked at 1 : 6) approximately 10 m long beneath the cap. The piles were driven into the dense sands underlying the layer that liquefied in 1987. The abutments are supported by 5 piles on the river side and 3 on the approach side without any approach slabs. The abutment backwall is tight-packed and bolted to the beam diaphragm.

In the early 1980's, five of the river channel piers suffered scouring and undermining damage which was remedied about 1985 by underpinning each pile cap with two 1.1 m diameter concrete cylinders. The enlarged piers can be seen in Figures 3.1 and 3.3.

During the 1987 Edgecumbe Earthquake, loose sediments liquefied a distance of approximately 300 m back from the true left bank of the Whakatane river. This caused lateral spreading of up to 1.5 m towards the river. It is understood that the true right bank sediments, which are older and have markedly greater cone penetration resistance, did not liquefy at all. Thus the superstructure, underpinned river piers and south-east abutment were essentially rigid in relation to the true left bank piers which resisted the soil movement. This meant that the buried section of the piers and underlying pile foundations were subjected to considerable lateral load. Mounding of the soil on the northern side of the piers gave and indication of a passive failure in the 1.0 to 1.5 m thick silt crust. Pier C had the most prominent soil mounding and was the focus of further investigation (see Figure 3.2).

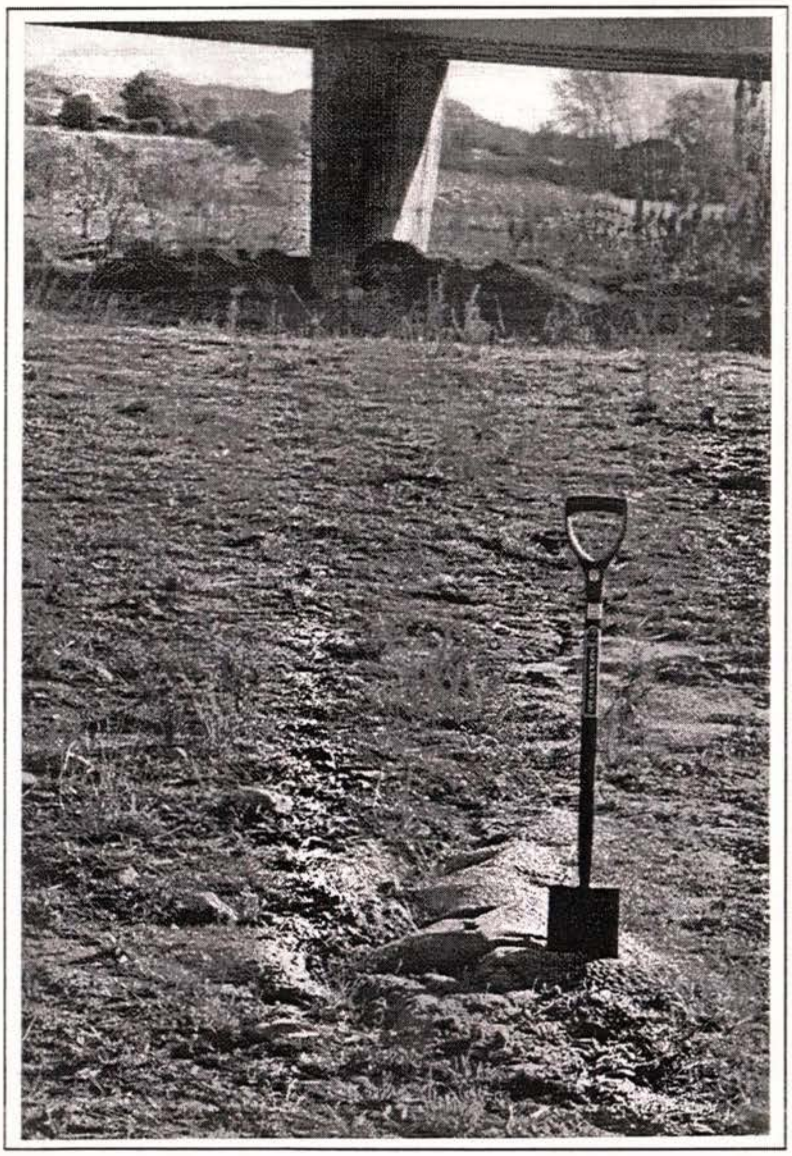

Figure 3.2 Sand boil in foreground with mounding of soil behind Pier C in background (courtesy of J. Berrill)

The bridge superstructure was not under any significant distress after the earthquake. Slight compression of the deck was indicated by the buckling of a concrete footpath slab. The approach side raked piles on the northern abutment were cracked on the river side through 75% of their width and repaired with epoxy resin. The ground surface of the true left bank settled 300-500 mm exposing the river side piles at the north-west abutment. Minor rotation of some of the piers on the northern bank of up to one degree was noticed (Christensen 1994). Large horizontal cracks appeared in piers H and J (the first two northern underpinned piers, which would have attracted added lateral load because of their additional stiffness) and went unnoticed for several years by the highway authority. These cracks were repaired in 1992, as shown in Figure 3.3, with epoxy resin.

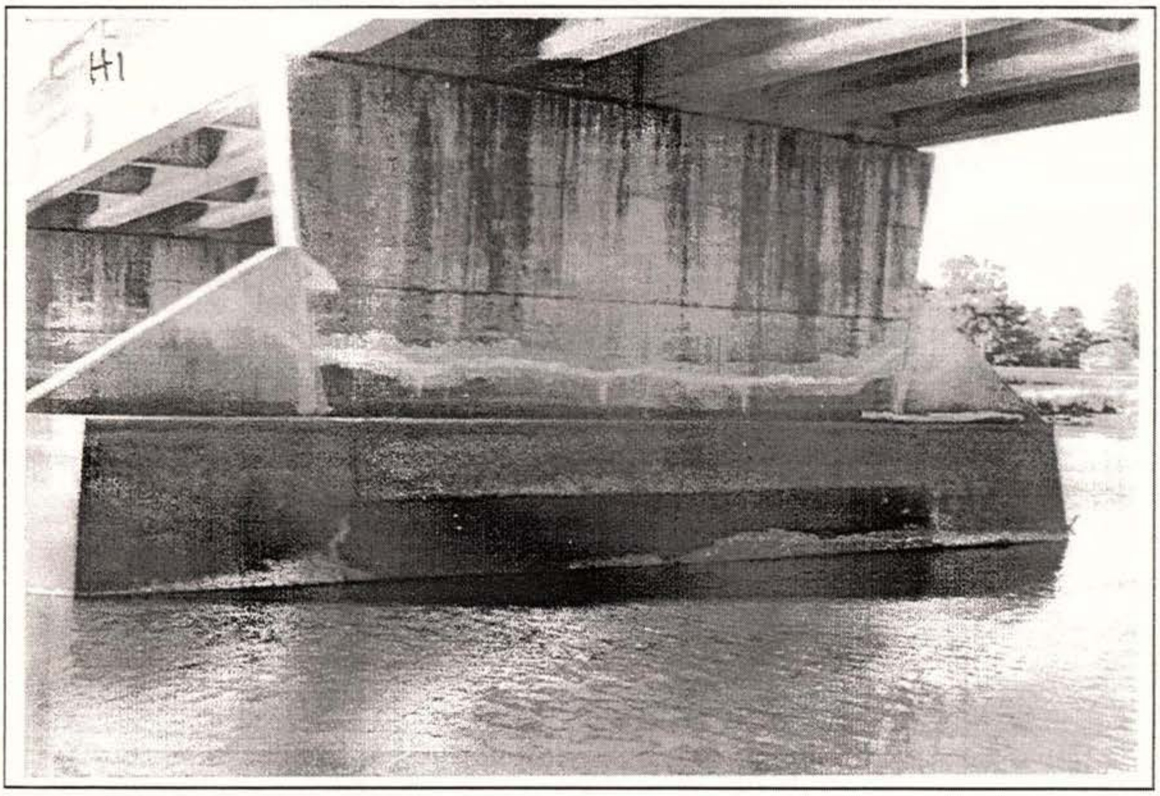

Figure 3.3 Repaired cracks at Pier H (courtesy of J. Berrill)

3.2 STRUCTURAL ANALYSIS OF THE BRIDGE

Using the construction plans drawn in 1960, it was possible to calculate the strength of the pile/pier system in the substructure of Landing Road Bridge. The superstructure is very much stiffer and stronger than the substructure, making it the redundant component in the structural system for longitudinal lateral loads The moment capacity top and bottom of the slab piers is small. The potential collapse mechanism in the pile/pier substructure due to liquefaction induced lateral spreading was defined (see Figure 3.4) and the ultimate lateral strength of it was found using an upper bound approach.

The chosen collapse mechanism is assumed to occur because of the nature of the lateral spreading loading. The centroid of the horizontal soil stress distribution is expected to be located just above the pile cap. Thus it is likely that the pile cap would translate with the moving soil but have very little or no rotation. The piles beneath and soil mass above the cap provide some rotational restraint. Where the pier and piles meet the pile cap, they are free to rotate and will translate with the cap. At the top of the pier and mid height of the piles, where they enter the denser soil, rotation only is assumed to occur.

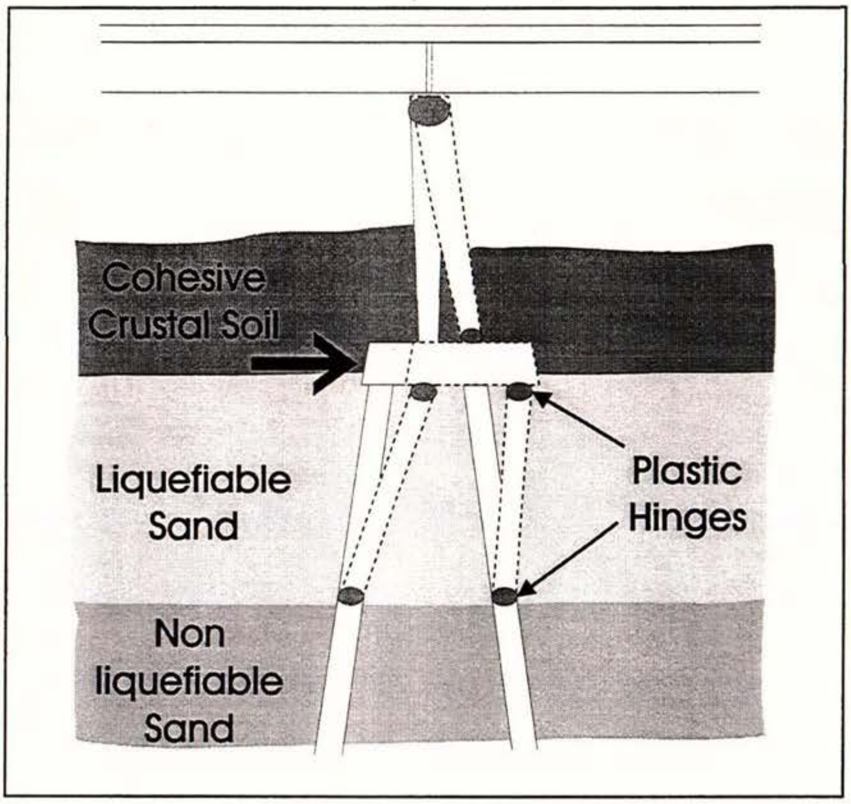

Figure 3.4 Substructure collapse mechanism

From the ground surface the crustal cohesive soil is approximately 1.5 m deep to the level of the top of the pile cap at piers B, C, D, E and F. Immediately below that there is loose, cohesionless, liquefiable sand approximately 4 m thick. At this depth there is a jump in density, with SPT N values of greater than 30 and the sand is unlikely to liquefy in strong ground motion.

Considering the research of Miura et al (1991), we would expect plastic hinges to form in the piles at the interface between liquefiable and non-liquefiable sand and the pile-pile cap interface during lateral spreading. The pile cap is quite heavily reinforced and hence very stiff so it would remain elastic without suffering any damage. Because of the small moment resistance of the tapered slab pier, it would contribute little to the lateral resistance of the system.

The plans for the bridge gave all of the necessary dimensions, reinforcing steel layouts and concrete properties in imperial units used in the calculation of the plastic moments. These details were easily converted to SI units but both the reinforcing and prestressing steel properties were more difficult to define.

Steel reinforcing and prestressing strand used in the 1960's had different properties from those currently used in modern design practice. Working stresses were used rather than yield stresses for design so often only the maximum allowable working stress was quoted in design charts and tables. Current New Zealand design codes use yield stresses and for the analysis of the bridge the current codes were followed. To assign a value for the yield stress at the time of the bridge construction, Works Consultancy Services guidelines used for the retrofit of old bridges were checked. For the early 1960's the yield stress of ordinary, non-prestressed steel reinforcing was assumed to be $f_y = 250$ MPa.

The precast prestressed concrete piles contained 16 seven wire helically wound prestressing strand with square helical transverse reinforcement. Obtaining properties for the strand proved to be difficult because only the nominal external diameter was known.

A prestressing strand catalogue (GKN Catalogue, 1960) gave the minimum breaking load (equivalent to the ultimate tensile strength) of the strand to be 21 000 psi (or $f_{pu} =$ 1810 MPa) and cross sectional area of 0.080 in^2 (or 51.6 mm^2). These values were used for the strength calculations.

It is important to consider the method used to construct the pile cap around the top of the eight piles; the practice at the time was as follows. After driving the piles the top of each pile had the concrete jack hammered away exposing the prestressing steel and square helical transverse steel. The pile cap reinforcing steel and formwork were placed around the exposed pile reinforcing so that the concrete could be poured in situ. Thus effectively all of the prestress was lost at the pile-pile cap interface. Under ultimate loads, the interface cannot fully develop the same strength as that of the prestressed part of the pile.

The development length for the prestressing strand was calculated to be 1460 mm (from NZS3101:1995) for the prestressed strand in the intact pile. But where the tendons have no initial stress, which is the case in the pile cap, the development length is much larger at 2280 mm. The pile cap is 760 mm high, so it is not possible to develop the full moment capacity from the strand, which results in a much lower strength. These calculations were done assuming that the prestressing strand was straight and they indicate that the maximum stress in the strand at failure is likely to be about one third of that for the mid height of the piles. It is possible that during construction the exposed strand was bent to form a hook in the pile cap. This may have occurred when some piles were not driven as far as the others and after removing the concrete surrounding the pile reinforcing, they were found to be too long for the height of the pile cap. If this were the case then the development lengths for the strand would be significantly less than for the straight strand, but it is likely that they are still not enough to utilise their ultimate tensile strength.

Ultimate flexural strength at the interface is therefore assumed to be governed by bond failure of the strand in the pile cap. If this failure mechanism was mobilised by lateral spreading of the ground one would expect to see some cracking around the top of the pile and possibly separation between the pile and pile cap.

Axial compressive loads of the order of 2.5 MN on each pier were insignificant when considering the interaction with plastic moments and so the flexural strength calculations for the top and bottom of the pier neglected them. The average axial load on each of the piles was determined to be 310 kN or approximately 5 percent of the ultimate axial capacity. This load is significant enough to increase the plastic moment capacity in the piles. As the substructure undergoes lateral deformation, the riverside piles have an increased axial compressive load whereas the river bank side piles have induced axial tensile forces. This means that the axial load could be significantly smaller in compression, or perhaps slight tension at ultimate loads under full collapse for these piles. Thus, moment-axial load interaction charts for the individual piles were calculated using a method based on first principles (Lin and Burns, 1981). Each of the anchorage and stress conditions in the piles gives a different curve (as shown in Appendix A):

- Firstly, at the interface between the liquefiable and non-liquefiable sand, the prestressing force in the strand is fully developed under ultimate loads.
- Secondly, at the pile/pile cap interface, the prestressing force is zero and the anchorage of the strand in the pile cap is assumed to be able to develop the full capacity of the strand in tension.
- Thirdly, at the pile/pile cap interface, the prestressing force is zero with the anchorage of 700 mm of straight strand in the pile cap developing one third of the ultimate tensile capacity of the strand.

Table 3.1 shows the calculated plastic moments for the pier and pile at each position. Axial dead loads did not give a significant difference to the plastic moments calculated in the pier, but show an increase for the case of the piles. The deformation causing changes in axial loads in the raked piles is not considered here.

M_p (kNm)	*Neglecting Dead Load*	*Considering Dead Load*
Top of pier	610	610
Bottom of pier	305	305
Top of piles - one pile, assuming full development of strand	195	225
Top of piles - one pile, assuming bond failure	80	130
Mid height of piles - one pile	200	230

Table 3.1 Ideal plastic moment capacities of substructure

The piles on the riverward side of the pier will sustain a greater plastic moment than that shown in Table 3.1, due to an increase in compressive load during lateral deformation, and the landward piles will develop a lower plastic moment. For the calculation of ultimate lateral loads, the increase in plastic moment in the riverward piles, as the pile cap translates, is assumed to be equal to the decrease in plastic moment for the landward piles. This allows the plastic moments determined under axial dead loads only to be used in the lateral load calculations as the effects of the deformation induced loads will cancel out.

Cracking moments were determined at each potential plastic hinge location using an iterative elastic analysis of the substructure, including axial dead loads and allowing for deformation induced changes in axial loads in the raked piles . The transformed area approach for the pile and pier sections was used in the calculations. At construction joints, it is common practice to assume that the concrete has no tensile strength. Thus the moments required to just cause zero concrete stress at the extreme fibre of the section were calculated. However, at the mid height of the piles, the tensile strength can be developed and the calculations allowed for the modulus of rupture of the concrete. Table 3.2 shows the first cracking moments for the substructure. The cracking moments for the piles are only approximate, since they depend on the axial load at first cracking. The elastic analysis can only be used to predict first cracking moments up to the formation of the first plastic hinge, where after this only approximations can be used as the mechanism begins to form.

CRACKING MOMENTS	*M_{crack} (kNm)*
Top of pier	215
Bottom of pier	140
Top of one riverward pile	~50
Top of one landward pile	~14
Mid height of one riverward pile	~150
Mid height of one landward pile	~100

Table 3.2 Ideal first cracking moments of the substructure

From observations above ground at the bridge, there is no evidence of cracking at the top of the pier due to the lateral spreading loads. But it is possible for the bottom of the pier and the top of the piles to be cracked. Excavation for examination of these two areas was undertaken to reveal if any cracks had appeared there, which is discussed in Chapter 4.

The smallest cracking moments occur at the bottom of the pier and the top of the piles, which is where cracks would first be expected after lateral displacement of the pile cap.

The large difference in the pile first cracking moments is due to the fact that all prestress is lost at the top of the pile, but is fully effective at mid height.

3.3 COLLAPSE LOAD OF THE SUBSTRUCTURE

With the ideal plastic moments determined, the mechanism method can be used to calculate an upper bound on the total horizontal force required to initiate collapse of the substructure (calculations are shown in Appendix A). This is assumed to act over the height of the pile cap.

When the bond failure mechanism is assumed to occur at the top of the piles, the resulting passive force is calculated to be about 950 kN for collapse of the foundations. If full development of the strand at the top of the piles is assumed, about 1130 kN is required to cause collapse. Since the anchorage of the strand in the pile cap can not be determined, a range for the upper bound collapse load can only be be stated.

Preliminary estimates of the total horizontal passive force, based on CPT probes 20 - 30 m from the bridge, indicate a load of around 500 kN which is quite significant considering that it is about half the collapse load of the substructure.

Based on this initial estimate, it is quite likely that cracking of some elements within the bridge substructure beneath the ground resulted from the Edgecumbe Earthquake. This is most likely at Pier C where soil mounding behind it is prominent. Thus it was proposed to trench at pier C, both to search for a failure surface within the soil and to obtain better estimates of soil strength, and to inspect the pile tops for damage.

Chapter 4

Site Investigation

4.1 PRELIMINARY INVESTIGATIONS

4.1.1 Field Work

A short trip in late March 1995 was made to the site to get a general perspective of the area and perform some hand augering beneath the bridge. Walking both upstream and downstream of the bridge on the true left bank revealed previous lateral spreading cracks and some partially buried sand boils, presumably resulting from the 1987 Edgecumbe earthquake. In the free field the cracks were more or less parallel to the river channel, in the vicinity of the bridge they tended to be at about 45° to the longitudinal direction of the deck (see Figure 4.1). This immediately suggested that the bridge had not been displaced significantly with the laterally spreading ground, but rather that it had restrained the free field movement. Considering that the piers were still near vertical indicated that the full collapse mechanism had not developed.

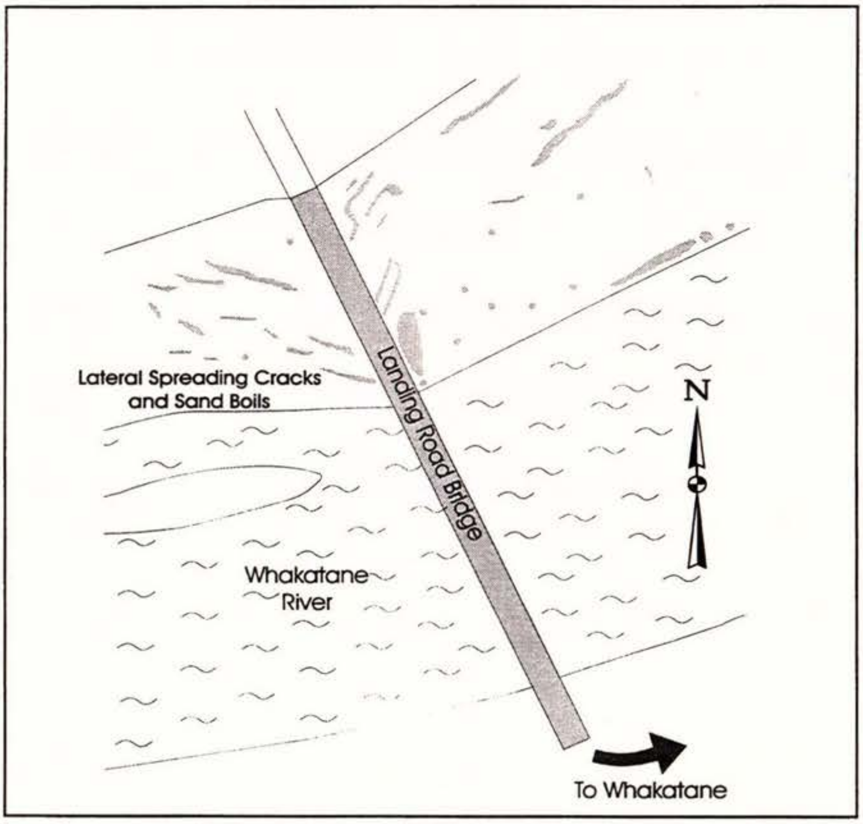

Figure 4.1 Lateral spreading cracks and sand boils on the true left bank

Both the piles and partially buried bridge piers would have been subjected to lateral spreading loads from two parts of the soil profile:

- Firstly, from the cohesive crustal silt from the ground surface to a depth of 1 - 1.5 m that did not liquefy during the strong ground shaking. This stratum moved on top of the liquefied sands toward the river channel while cracking and breaking into large blocks. Passive failures of this soil were indicated by mounding behind the bridge piers.
- Secondly, from the approximately 4 m thick liquefiable pumiceous sand beneath the crustal soil which may also have moved toward the river channel and in doing so subjected the piles to drag forces.

A 50 mm diameter hand auger was used to probe to a depth of 2.5 to 3 m at four positions beneath the bridge deck and 2 sites upstream of the bridge. Figure 4.2 shows a plan of the auger locations. Samples were taken at various depths for grain size analysis in the laboratory. Appendix B contains the bore logs and particle size distributions for these samples.

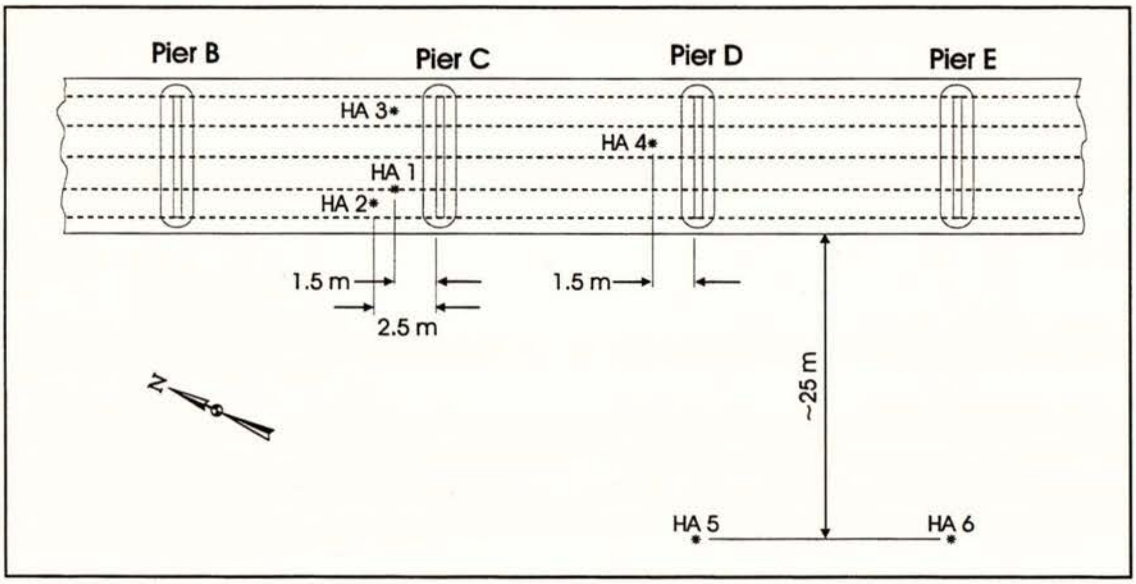

Figure 4.2 Hand auger locations

An initial guess at the geometry of the passive failure surface, based on the soil crust thickness and typical silt shear strengths, suggested the head of the slip surface would be

4 to 5 m from the pier face. North of pier C three auger holes were attempted within this length. HA 1 was taken to a depth of 2.6 m where it could no longer be continued due to caving problems in the loose, saturated sand. Six samples were taken from this hole including some fine angular gravels with lots of bark and wood chips. It also gave a good indication of the depth to the water table and how it varied with the tide over a few hours. The cohesive silt containing organic material, gravels and wood chips terminated at about 1.8 m with the sandy layers below this. This interface was at approximately mid height of the pile cap.

HA 2 could not be continued past 650 mm in depth because of coarse gravels that could not be penetrated with the small auger. HA 3 had a similar profile to that of HA 1. Angular gravels at depths of 350 mm prevented further penetration in a number of locations north of Pier D.

The final two auger holes, located about 25 m upstream from the bridge, showed 600 - 800 mm of tan gravelly silt overlying a grey, clean sand. Caving occurred in the sand at depths of about 1.3 m in both cases. As before, woodchips were found in the silt layers at each location. The Whakatane Board Mill is located back further from the rivers edge and is most likely the source of these wood chips. It is thought that the mill's waste was dumped on the river bank in the past and during high water times the river would have transported this waste downstream, depositing it on the true left bank.

4.1.2 Laboratory Work

The data provided by these borings and the general inspection of the site gave information for a more detailed investigation. The bag samples of disturbed soil were taken back to the laboratory for the following tests:

- NZS 4402:1986 test 2.7.2 Solid Density of Solid Particles (for medium and fine soils).
- NZS 4402:1986 test 2.8.1 and 2.8.2 Particle Size Distribution by Sieving.
- NZS 4402:1986 test 2.8.4 Particle Size Distribution by the Hydrometer Method.

The presence of wood chips and bark in some of the samples meant that certain dry density test results (ρ_s) for the parent soil were unrepresentative of the mineral content of the soil. Of the tests that did not have any wood particles, ρ_s varied between about 2.10 - 2.60 t/m^3. In the hydrometer analysis, the wood particles all floated to the top of the container rather than settling out of the mixture, and it is likely that the readings were not accurate. Before dry sieving tests begin, soil is softly ground down to its individual particles. Woodchips present in some samples generally splintered up in to many small pieces so that the resulting particle size distribution is likely to be altered slightly.

Some of the sand samples that did not have any wood particles in them fit within Tsuchida's Grading Curves for liquefiable soils (see Figure 4.3). D_{50}'s ranged from 0.1 to 0.6 mm with some sands being quite uniform and others more well graded.

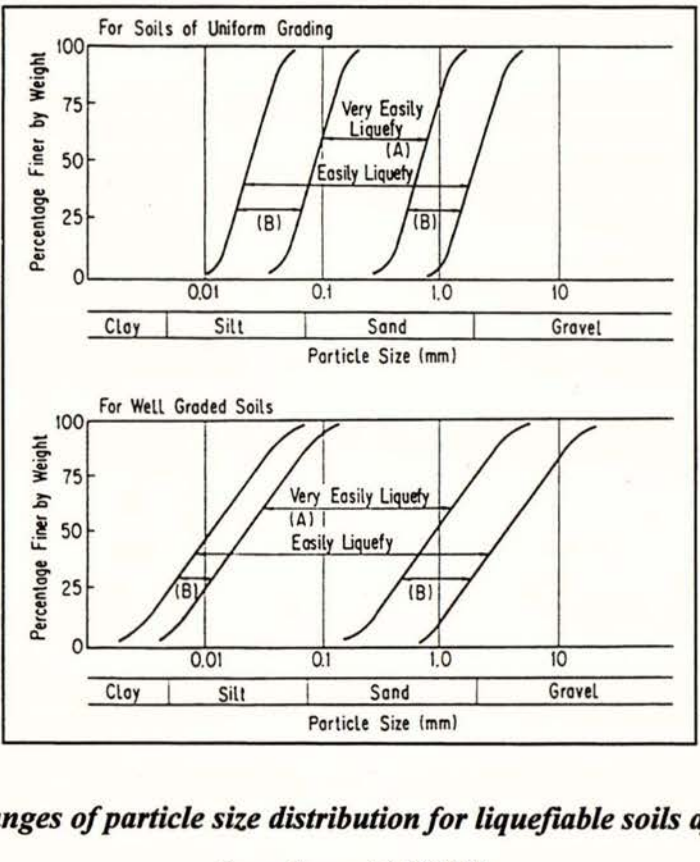

Figure 4.3 Ranges of particle size distribution for liquefiable soils after Tsuchida, from Iwasaki (1986)

4.1.3 Conclusions from Initial Investigation

The most important points gained from this preliminary investigation were:

- The cohesive soil crust in the free field varies from 0.7 to 1 m thick. It is a medium tan silt with some gravels and wood particles.
- Beneath the bridge, where mounding of the soil behind the bridge piers has occurred, the crustal soil is complex with silts, gravels, organics and wood chips and is about 1.5 m thick. This soil is presumably representative of the backfill placed at the time of construction rather than the free-field material.
- The Whakatane Boardmill was probably the source of the wood particles in the upper soil layers and they may have an important effect on the shear strength of this soil.
- Gravels are present beneath the surface adjacent to the bridge piers and were probably used as a construction back fill. The full extent of the gravel layers is not known.
- The ground water table beneath the bridge piers is significantly affected by the tide with the tidal river channel located close to the auger holes.
- Some test results were unreliable due to the presence of wood chips.

4.2 DETAILED SITE INVESTIGATION

The passive failure surface in the crustal cohesive soil was expected to be initiated at about the level of the pile cap base where it meets with the liquefiable sand beneath. A failure such as this would be three dimensional as shown schematically by Figure 4.4. Small scale in situ tests in wet sand were used to define the expected shape. A passive failure was formed by pushing a spade horizontally in the sand. The main failure plane was expected to be flat and perhaps have some curvature near the pile cap. The sides of the failure are expected to curve upward to the surface as shown.

To examine the expected failure mechanism and inspect the pile tops for damage, it was decided to excavate trenches along the centreline of the bridge deck. Piers C and E had the most prominent bulging behind them and they were selected as the best of the five riverbank piers to investigate. A two dimensional picture of the failure surface could be seen and this technique can also allow for relatively undisturbed sampling of the soil. The three dimensional aspects of the failure surface were not investigated in detail.

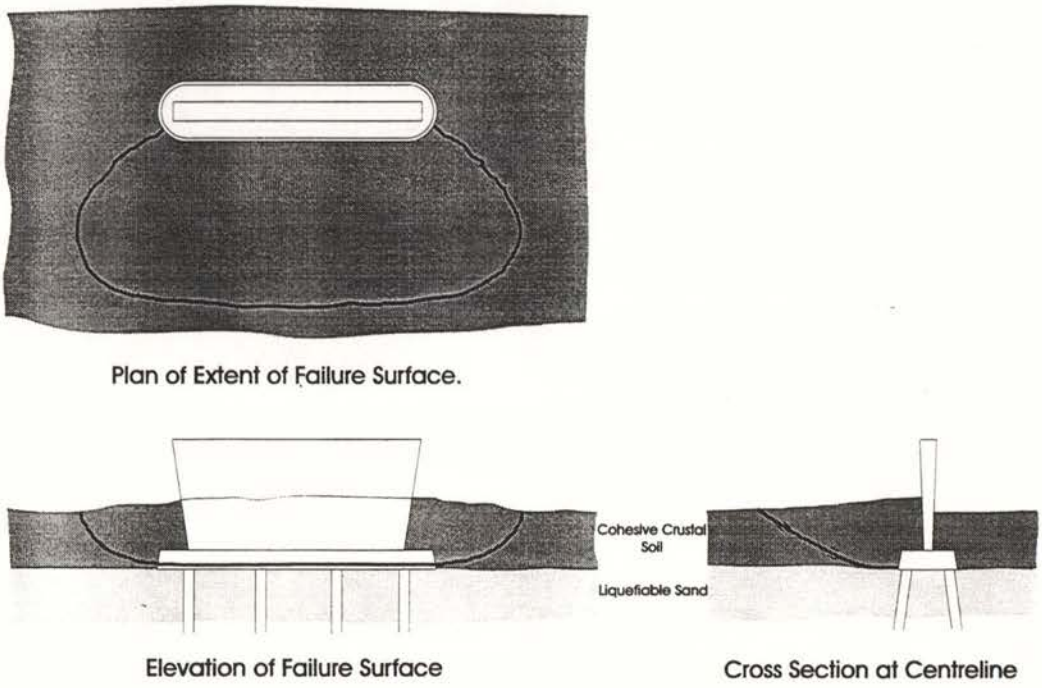

Figure 4.4 Expected passive failure surface geometry

4.2.1 Trenching

Headroom beneath the bridge was a very important consideration when choosing a hydraulic excavator to fit beneath the bridge superstructure and trench deep enough to examine the top of the piles. The minimum headroom available of 2.5 m occurred at pier C due to the bridge beams above. Approximately one metre extra working room was present in between the beams. Maximum excavation depths required were 2.5 to 3 m which is deep enough to inspect the top of the piles. Research of hydraulic excavators that could meet this criteria suggested that a 3 to 5 tonne machine would suffice. A Komatsu PC-45 hydraulic excavator owned by a local contractor in the Whakatane area was available and proved to be very versatile for this job. Figure 4.5 shows the start of excavation on the riverbank side of Pier C.

Figure 4.5 Start of excavation at Pier C

After excavation of a trench was complete, one side of the trench was cleaned up by scraping off the loose material and creating a clean, smooth surface. A 0.5 m square gid was created on the face using string lines, plumb bobs, a dumpy level and staff to within about 2-3 cm accuracy for logging the face. Permatrace film placed on a metric grid was used to draw the features of the trench face at a scale of 1:20. Working in pairs, a tape measure was used to accurately position certain important features such as shear surfaces and layer boundaries, while the other person recorded the information by following the grid and scale. Photographs of the trench face were also taken for the final reproduction and presentation of the trench logs.

A plan of the five trench locations with the logged face indicated is shown in Figure 4.6. The final trench logs are in Appendix C.

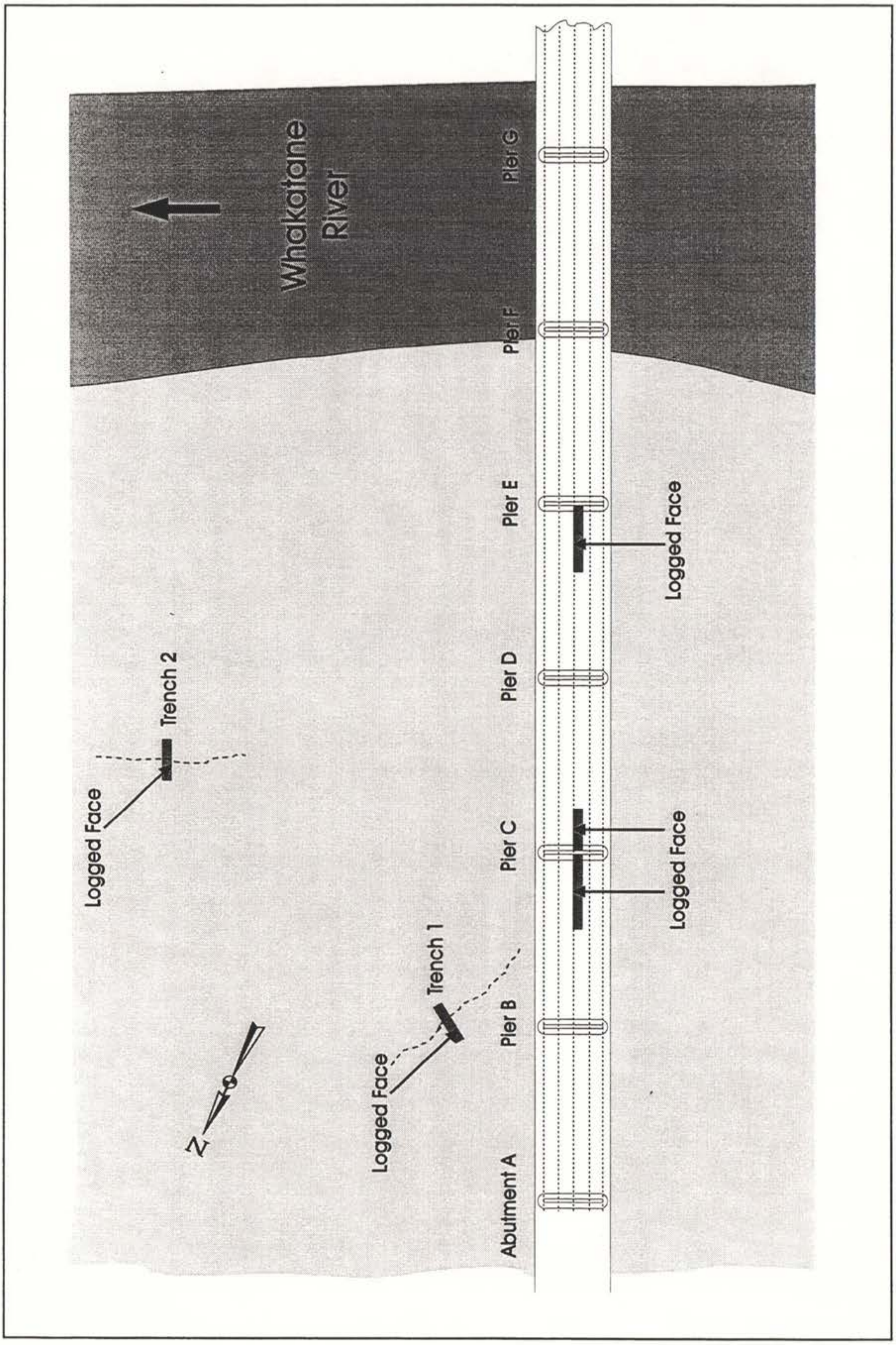

Figure 4.6 Plan of trench locations

4.2.1.1 Pier C

Trenching at Pier C revealed some interesting results which gave clues as to what occurred there during the lateral spreading movement. Two trenches, approximately 1.5 m wide were excavated on each side of the pier with the east face positioned along the centreline of the bridge deck above (see Figures 4.5 and 4.6). This enabled close examination of the passive failure surface on the north side of the pier and lateral spreading cracking in the soil on the south side. Face logs for these trenches are shown in Appendix C.

Soil mounding was clearly obvious from about 2.5 m north of the pier face. The elevation difference of the topsoil between the two sides of the pier was about 450 mm. Upper laminated silt horizons exhibiting curvature in the heaved soil zone show clearly that the crustal soil has been forced upward. A small shear in the sandy silt near the surface could be seen clearly. Angular gravels, which were probably used as backfill material, were found and this explains why some of the preliminary hand augering work could not penetrate past this depth.

The soil profile was quite disturbed and complex due to the methods used for the bridge foundation construction and subsequent back filling. The natural in situ material, which was not excavated during construction of the bridge, could easily be seen but some disturbance and warping of it was indicated by curving sand lenses at the north end of the trench. This could have been caused by lateral spreading stresses, settlements or perhaps heavy machinery loads imposed during the bridge construction. These buried sand lenses within the silty clay may also indicate previous episodes of liquefaction at the site.

Near the pile cap some rubbish material was found such as old wire, logs, sawn timber formwork and permanent shoring for the pile cap construction. Woodchips, bark, organic material and gravels were present in a disturbed state. Two large shear zones could be seen in this fill debris but termination of them could not be accurately found. It is possible that one originated at the base of the pile cap and the other where the pier meets the pile cap. These positions may have acted as stress concentrations and initiated the passive failure when lateral spreading occurred.

This excavation was deepened and widened in an effort to examine the river side of the two upstream piles (see Figure 4.7, No.'s 1 and 2) at their interface with the pile cap. This proved to be very difficult to achieve in the loose saturated sands since bark and woodchips continually clogged the pump filter, which was used to lower the water table, and stability was marginal. The top of piles 1 and 2 could just be seen and they appeared to be undamaged. No cracks could be felt along the north face of these piles, or on the east and west faces through about 50 percent of their width. The inner faces of these piles could not be reached for inspection. Thus it is certain that there was no concrete crushing on the north face; however nothing can be said about the inner face of these piles.

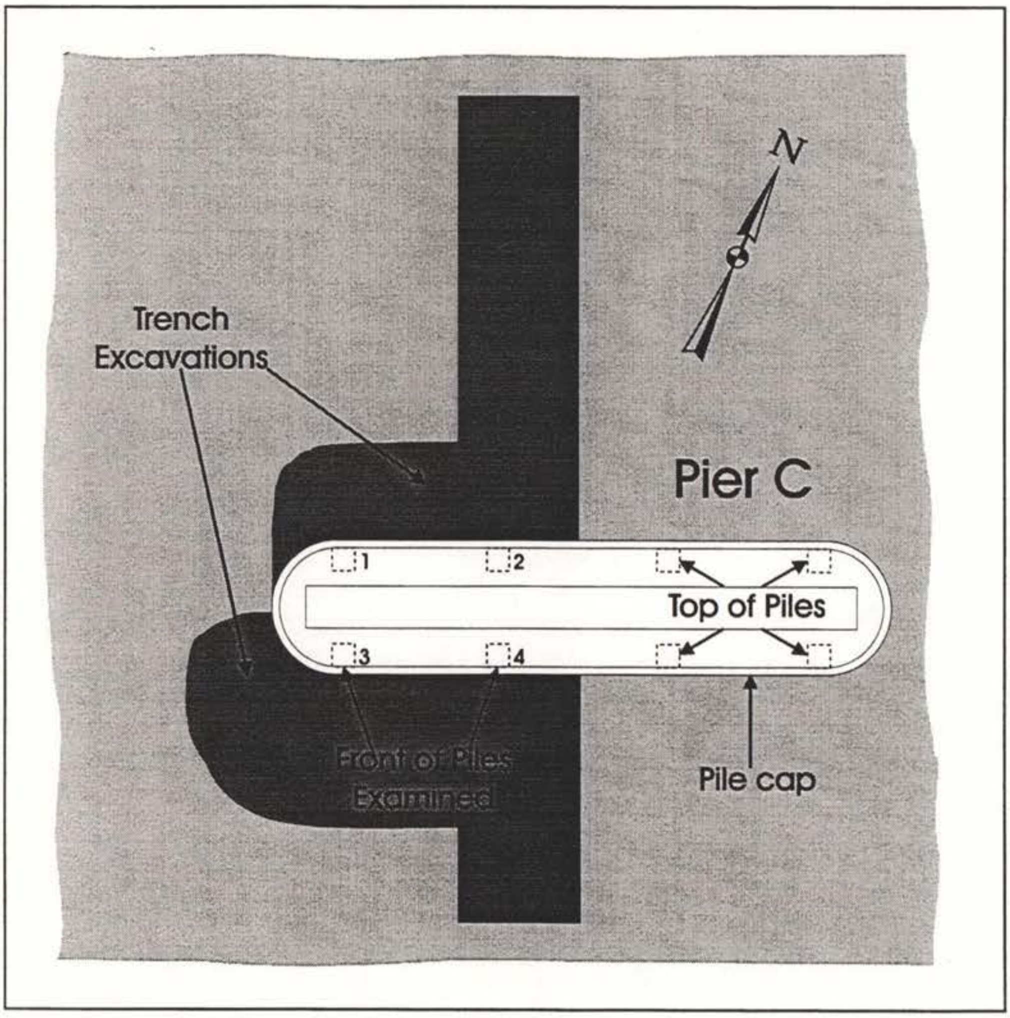

Figure 4.7 Excavation at Pier C

Trenching south of pier C revealed two lateral spreading cracks in the crustal soil (see Figures 4.8 and 4.9). The first crack began at the edge of the pile cap with an 80 mm average width. The second crack was much wider at approximately 140 mm and positioned about 2.5 m from the pier face. Sand had jetted up the fissures presumably during or after the 1987 earthquake and remained at a significant height. It is likely that the sand was forced to the surface but there was no evidence of past sand boils there. High water episodes during subsequent flooding may have eroded the sand away from the ground surface and filled the cracks with debris.

The 80 mm fissure beside the pile cap was investigated further by widening the trench in the upstream direction. It remained essentially vertical along the edge of the pile cap until the pile cap terminated where in cross section, the crack turned vertically away from the river channel at an angle of approximately 40° to the horizontal (see Figure 4.10). Further excavation showed that in plan view, it connected to one of the cracks at 45° to the bridge in the field upstream.

The two upstream piles (No.'s 3 and 4) on the river side were examined for possible cracking and distress by excavating further (see Figure 4.7). As on the other side of the pier, loose unstable saturated sands made it difficult to excavate very far. But here, it was possible to lower the water level sufficiently to see the upper 200 mm or so of the south face of the piles.

Figure 4.11 shows pile 3 which is 406 mm wide and a very small crack could be seen just beneath the interface over the width of the pile, but overall, the pile was very much intact at this location. This crack could have occurred during construction or perhaps by lateral spreading loads and we can not be certain what caused it to form. Figure 4.12 reveals that there are has no cracks in the upper 200 mm of pile 4. In both cases there did not appear to be any separation between the top of the pile and the bottom of the pile cap. Some formwork (100 by 50 mm cross section timber) and non structural concrete was found beneath the pile cap and could not be removed. This may have hidden some of the possible movement or cracks.

Figure 4.8 Lateral spread crack near the river side of Pier C

Figure 4.9 Lateral spread crack about 2.5 m from the river side of Pier C

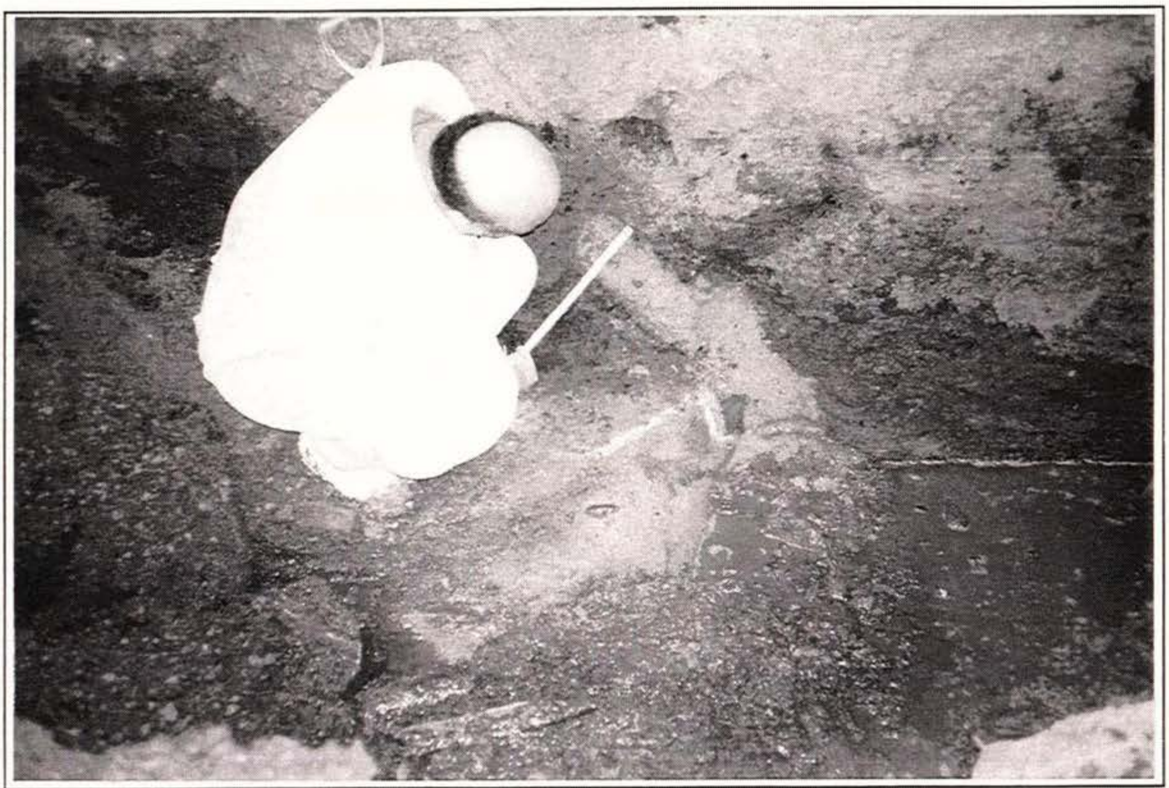

Figure 4.10 Lateral spread crack at the edge of the pile cap at Pier C

Figure 4.11 Riverside view of the top of pile 3

Figure 4.12 Riverside view of the top of pile 4

From the inspection of piles 3 and 4, overall the top of the south face of the piles showed no visible indication of structural damage and one would expect the other two on the south side of the pile cap to be the same. The collapse mechanism for the substructure indicates that the piles on the river side would undergo increased compression while the piles on the landward side would reduce in compressive load and perhaps go into tension. Concrete crushing would have been greater on the riverward piles and there was no evidence of this. Similarly, one would expect greater tensile stresses and thus a greater likelihood of cracking on the river side of piles 1 and 2 (the inland piles). At the time, it was decided that attempting to examine these piles was too difficult and dangerous with the resources available. Nevertheless, it was clear that plastic hinges had not formed in piles 3 and 4, and it appeared unlikely that they had done so in piles 1 and 2.

4.2.1.2 Pier E

One trench was excavated on the north side of Pier E (see Figure 4.6) with the eastern face along the centreline of the bridge. Appendix C shows the trench face log. Similar soil types to those at Pier C with a complex, disturbed fill were observed. Soil heaving near the pier face was not as pronounced but right at the pier face it appeared that nearly 0.5 m of mounding occurred, which is slightly greater than at Pier C.

A small shear in the topsoil and sandy silt was found at the pier face. Curvature of the upper silts could be seen clearly in the heaved soil because of the laminations present. Angular gravels deeper down matched those found at Pier C. More debris such as logs, wood, reinforcing steel and wire were found. Wood chips, bark and more organic material were also present in the fill.

One large passive shear, originating from the top edge of the pile cap, through the fill was observed but it was difficult to determine if it penetrated through to the ground surface. A disturbed bag sample of the material in the shear zone was taken for testing. Undisturbed block samples were difficult to remove because the fill was hard to cut through but when some progress was made it would fall away in a brittle manner. Sand lenses present in the in situ silty clay showed similar curvatures to those near pier C. Some large gravels were found further away from the pier wall. The tops of the piles were not inspected here.

4.2.1.3 Lateral Spreading Cracks Downstream of the Bridge

Two more trenches away from the bridge were excavated at right angles across old lateral spreading cracks. Trench 1 was located through one of the cracks at 45° to the bridge and trench 2 passed through a crack parallel to the river channel (see Figure 4.6).

Two clearly defined cracks filled with sand and a third that did not quite penetrate to the surface, were visible on the exposed face (see Figure 4.13). Sand boils from the 1987 earthquake above the two main fissures were slightly covered with topsoil. They show that as the sand was ejected from below it flowed down slope toward the river channel.

At least two previous episodes of liquefaction at this site, since the true left bank sediments were laid down, are indicated by two buried sand boils. An earthquake producing a Modified Mercalli intensity of at least MM 7 is needed to cause liquefaction. Using this basis and examining isoseismal maps (Downes 1995), the earthquakes which are most likely to have produced liquefaction at this site are the 1914, October 6, M_s 6.5 East Cape Earthquake and the 1977, May 31, M_L 5.4 Matata Earthquake.

The texture and fabric of the lateral sand deposits show how the sand had moved away from the fissures, not unlike lava from a volcano. Bag samples taken from both sand boils have D_{50}'s ranging between 0.2 and 0.5 mm. When plotted against Tsuchida's grading curves, the particle size distributions fit well within the range for liquefiable uniform sands.

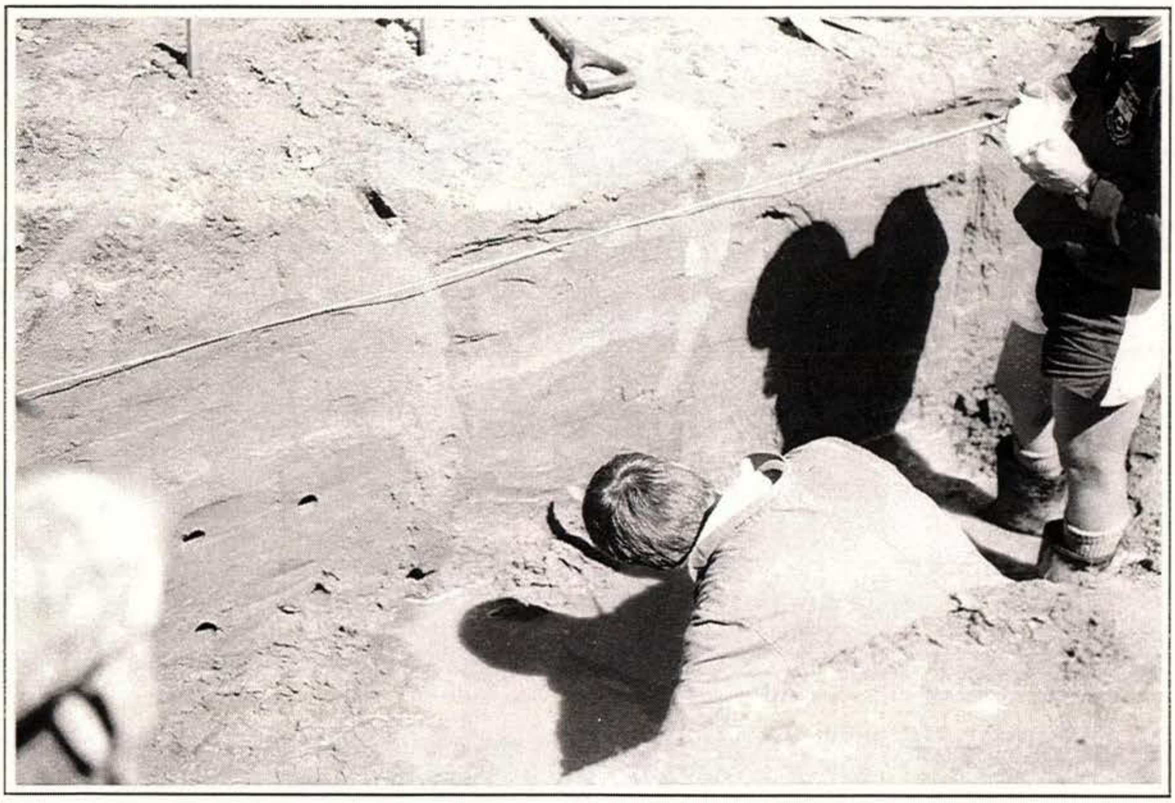

Figure 4.13 Exposed face of trench 1 (courtesy of S. Pasa)

A vertical offset of 50 - 60 mm was measured on the left hand side of the first fissure at two locations. This can be clearly seen in the trench logs where the two halves of each buried sand boil on either side of the fissure are offset.

The strike of the cracks in plan view was found to be about 205° and the average bearing movement vector at the base of the trench was 110°, which is nearly perpendicular to the crack strike.

Excavating deeper into the sand below the water table showed the source of the sand in the fissures. Particle size distributions for this sand had a D_{50} of 0.4 mm. Woodchips and bark were not found in the sides of this trench except for a few in the topsoil layer. This suggests that the woodchips were mixed with the backfill used around the piers at the time of the construction of the bridge.

Both of the sand filled fissures were traced back toward the bridge along the ground surface. Shallow excavation in the topsoil revealed other crack sequences in the crustal soil and other buried sand boils. Figure 4.14 shows some of the sand filled cracks just south of trench 1.

Figure 4.14 Sand Filled Lateral Spread Cracks South of Trench 1

Trench 2 located about 40 m downstream from the bridge revealed a single lateral spread crack of 80-90 mm in width. A similar soil profile to that of trench 1 was found but slightly more woodchips were found at this site. Some rounded gravels were also present at the base of the topsoil layer. Appendix C shows the trench log and Figure 4.15 shows the sand filled crack in the trench.

The top 0.5 m of the fissure was filled with organic material, debris, wood chips and gravels in a disturbed arrangement. This may have occurred due to the sand being removed during flood episodes and rubbish filling up the opening. No buried sand boils were found at this site.

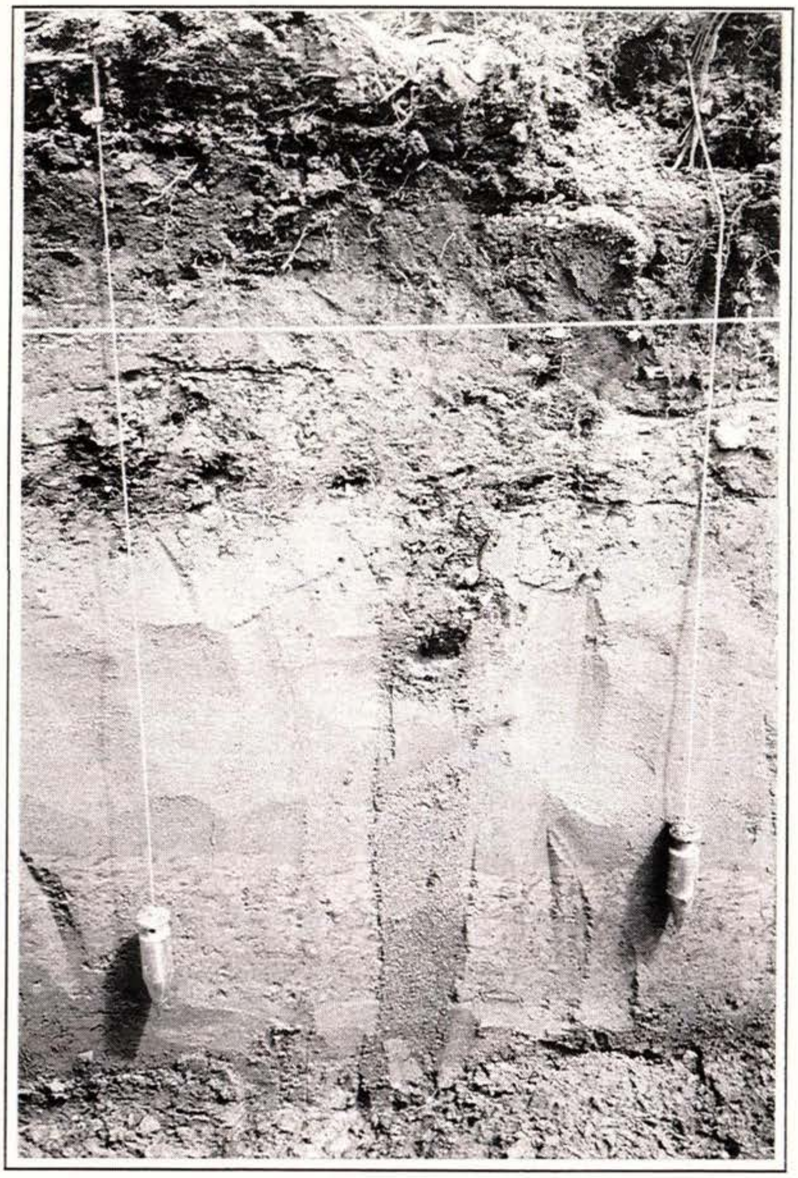

Figure 4.15 Lateral Spread Crack in Trench 2

Chapter 5

Laboratory Testing

Both block and bag samples were taken from the east face of the trenches at Piers C and E, in the vicinity of the passive failure surface. Triaxial and direct shear testing of these samples enabled shear strength parameters to be determined so that a more accurate estimate could be placed on the total passive load applied to the bridge substructure at each pier. The disturbed fill was the most dominant part of each failure and thus only the shear strength parameters for this soil were investigated. The extent of the shear failure plane at each pier was examined carefully and it was difficult to determine whether or not they penetrated into the sandy silts and gravels near the ground surface (see trench logs in Appendix C).

5.1 DIRECT SHEAR TESTS

An effort was made to take test specimens directly from a large block of soil with minimum disturbance, but this proved to be impossible because of large woodchips, some in excess of 80 mm long. Thus, reconstituted samples were created in a 60 mm square shear box with soil from block and bag samples. In the field, this soil was partially saturated or completely saturated at times since the ground water table moved with the tide. Each sample, from the complex disturbed fill material, was compacted in the shear box until water was forced to the surface. Thus it was essentially saturated and it was felt that this gave the best representation the in situ conditions in the fill beneath the bridge. Relatively high shearing rates of 0.60 mm/min were used in testing. Graphs of shear force versus lateral displacement at varying normal loads are shown in Appendix B.

Testing was undertaken in two parts:

- Firstly, samples of the backfill that included woodchips small enough to fit in the shearbox.
- Secondly, specimens using the soil only by removing the large woodchips. It is likely that some small wood particles were present in the second series of tests, but their influence on soil strength was thought to be very minimal.

5.1.1 Pier C

Block sample number 6, taken from the trench on the north side of Pier C (see Appendix C), proved to be very difficult to remove and keep intact. A block sample could not be taken directly from the passive failure region, because it was difficult to penetrate the trench wall with a spade and keep the soil mass intact. Woodchips in the soil were the main cause of this problem. Block 6, located near the failure surface, was examined carefully and appeared to be representative of the material in the failure area.

Test specimens created from the block sample had consistent densities, as shown in Table 5.1. The high water content and low bulk density values determined for the reconstituted specimens are most likely caused by the presence of wood chips, which are inherently less dense than the solid soil particles. The water content is defined as the ratio of the mass of water, (M_w), to the mass of the solid particles, (M_s), for a single specimen. The wood appeared to be saturated and thus would retain more water than the soil around it, which would tend to increase M_w, and when dried out, the wood is much less dense than the soil, thus giving a lower value for M_s.

BLOCK SAMPLE 6	*Water Content (w)*	*Bulk Density (ρ in t/m^3)*
Large Woodchips Included	0.8-1.0	1.2-1.3
Large Woodchips Removed	0.8-0.9	1.3-1.4

Table 5.1 Results from reconstituted specimens from Block 6, Pier C

The direct shear test results for Pier C are shown in Figure 5.1 with a best fit line drawn for each data set.

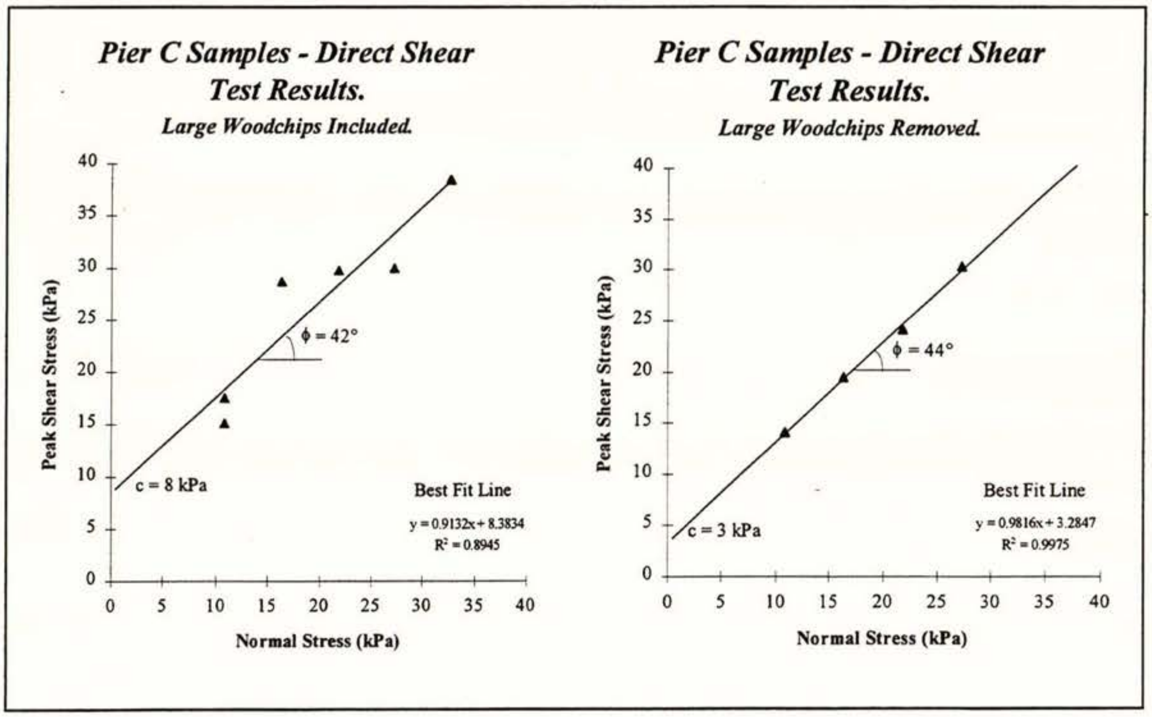

Figure 5.1 Direct shear test results for soil from Block 6, Pier C

5.1.2 Pier E

Reconstituted test specimens were created from bag sample No. 17 (see Appendix C), removed from the passive failure region, approximately 0.8 m below ground level, at Pier E. Bulk densities of the reconstituted specimens were in the same range as those tested for Pier C (which was expected as the fill material appeared to be the same at each pier), but water content determinations for the reconstituted specimens were found to be slightly higher (see Table 5.2). This may be explained by the fact that bag sample 17 was taken at a greater depth than block 6, and the ground surface is slightly lower than at Pier C. A small pond had formed on the surface beneath the bridge deck at Pier E, which in turn may have resulted in the higher water content of the fill material. Figure 5.2 shows the test results for Pier E, which are comparable to those in Figure 5.1 for Pier C.

BAG SAMPLE 17	*Water Content (w)*	*Bulk Density (ρ in t/m^3)*
Large Woodchips Included	1.0-1.1	1.2-1.3
Large Woodchips Removed	0.7-0.8	1.3-1.4

Table 5.2 Results from reconstituted specimens from Bag 17, Pier E

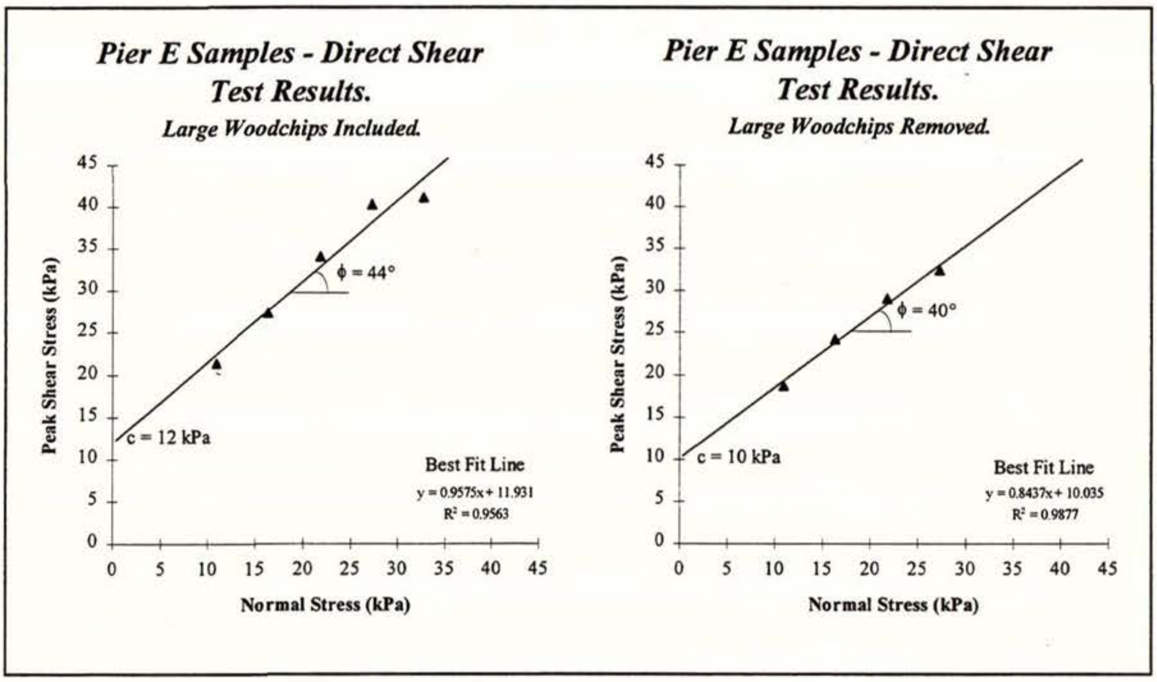

Figure 5.2 Direct shear test results for soil from Bag 17, Pier E

5.2 TRIAXIAL TESTS

One of the aims of this project was to estimate the shear strength of the soil on the failure surface so that a more accurate estimate could be put on the total passive load applied to Piers C and E. Since it proved impossible to remove blocks of soil from the region of the failure surface in both trenches, soil adjacent to this, which remained intact, was used. 38 mm diameter specimens from Block 6 were intended to be formed by pushing a sampling tube through the block. The orientation of the failure planes expected in these samples would be close to that seen in the field.

Soon after pushing the drive tube into the block, large resistance was encountered which prevented retrieving a specimen long enough to test. When more force was applied to the drive tube, the block simply crumbed and broke up around it because woodchips hindered the penetration of the drive tube.

Another attempt at creating relatively undisturbed samples was to simply cut them out of the block and form cylindrical samples with a sharp blade. But as before, woodchips, glass and other rubbish in the block interfered with this. The last option available was to create reconstituted specimens, similar to the method employed in direct shear testing, which meant that the shear failure of the block in the preferred orientation could not be established.

One way to possibly achieve this would be to remove a very large block, say 0.1-0.2 m^3, and test large samples from the block. Direct shear tests could be undertaken with the direction of lateral shearing corresponding to the failure surface seen in the field, or triaxial testing of large diameter samples from the block which include the large woodchips. The resources available at the time and increased cost meant that this option was not viable.

Testing of reconstituted 76 mm long, 38 mm diameter specimens formed in a split mould was employed for the fill taken from Pier C. Insufficient material remained from Pier E to test; but one would expect very similar results, as seen in the direct shear tests, since they appear to be the same material. Specimens from Block 6 were created for two different test series as before; firstly, samples with some woodchips present and secondly, samples that avoided the woodchips as much as possible.

Undrained tests were used since in the field, the soil undergoes rapid loading during an earthquake, and there is little time for pore water pressures to dissipate. Samples were not saturated so pore pressure time histories could not be determined in each test. Any excess air would compress and dissolve into the de-aired pore water. Loading rates of about 1.10 mm/min were used (or about 1.5% axial strain per minute). Load versus displacement plots at different cell pressures can be seen in Appendix B.

Since Block 6 was under low confining stresses in the ground, testing began with similar cell pressures and increased up to 100 kPa (over five times the in situ confining stress). This low maximum confining pressure causes problems because the lack of confinement prevented the specimens forming the desired shear failure and in each test, the soil failed by bulging laterally.

The value of cohesion determined for these tests was comparable with the direct shear test results, but the angle of internal friction was much less. This could be explained by the nature of each test method. In direct shear testing, the constraints of the shearbox force a shear failure surface to occur, which in this case is likely to be quite irregular because of the large particle sizes. A high angle of internal friction occurs because the irregularity of the failure surface is great compared with that of a fine grained soil. During triaxial testing, samples have little constraint and the failure is progressive. The larger particles in the sample have less influence on the progressive failure, because the deformation is not necessarily concentrated on a prescribed plane as in direct shear tests. Figures 5.3 and 5.4 show the Mohr diagram for each test series.

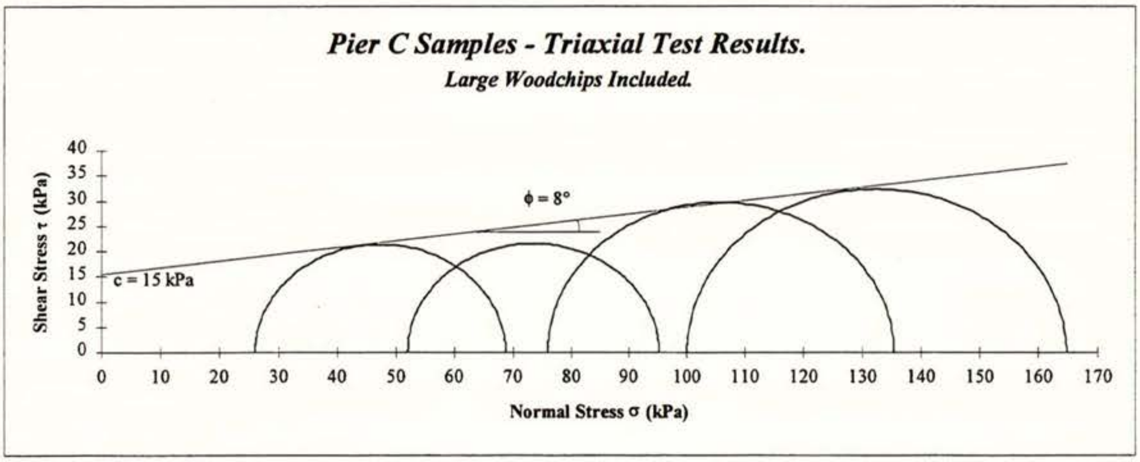

Figure 5.3 Triaxial test results for samples from Block 6, Pier C that included woodchips

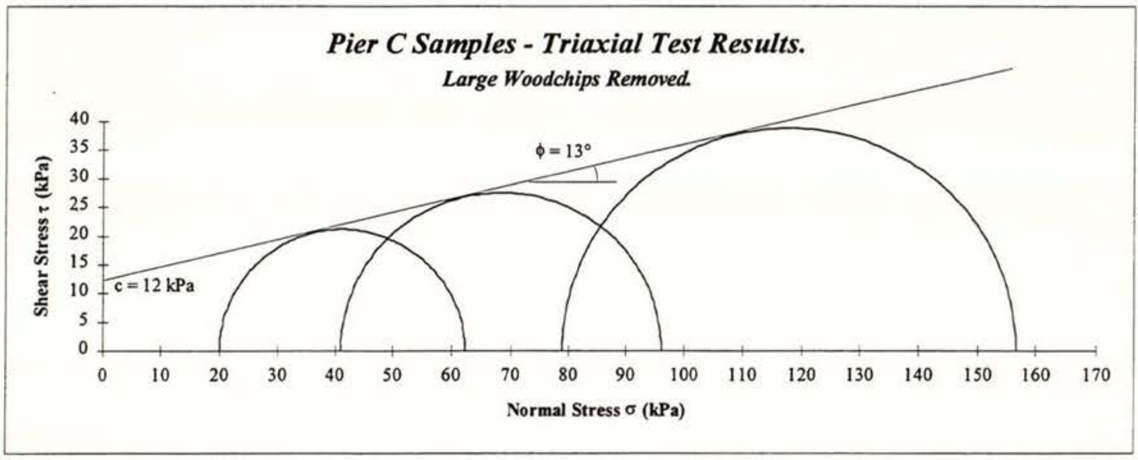

Figure 5.4 Triaxial test results for samples from Block 6, Pier C without woodchips

5.3 WOODCHIPS AND THE FILL MATERIAL

In the soil, the large woodchip particles create an interesting problem when considering the shear strength of the soil mass. In both direct shear tests and triaxial tests, they are likely to have a significant influence on the experimental values of c and ϕ.

In direct shear tests at low confining pressures, one would expect shear failures in the soil to move around the woodchips, creating an irregular failure surface. This was seen clearly in the results and somewhat in the field. They will act to strengthen the failure surface, giving the soil an apparent strength increase. This is reflected in the high angle of internal friction of 40 - 45° determined from direct shear testing. For triaxial testing, the low confining pressures allow the sample to fail by bulging radially in a progressive nature. Failure was defined for a fixed strain of 20 percent because there was often no definitive peak deviator stress in the results (see Appendix B). Samples will continue to take added loads until very high strains are reached, by which stage, results have little meaning. Low angles of internal friction occur since a small increase in confining pressure gives little increase to the deviator stress.

At moderate confining pressures in direct shear tests, the woodchips would still cause an irregular failure surface. They may also undergo some rotation and warping as the sample is sheared. Some chips may split if the orientation of the grain is close to that of the failure surface but otherwise they should remain intact. The friction angle is expected to be somewhat smaller, since the influence of the woodchips on the shear strength is not as great. Failure surfaces may be less irregular, with the wood chips causing a reduction in strength. In triaxial tests, both bulging and shear plane type failures could be expected, with the angle of internal friction being greater than at low confining pressures. The increase in confinement means that the progressive type failure will be limited.

Direct shear testing at high normal loads (hence high confining pressures) is expected to reduce the influence of the woodchips as they may be sheared completely through and the failure surface would be much more uniform and flat. Some particle degradation could be expected as the shearing motion grinds particles into smaller fractions. Triaxial testing of this type of soil at high confining pressures is most likely to give shear plane failures because the added confinement constraints will prevent bulging type failures. In both types of test, the angle of internal friction would be at its lowest value since the specimens do not get a great strength increase for an increase in confining pressure and thus the failure envelope will have a very mild slope.

The woodchips have an important influence on other soil properties. If there is a significant proportion present in a soil mass, then the bulk density of the soil will be lower and water content is likely to be higher than for the parent material.

5.4 SHEAR STRENGTH PARAMETER SUMMARY

For the passive wedge failure analysis to calculate the lateral loads exerted on the pier wall, the following range of parameters, (shown in table 5.3) based on the test results, are used.

RESULTS	*Direct Shear Tests*	*Triaxial Tests*
Parameter	*Range*	*Range*
Unit Weight, γ (kN/m^3)	12 - 14	12 - 14
Cohesion, c (kPa)	8 - 12	12 - 15
Angle of Internal Friction, ϕ (°)	40 - 45	8 - 13

Table 5.3 Laboratory test results summary

Chapter 6

Lateral Load Analysis

At the Landing Road Bridge site, liquefaction-induced lateral spreading has subjected the bridge foundations to horizontal loading from two sources. Firstly, drag forces from the moving liquefied sand are likely to have been induced on the piles during the period of shaking, as the sand moves horizontally in a cyclic manner toward the river channel. Once shaking ceases, the drag forces no longer exist since the liquefied sand gradually regains strength and its lateral motion stops. The second, and most dominant source of lateral loading in this case, is passive soil pressures in the cohesive silty crust. They are a result of laterally spreading soil being restrained from movement by the bridge piers on the northern bank. Trenching at Piers C and E indicates the extent of these failures.

6.1 DRAG FORCE ON THE PILES

A fluid mechanics approach to calculating the magnitude of the total drag force exerted on the piles in the horizontal direction may be used. With estimates of the viscosity of the liquefied sand, the velocity of movement and knowing the geometry of the piles and thickness of the liquefied layer, a rough estimate of the total drag can be determined.

The total drag force F_D on an infinitely long cylinder (two dimensional) in a moving fluid is given by Newtons quadratic resistance law (Vargas and Towhata 1995):

$$\begin{aligned} F_D &= \tfrac{1}{2} C_D A \rho V^2 \\ &= \tfrac{1}{2} f(Re) A \rho V^2 \end{aligned}$$

where C_D = drag coefficient

A = projected area of the cylinder on a plane perpendicular to the flow

ρ = mass density of the fluid

V = flow velocity of the fluid

$Re = \dfrac{\rho VD}{\eta}$ = Reynolds number of the flow

D = diameter of the cylinder

η = viscosity of the fluid

The drag coefficient C_D is dependent on the Reynolds number (Re) of the viscous flow and the geometry of the cylinder. Often charts of C_D versus Re are plotted for different shapes because the relationship between them is complex. Rouse (1938) noted that for the case of an infinite cylinder in a moving fluid at low Reynolds numbers (less than 1), the curve for is asymptotic to a straight line with a slope of -0.75 (see Figure 6.1). The approximate equation of this line is:

$$\log_{10}C_D = -0.75\log_{10}Re + 2.05 \quad (6.1)$$

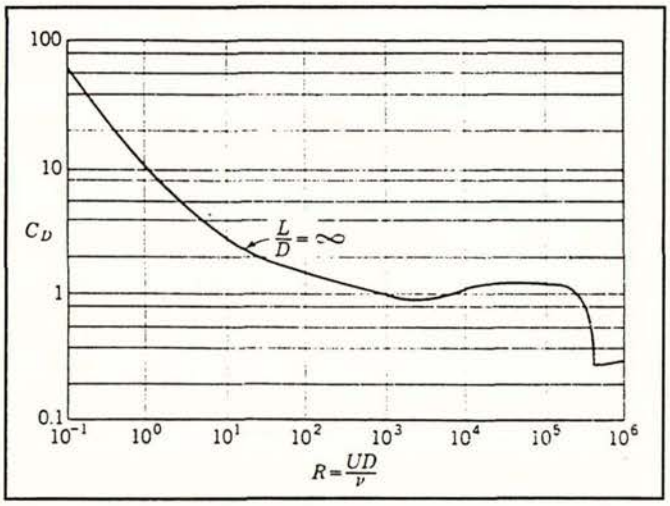

Figure 6.1 Drag coefficients for circular cylinders (from Streeter and Wylie 1985)

Reynolds numbers of the order of 10^{-2} were calculated for the piles at Landing Road Bridge and at low values of Re, a cylindrical approximation of the square piles is valid since the drag coefficients for the two shapes are virtually the same (pers. comm. B. Hunt).

The calculation of the total drag force for a uniform velocity distribution is simple, but for more complex distributions, numerical integration must be used. The velocity and displacement distributions of the liquefied sand over the depth of the layer were assumed to be triangular for these calculations, as shown in Figure 6.2. Given that the displacements can vary in a curved nature with zero lateral displacement at the bottom of the layer to maximum displacement at the top, it is felt that this approximation is close enough considering the accuracy of the other parameters used in the drag computation.

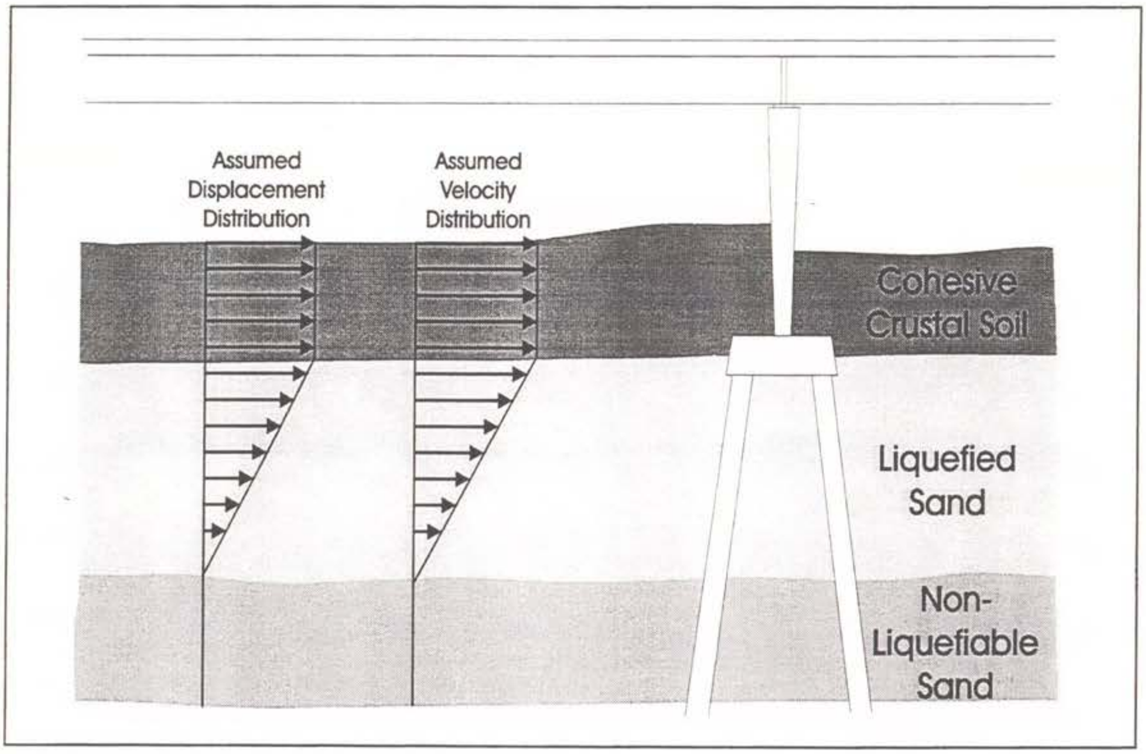

Figure 6.2 Assumed displacement and velocity distributions

The density of the liquefied sand was estimated to be between 1.8 and 2 t/m^3. Estimates of the viscosity of the liquefied sand are based on Vargas and Towhata's research, and the range of 0.5 to 1.5 kPa.sec was used in calculations. During the earthquake shaking, lateral spreading of the liquefied sand will occur in steps as the ground moves cyclically in a horizontal plane. With each cycle, the displacement towards the river channel is greater than away from it, giving a net movement of about 1.5 m at the ground surface in this case. Given that about twenty to thirty cycles of movement may have occurred, the average displacement of the top of the liquefied layer per cycle is 50 - 75 mm. If each cycle of motion takes up to one second, peak velocities of the order of 100 mm/sec would have occurred.

Calculations were done for one pile by integrating over the height of the liquefied layer and multiplied by eight piles. The maximum total horizontal drag force on the piles during the strong ground motions for one pier is estimated to be about 50 kN. Clearly, this is low in comparison to the loads imposed by the cohesive crust, which are perhaps more than ten times greater.

6.2 PASSIVE WEDGE FAILURE ANALYSIS

Rankine and Coulomb passive earth pressure theory was used to analyse the failures observed in the crustal soil in trenches at Piers C and E. Parameters determined from the direct shear and triaxial tests were used in conjunction with trench logs in Appendix C.

These methods use a two dimensional approach which gives a lower bound to the three dimensional passive failure. The total passive load was determined for a two dimensional wedge and applied over the width of the base of the piers. Each pier is over eight metres wide with the greatest bulging of soil at the centreline of the bridge. Towards the sides of the pier, this bulging is less and it is felt that the horizontal passive pressures will be slightly lower, which means the two dimensional approximation might give a reasonable estimation of the total passive load, albeit a lower bound.

6.2.1 Rankine Analysis

Rankine's analysis assumes an initially horizontal or sloped backfill behind a wall and does not allow for unusual wedge shapes. Friction between the soil and the supporting wall is usually neglected. In this analysis the ground surface was assumed to be horizontal and the pier wall vertical (it is about 2.5° from vertical in reality) for simplicity. The depth to the water table was assumed to be level with the top of the pile cap.

A range of values were used in the calculations for cohesion, angle of internal friction and density of the soil. Results were sensitive to the first two parameters with the third having less significant influence. Tables 6.1 and 6.2 summarise the results of the total passive load calculations using Rankine's theory of earth pressure.

TOTAL PASSIVE FORCE (kN)	*Direct Shear Tests*	
Direct Shear Test Parameters	*Pier C*	*Pier E*
Maximum P_p $c = 12$ kPa, $\phi = 45°$, $\gamma = 14$ kN/m^3	1030	910
Minimum P_p $c = 8$ kPa, $\phi = 40°$, $\gamma = 12$ kN/m^3	650	580
Best Estimate P_p $c = 10$ kPa, $\phi = 42°$, $\gamma = 12$ kN/m^3	790	700

Table 6.1 Rankine results using direct shear test parameters

TOTAL PASSIVE FORCE (kN)	*Direct Shear Tests*	
Triaxial Test Parameters	*Pier C*	*Pier E*
Maximum P_p $c = 15$ kPa, $\phi = 13°$, $\gamma = 14$ kN/m^3	490	440
Minimum P_p $c = 12$ kPa, $\phi = 8°$, $\gamma = 12$ kN/m^3	360	320
Best Estimate P_p $c = 13$ kPa, $\phi = 11°$, $\gamma = 12$ kN/m^3	410	370

Table 6.2 Rankine results using triaxial test parameters

The best estimates of the total passive pressure shown in each table are based on average values of c and ϕ, determined from testing reconstituted samples of the fill from near piers C and E. The in situ density of the fill was estimated by using a large intact part of Block 6. The volume of the specimen was determined using water displacement; its mass using electronic scales, giving a density of 1.2 t/m^3. The in situ water content of Block 6 was estimated to be 1.0, but the reliability of this is questionable due to significant humidity changes and disturbance from strength testing.

The triaxial test results gave the best representation of the field conditions and loading using undrained, high strain rate tests. The direct shear tests were essentially drained, high strain rate tests and the calculations show much greater passive loads, which obviously did not occur because significant structural damage would have been evident at Pier C where the top of the piles were examined. Using this basis, then the total passive loads seem likely to have been about 400 kN.

6.1.2 Coulomb Analysis

Any wedge shape can be accommodated in Coulomb's method and wall friction can be taken into account. Graphical methods are used to solve the force vectors for passive pressure. Trench logs defined the wedge geometry and shear strength parameters gained from laboratory test results were used.

At pier C, two possible shear planes were identified; one originating at the top of the pile cap where the pier meets it and a second one at the bottom edge of the pile cap. The first shear failure is at an angle of θ = 25 - 30° with respect to the horizontal and consistent with a passive failure in the soil. This indicates an angle of internal friction for the material of ϕ = 30 - 40°. The second failure is at about θ = 50 - 55° to the horizontal which is perhaps a secondary shear and is not representative of a passive failure, where failure angle is normally less than 45°. At pier E, one shear failure surface was evident and it appeared to start at the level of the top of the pile cap, with an angle to the horizontal of about θ = 30 - 35°, which indicates an angle of internal friction of ϕ = 20 - 30°.

Tables 6.3 and 6.4 summarise the results of the total passive load calculations using Coulomb's theory of earth pressure.

TOTAL PASSIVE FORCE (kN)	*Pier C*		*Pier E*	
Direct Shear Parameters	$\theta = 25°$	$\theta = 30°$	$\theta = 30°$	$\theta = 35°$
$\gamma = 12\ kN/m^3$, $c = 8\ kPa$, $\phi = 40°$, $\delta = 0°$	770	980	790	1090

Table 6.3 Coulomb results using direct shear test parameters

TOTAL PASSIVE FORCE (kN)	***Pier C***		***Pier E***	
Triaxial Test Parameters	$\theta = 25°$	$\theta = 30°$	$\theta = 30°$	$\theta = 35°$
$\gamma = 12\ kN/m^3,\ c = 12\ kPa,\ \phi = 11°,\ \delta = 0°$	490	530	480	530
$\gamma = 12\ kN/m^3,\ c = 12\ kPa,\ \phi = 11°,\ \delta = 10°$	580	650	580	660
$\gamma = 12\ kN/m^3,\ c = 15\ kPa,\ \phi = 11°,\ \delta = 0°$	570	630	560	620
$\gamma = 12\ kN/m^3,\ c = 15\ kPa,\ \phi = 11°,\ \delta = 10°$	680	760	680	780

Table 6.4 Coulomb results using triaxial test parameters

The results from these analyses are quite different from those shown in Tables 6.1 and 6.2, due to the allowance for the angle of the failure surface, θ, and wall friction, δ. In the calculations using the direct shear parameters with wall friction $\delta = 0.66\phi$ ($\delta = 27°$), the total passive load was well in excess of that required to cause collapse of the foundations. Even when $\delta = 0$, the calculated passive loads are high, and they could not have occurred because severe structural damage would have resulted. Calculations using the triaxial test parameters show slightly higher loads than those in Table 6.2.

The best estimate of the total passive load from the Coulomb analyses is made by averaging the total passive load values at each pier over the range of parameters considered. This gives a value of $P_p = 610$ kN for both piers.

This magnitude of load is likely to cause tensile cracking of all eight pile tops and noticeable deformation. This was not observed at pier C, and thus this analysis has probably overestimated the total passive force.

6.3 STRUCTURAL ANALYSIS

An elastic structural analysis was used to place a limit on the total passive force on the substructure by considering the observations made in the trenches at Pier C. Properties of the structural members used in the analysis were derived from the bridge construction plans. An iterative approach to determine the stresses in the raked piles was required, since the lateral deformation induced axial loads govern the moment required for first cracking and yielding. Two models of the foundations were used in the analysis; Model

1 allowed the pile cap to translate, but not to rotate, and Model 2 allowed both translation and rotation to occur (see Appendix B). The important results from these analyses are shown in Table 6.5.

<table>
<tr><th colspan="3"><i>MODEL 1</i></th></tr>
<tr><th><i>Position</i></th><th><i>P_p (kN)</i></th><th><i>M_{crack} (kNm)</i></th></tr>
<tr><td><i>Landward Pile Top</i></td><td>260</td><td>14</td></tr>
<tr><td><i>Bottom of Pier</i></td><td>405</td><td>140</td></tr>
<tr><td><i>Top of Pier</i></td><td>410</td><td>215</td></tr>
<tr><td><i>Bottom of Pier</i></td><td>870</td><td>yielding</td></tr>
<tr><td><i>Riverward Pile top</i></td><td>>870</td><td>>50</td></tr>
<tr><th colspan="3"><i>MODEL 2</i></th></tr>
<tr><th><i>Position</i></th><th><i>P_p (kN)</i></th><th><i>M_{crack} (kNm)</i></th></tr>
<tr><td><i>Landward Pile Top</i></td><td>155</td><td>19</td></tr>
<tr><td><i>Riverward Pile Top</i></td><td>220</td><td>27</td></tr>
<tr><td><i>Top of Pier</i></td><td>330</td><td>215</td></tr>
<tr><td><i>Landward Pile Top</i></td><td>770</td><td>yielding</td></tr>
<tr><td><i>Top of Pier</i></td><td>>770</td><td>yielding</td></tr>
</table>

Table 6.5 Iterative elastic analysis results for models of the bridge foundations

Each model showed the formation of cracks and hinges to occur in a different order. In both models, first cracking at top of the landward piles would occur at a low lateral loads but the range of loads to crack the top of the riverward piles, which were inspected, is large. Model 2 cracking moments for the top of the piles were much lower because the pile cap rotation was not constrained, thus the distribution of structural actions is different.

The reality of the situation at Landing Road Bridge is expected to be somewhere in between these two models. The examination of the pile tops, described in Chapter 4, showed that there was no evidence of concrete crushing in the northern piles. One possible tensile crack in pile 3 on the southern side was observed, which may have been caused by lateral spreading, but it is also possible that this crack occurred during the construction of the bridge foundations. The condition of the inner faces of these piles could not be determined since the inspection did not go far enough to either confirm or eliminate the presence of cracks in the northern piles. Nothing can be stated about the condition of the piles at the bottom of the liquefiable layer and the bottom of the pier was not inspected for cracks at the time. However, because of the form of the raked piles and the certain loss of prestress at the top of the piles, the pile-pile cap interface is the most vulnerable location. The moment required for first cracking of the top of the landward piles is very small at less than 20 kNm per pile (see Table 6.5) because the interface with the pile cap is a construction joint, and the concrete is assumed to be unable to sustain any tensile stresses.

Considering the estimated lateral loads from the passive wedge analysis, this analysis suggests that cracking of the top of the piles, as a result of lateral spreading, is likely to have occurred. With large differences in the loads to cause the riverward piles to crack, it is not possible to place an accurate upper limit to the horizontal passive load on the substructure at Pier C. Had cracking occurred there after cracking of the landward piles, the maximum passive load is likely to be between 200 and 900 kN, which is encompasses part the range of values determined in the passive wedge analysis. Observations of the upper 200 mm of the riverward piles showed that there did not appear to be any flexural cracks present, thus 200 to 900 kN range places an upper limit on the lateral spreading loads.

It can only be concluded that in this case for the elastic analysis, there appears to be too many variables and influences to make a clear judgement on the behaviour of the substructure.

Chapter 7

Design for Lateral Spreading

The lateral loading of piles and walls due to static and dynamic horizontal soil movement is a difficult design issue for engineers. The interaction of soil and the structure influences the behaviour of the system as a whole, with the main influences being geometry, structural strength and stiffness, and soil strength and stiffness. Various methods have been used to analyse the behaviour of laterally loaded piles and walls which include analytical and numerical techniques. In the case of piles, static loading from above the ground can be estimated by using relatively simple formulae, as shown in Poulos and Davis (1980) and Elson (1984). Pender (1993) summarised methods for predicting the stiffness and capacity of pile foundations subjected to seismic loading, considering both axial and lateral loads.

Lateral spreading loads exerted on walls, pipes and piles are more difficult to predict and currently there are not any simple methods to estimate them. Based on the theory outlined by previous researchers and using a common sense approach, a simple method for estimating this type of loading is proposed.

7.1 LATERAL SPREADING LOADS

Liquefaction-induced lateral spreading loads will only be imposed on buried structural elements if some form of restraint against movement is present. This restraint may be above ground, around the structure or below it. Without any restraint present, it is likely that the structure will simply move with the lateral spread and be subjected to small differential loads. But since most engineering structures are designed to remain in-place, some form of restraint will always be present. Walls, lifelines and bridges constructed on piles usually all have restraint against horizontal movement and lateral spreading will inherently impose passive loads on these. Considering the case of Landing Road Bridge, longitudinal movement restraints were provided by the stiff superstructure, piers that were not subjected to lateral spreading loads and the piles embedded in to the dense sands, which did not liquefy, on the true left bank of the Whakatane River.

Two sources of liquefaction induced lateral spreading horizontal loads are likely to occur during an earthquake (as outlined for Landing Road Bridge in Chapter 3):

- Firstly, the cohesive or cohesionless material above the water table, which can form passive failures against buried structures as they resist lateral movement.
- Secondly, drag forces from the motion of liquefied soil are imposed on buried structures.

At Landing Road Bridge, the first source of loading is most significant (estimated at over ten times the drag forces) but in other situations, the second loading source could dominate.

It should also be noted that vertical deformations associated with liquefaction and lateral spreading can cause very significant structural damage, such as negative skin friction on piles, but this deformation mechanism is not considered here.

7.2 ANALYSIS FOR LATERAL SPREADING LOADS

A simple procedure for analysis of the lateral spreading load mechanism is presented, giving some guidelines for approaching this problem. Firstly, the liquefaction potential of the site of interest must be established, followed by estimates of the likelihood and magnitude of lateral spreading. The geometry of the structure and soil must be defined, considering restraints against lateral movement and collapse mechanisms. Soil parameters for the analysis need to be established and finally calculations of lateral loads can be undertaken. Design for these lateral loads to be sustained by the structure can be achieved by providing adequate strength in the structure.

7.2.1 Evaluation of Liquefaction Potential

The susceptibility of a particular site to liquefaction should be established first. Some in situ testing such as bore holes, CPT and SPT tests would be required for the prediction models. Some of the well known models that have been published include those by Zhou (1980), Davis and Berrill (1982), Taiping et al (1984), Robertson and Campanella

(1985), Shibata et al (1988) and Law et al (1990). As a general rule of thumb, if a site has a layer with young, loose, fine grained saturated deposits, then liquefaction is likely to occur in strong ground motions.

7.2.2 Lateral Spreading

The possibility of lateral spreading as a result of liquefaction should be investigated. The important aspects to consider were given by O'Rourke and Hamada (1992) involving seismic, geological, topographic, and soil factors (see Chapter 2). Empirical techniques for the prediction of lateral displacement (as shown in Chapter 2) could be used to estimate the likely magnitude of movements based on assumptions of different parameters.

7.2.3 Soil/Structure Configuration

Given that the site of interest has a high potential for liquefaction and lateral spreading to occur in an earthquake, the geometry of the structure and soil needs to be defined. This will include the thickness of non-liquefiable layers above the water table, thickness of liquefiable layers, depth of foundations, pile penetration and sources of restraint against lateral movement. The position of the buried structural elements with respect to the soil layers is important since this will influence what type of horizontal loading they might be subjected to during lateral soil movement. In the case of bridge and building foundations, it may be important to identify potential collapse mechanisms for this type of loading. Areas where failure may occur need to be identified so that measures can be taken to allow for or avoid this.

7.2.4 Soil Parameters

Without any soil sampling, educated estimates of the soil properties may be used for establishing parameters to be used in calculations. However, to make the best guess of the potential horizontal loads, soil samples should be taken for testing in the laboratory. Direct shear and undrained triaxial tests with high strain rates should be undertaken. Partially saturated soils may cause problems with testing because their true undrained strength can not be determined without saturating the samples first, which can take considerable time for low permeability soils. In situ bulk densities of the soil need to be determined for calculations.

7.2.5 Horizontal Load Calculations

The horizontal passive loads can be estimated for each part of the structure using all of the information about the soil and structure compiled so far. Methods for the calculation of lateral load are defined for slender structural elements (such as piles) and large elements with high cross section aspect ratios (such as piers and walls).

7.2.5.1 Non-Liquefiable Soil Above the Water Table.

Firstly, cohesive and cohesionless soils will be considered with different geometries of the soil and large elements. Secondly, small elements will be considered.

(a) The bottom of the non-liquefiable layers is lower than the bottom edge of a large structural element (see Figure 7.1).

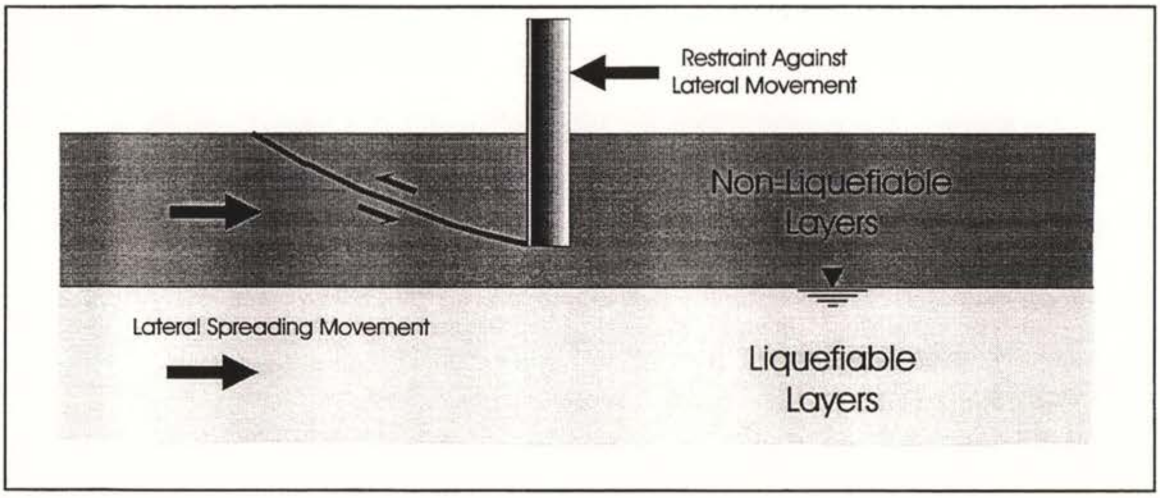

Figure 7.1 Large element over partial depth of non-liquefiable soils

Assume a passive failure originates at the bottom edge of the large element and penetrates to the surface. A two dimensional approach is suggested for calculation of the total passive load per unit length, then multiply this result by the width of the structural element. For a uniform soil, the simplest estimate of the passive failure surface will be a straight line at an angle of $\theta = 45 - \phi/2°$. More complex surfaces, such as logarithmic spirals, parabolas and circles can also be assumed but generally, they make computations more difficult. Friction between the structural element and the soil can be taken into account which will increase the passive load on the element. A Rankine or Coulomb passive earth pressure analysis can be used with undrained shear strength parameters for calculations. It is important to remember that cohesive soils have an added component of load because of their cohesion and in the case of passive failure, this can be quite significant. Multi-layered soil can be taken account of in the analysis by summing the components of each layer.

The total passive pressure, when multiplied by the element width, gives a lower bound to the loads imposed on the structural element by the true three dimensional passive failure.

(b) The bottom of the non-liquefiable layers is above the bottom edge of a large structural element (see Figure 7.2).

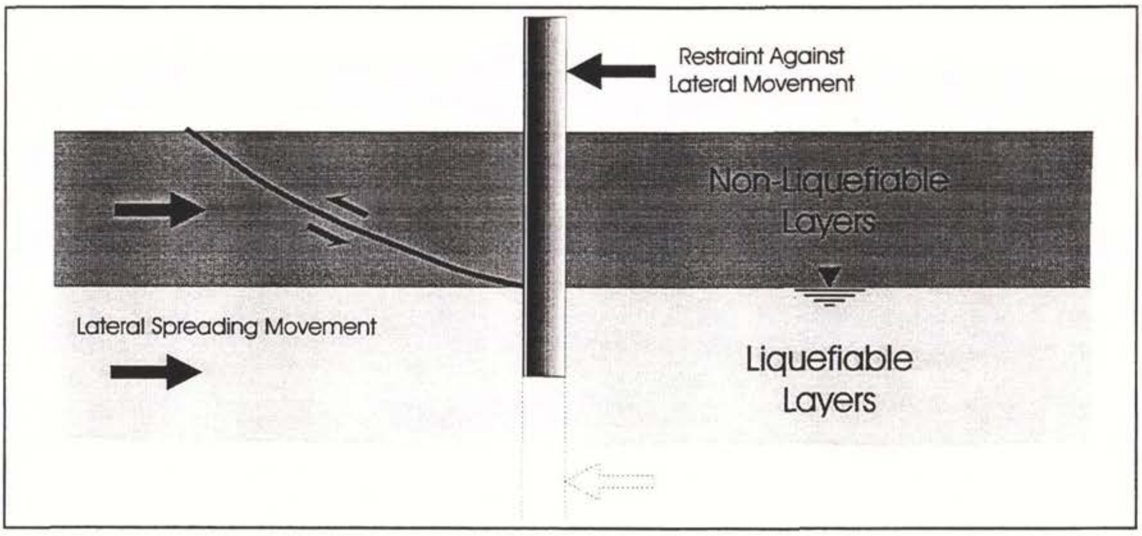

Figure 7.2 Large element over full depth of non-liquefiable soils

The same process as that used in (a) can be used in this case, but one can assume that the passive failure originates at the bottom of the non-liquefiable layer.

When passive failures occur around small elements such as piles, three dimensional effects can not be ignored. Using the theory outlined in Poulos and Davis (1980), Elson (1984) and Pender (1993) for the ultimate lateral resistance of piles subjected to horizontal loading from above ground, it is possible to infer likely soil pressures that may occur against piles when horizontally moving soil imposes loads against them. In order for these loads to develop, significant restraint against lateral movement must be present as discussed earlier. The end conditions of the piles are important as well as the influence of piles in a group. The pile strength and stiffness is also important in relation to the soil strength and stiffness. Plastic hinges may form in the pile resulting in the formation of a collapse mechanism. In general flexural failure of this type is to be avoided because usually it is difficult to detect and repairing these failures can be very costly.

Assuming there is rotational and lateral restraint present at both ends of a small structural element and it behaves as a rigid member, then the maximum horizontal soil pressures due to liquefaction induced lateral spreading can be estimated simply.

(c) The total passive horizontal force induced by a cohesive soil moving laterally against a small structural element, as shown in Figure 7.3, is given by (Elson 1984):

$$P_p = 9\ c_u\ D\ (L-1.5D) \tag{8.1}$$

where P_p = total passive force (kN)

c_u = undrained cohesive strength of soil (kPa)

D = small element diameter/width normal to movement (m)

L = embedded length of small element in layer (m)

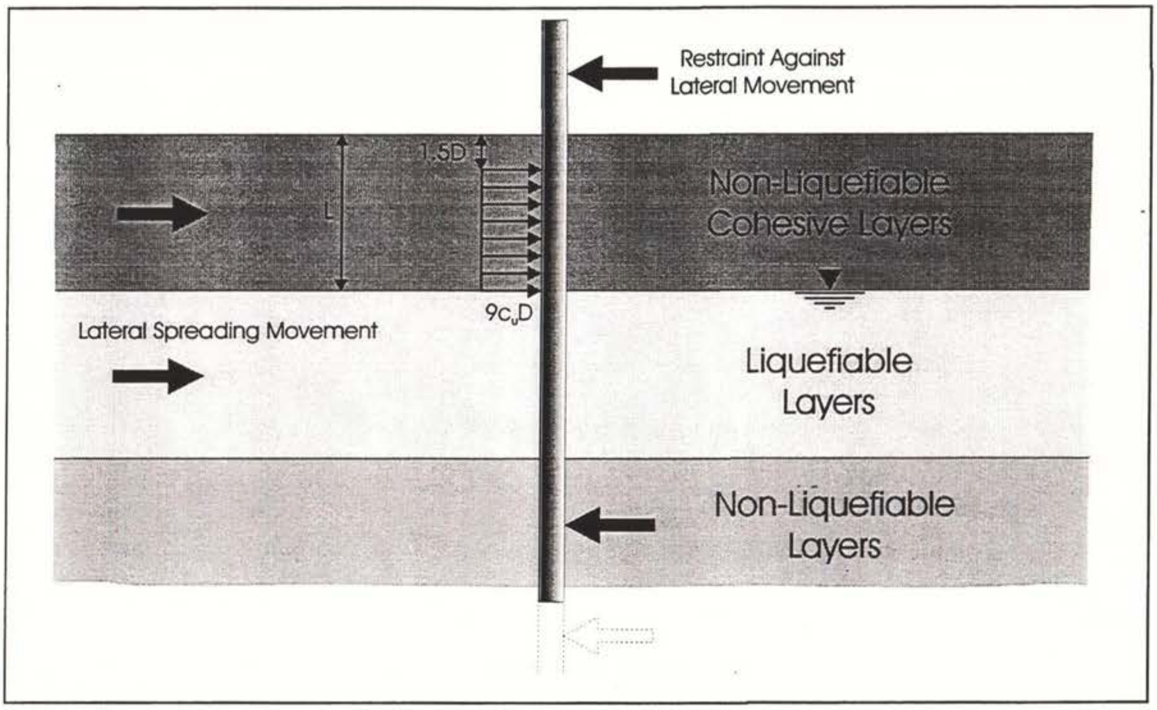

Figure 7.3 Lateral spreading stresses on small elements from cohesive soil

If there is more than one cohesive layer, the passive load can be summed for each layer. When cohesive soils move laterally, the induced stresses can be assumed to be uniform over the depth of the layer, except near the ground surface where for a depth of 1.5D, no passive pressure is assumed to occur. It can also be applied for cohesive layers below the water table which move laterally. This approach is used in design of short piles when they are pushed laterally from above the ground and gives a good idealisation of the total passive resisting force.

(d) The simplest approach to determining the total passive horizontal load from cohesionless soils on a small structural element, as shown in Figure 7.4, is to take three times the Rankine passive value (Elson 1984):

$$P_p = 1.5\,\gamma\,DL^2K_p \qquad (8.2)$$

where P_p = total passive force (kN)

γ = unit weight of the soil (kN/m^3)

D = small element diameter/width normal to movement (m)

L = embedded length of small element in layer (m)

K_p = Rankine passive pressure coefficient

$$= \frac{1+\sin\phi}{1-\sin\phi}$$

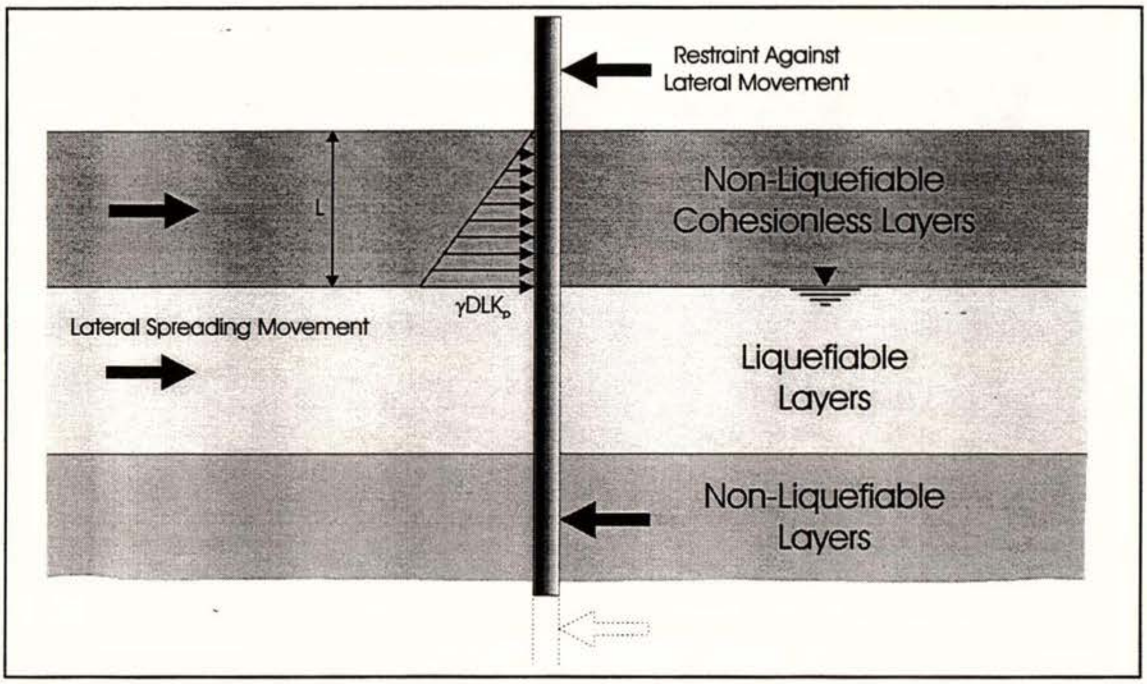

Figure 7.3 Lateral spreading stresses on small elements from cohesionless soil

This also can be extended to account for layers of different properties quite simply by considering first principles used in deriving the equation. It can also be used for cohesionless layers that do not liquefy and are below the water table.

When small structural elements have only partial restraint against lateral movement (restraint at only one end for example), it is more difficult to predict the lateral loads. The methods shown in (c) and (d) could be applied if the element is stiff enough to prevent flexural failure, but they will have their limitations. Passive failures in the soil can be assumed to start from the bottom of the element and project toward the surface. Other approaches may be taken by following the ideas presented by Poulos and Davis (1980) and Elson (1984).

7.2.5.2 Soil Below the Water Table.

Lateral loads imposed by cohesive and saturated cohesionless soils that do not liquefy but undergo lateral spreading in an earthquake can be treated similarly to methods (a)-(d). Effective stresses will need to be used in place of total stresses and the influence of pore water pressure may be neglected for symmetrical structures as the pore water pressure distribution will cancel out (usually one would expect this in most situations). Thus the last component of horizontal loading to consider is that of the moving liquefied soil.

In most situations, it is likely that liquefied soil drag forces will be insignificant compared with the loads from the soil above the liquefied layer. However, certain situations may necessitate the estimation of these loads, especially when there is little or no non-liquefiable soil present above the liquefied layer. The drag forces induced on buried structural elements are expected to be of short duration and dynamic in nature, occurring only during earthquake shaking and will cease to load the structure when movement stops. The loads imposed by soil above the liquefied layer are likely to be sustained in the soil for some time after shaking has stopped.

The drag force on small structural elements exerted by a moving liquefied soil could be estimated using the method outlined in Chapter 6. Estimates of the liquefiable soil properties such as its viscosity when liquefied, velocity distribution and density would be required.

For large structural elements subjected to liquefied soil drag forces, it may be difficult to estimate the total load since the inertia of the element itself may play a more important role in its loading.

7.3 DESIGN FOR LATERAL SPREADING LOADS

Damage to engineering structures caused by liquefaction induced lateral spreading can be minimised by well thought out design and construction solutions. It may be possible to prevent most structural movements and associated failures during lateral spreading by minimising the imposed load on the structure or increasing the strength of the structure.

7.3.1 Load Minimisation

A simple way to ensure that the horizontal loads imposed on a structure by moving soil above the liquefied layer are minimised would be to create a weak fill around the foundations (as suggested by the woodchips in the fill at Landing Road Bridge), oriented for the expected lateral spread movement. The fill would act as a buffer zone for lateral soil movement so that it may still occur, but the strong soil behind the weak fill will exert little force on the structure. This would be particularly useful in foundations with pier walls and piles, such as at Landing Road Bridge. The extent of the weak fill surrounding the foundation would be governed in part by the magnitude of expected lateral displacements. Vertical load carrying capacity of the foundations should not be compromised by the weak fill, so it would be important to ensure that foundations are sited on soil with sufficient bearing capacity. This can be accomplished by using piles that penetrate to depths where the soil provides this capacity.

The lateral dynamic properties of such foundation with weak fill surrounding it may be significantly different than if it were not present. Since earthquake shaking is required to initiate liquefaction induced lateral spreading, dynamic inertia loads will be effected by the soil properties. A weaker, less stiff, fill would provide less lateral stability and the consequences of this would need to be investigated. Scouring of fill around the substructure during flood episodes may also be an important design consideration.

Lateral spreading loads imposed by liquefiable layers themselves would be difficult to minimise using this approach because of the difficulty in working below the water table in loose material. These loads are expected to remain only for a short time since they are essentially dynamic and because of the low strength of the liquefied soil, are likely to be less significant than lateral loading from non-liquefied soil layers. When there is a significant thickness of potentially liquefiable material present, foundations would usually consist of piles that penetrate through the weak liquefiable layer into denser, stronger soil. Other approaches need to be adopted to minimise damage in these situations.

7.3.2 Increasing Structural Strength

Engineering structures could be designed and constructed so that any lateral spreading loads are resisted internally by the structure within its elastic capacity. By estimating the magnitude of the potential lateral spreading loads and deciding what sort of load distribution is likely, the designer can choose a structural strength to sustain these loads. For example, flexural strength at potential plastic hinge locations in concrete piles and piers may need to be increased, larger structural members may need to be employed in steel and timber construction.

External means of preventing structural damage could be applied by making use of tensile rods and anchor blocks. Piles raked at 1:1 could be used in compression to sustain lateral spreading loads. For the situation of Landing Road Bridge, the five river bank piers subjected to lateral spreading loads could be prevented from lateral movement by using one of the following approaches:

- Option 1 - Each pier could be secured individually with soil anchors, tensile rods and blocks placed in the denser material below the liquefiable sand (see Figure 7.5).
- Option 2 - Piers B to F could be linked by tensile rods and tied back with a number of soil anchors, tensile rods and blocks placed in material that will not move. The left abutment could be treated as in option 1 (see Figure 7.6).

In this case, it is likely that the ground anchors would need to be large because large forces could be expected. Similar methods could be applied in other situations such as building foundations, wharves and walls.

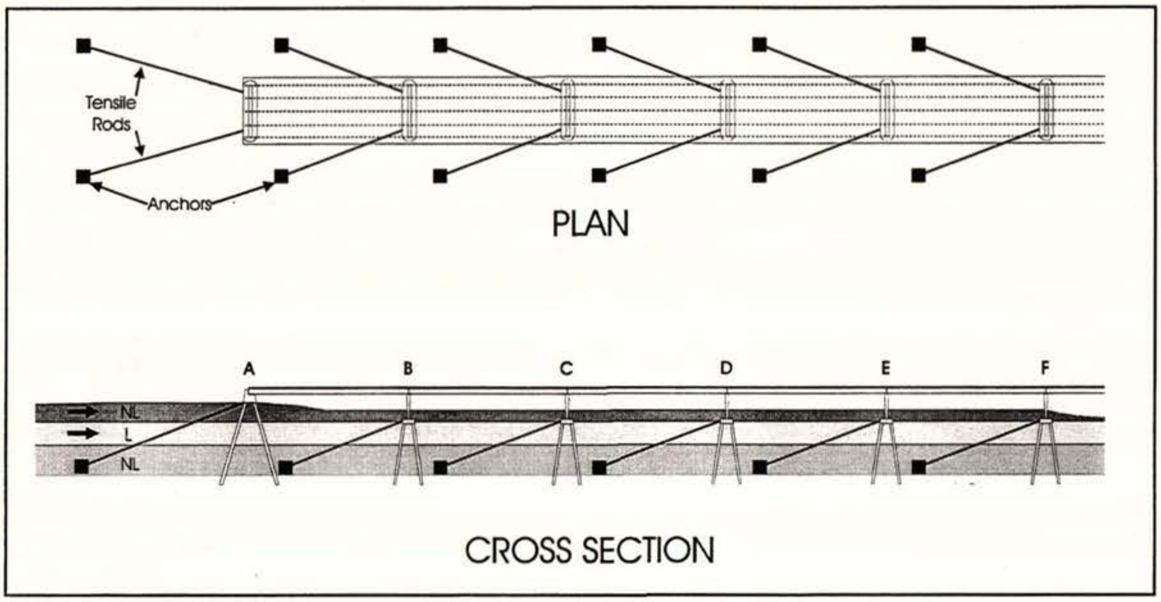

Figure 7.5 Construction to resist lateral spreading loads - Option 1

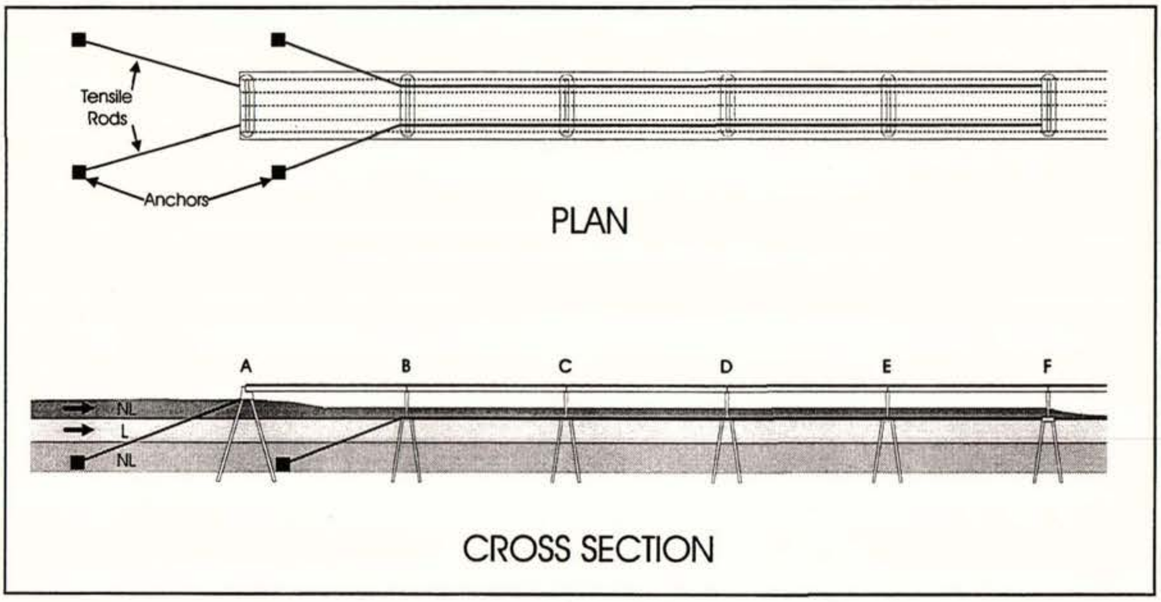

Figure 7.5 Construction to resist lateral spreading loads - Option 2

Chapter 8

Summary and Conclusions

8.1 SUMMARY

This research has investigated the phenomenon of liquefaction-induced lateral spreading, considering horizontal foundation loads that are exerted on engineering structures, with a case study at Landing Road Bridge, Whakatane. Examination of the bridge site, where extensive lateral spreading occurred following the 1987 Edgecumbe Earthquake, provides a useful account of the sorts of magnitudes which can be imposed on foundations by liquefaction induced lateral spreading.

Preliminary estimates of the horizontal passive load applied at the bridge piers, on the true left bank of the Whakatane River, suggested that the passive load was of the same order as the collapse load of the piled foundations. Consequently, a more detailed investigation of the soil conditions and more precise analysis of the structural capacity was undertaken in the project.

Excavation at two of the piers at which failures occurred revealed shear surfaces within the backfill, confirming the passive failure hypothesis. The main backfill used around the piers appears to have had woodchips mixed in with the soil during backfilling around the foundations, which has produced a very complex, disturbed material at the site. Block sampling of the fill proved to be troublesome due to the difficulties in forming a block, keeping it intact and transporting it to the laboratory with minimum disturbance. Soil testing of the fill posed many problems as the influence of the woodchips proved to be significant in some of the tests undertaken. For strength testing in particular, often wood particles were greater than specimen dimensions so that tests using the in situ fabric of the fill could not be performed. Strength testing of reconstituted specimens was found to be influenced by the woodchips, as only small specimens could be tested and low confining pressures were used to represent the natural stresses in the field. Test results showed that in general, woodchips produced scatter about the expected failure envelope and weakened the strength of the fill.

During the trenching at Pier C, it was possible to make a limited inspection of the pile-to-pile cap interface. It was not possible to inspect the most vulnerable region, the tensile zone at the top of the northern piles. But it appeared that cracking had not occurred at the second most vulnerable joint, at the top of the southern piles. Assuming that no cracking had occurred there, in Chapter 6 we saw that from the use of iterative elastic analyses, a wide range of 200 to 900 kN could placed on the passive loads applied to the foundations. From the soil properties obtained by strength testing of reconstituted soil samples, and ignoring three dimensional effects, the calculated passive load was estimated to lie in the range of 400 and 600 kN. This indicates that the ability of placing an accurate value on the passive loads is influenced by many variables, including both the soil and structure properties, and the final estimates have, in this case, shown a similar precision to the initial estimates.

Evidence of two previous episodes of liquefaction at the Landing Road Bridge site was found while trenching across one of the lateral spreading cracks. Records of the past 150 years of New Zealand earthquakes give the likely sources of buried sand boils in the trench to be the 1914 East Cape and the 1977 Matata Earthquakes.

Drag forces exerted on the piles by the liquefied sand during shaking were estimated to be about one tenth of the passive loads from the backfill. The cohesive soil above the water table clearly dominated the lateral loading in this case study.

Simple approaches to analysing lateral spreading loads were presented with possible design methods to minimise potential structural damage. Application of these in future construction practice may be possible.

8.2 CONCLUSIONS

While in this instance, there appears to be a good margin of safety against collapse, the passive force applied by lateral spreading could easily have been much greater; the cohesive layer could have been thicker and the soils easily two to three times stronger. Thus this case study illustrates a major potential source of foundation loading when lateral spreading may occur.

Trench excavations showed that the backfill was quite heterogeneous, containing gravel, sand, woodchips and other rubbish. Because of this, it was difficult to sample and test, and the final estimates of soil loads were probably no better than the preliminary one. However, the details of this particular case study are not as important as the information obtained about the overall mechanism; namely that in lateral spreading, the unliquefied crust can impose large loads on buried structures, limited only by the passive capacity of the soil.

In this case, the weak backfill around the piers saved the foundations from damage. Had the crushed stone fill been placed through the full depth of the overlying crustal layer, it is likely that the foundations would have attracted a much greater load and, possibly, failed. This, in turn, suggests that in similar circumstances, weak fill may be employed to protect the foundations from lateral spreading loads.

An accurate estimate can not be placed on the lateral spreading loads for three reasons. Firstly, due to inabilities in gauging the strength of intact samples of the weak backfill (when only reconstituted samples were able to be tested); secondly, the sensitivity of the parameters used in calculations; and thirdly, the uncertainties in the flexural strength of the piles at their interface with the pile cap and the structural behaviour under ultimate lateral loads.

Site investigation using trenching methods shows extensive detail of in situ soil conditions and provides the means for relatively undisturbed, accurate soil sampling. The data gathered from a trench can show vast detail of the near surface soils; more than would ever be possible using boring methods, giving a better picture of subsurface soil behaviour and enabling discontinuities in the soil strata to be located easily. Its application to site investigation is only limited by the depth of excavation, whereas using boring methods, great penetration depths can be achieved. In this case study, the versatility and simplicity of trenching methods made this technique the obvious choice for subsurface site investigation, and was invaluable for gathering information about the backfill around the bridge foundations and lateral spreading fissures in the field.

One of the objectives of this project was to develop a simple approach to determining the magnitude of lateral spreading loads on buried structures and possible design solutions to minimise damage to structures. Foundation loads due to lateral spreading have not been investigated extensively in the past. Simple approaches to calculating the magnitude of lateral spreading loads exerted on buried structures have been presented, in the hope that they will provide some guidelines for the designer in the future. Possible methods of sustaining these loads with minimum damage are presented which include modifying the soil or the structure by internal or external means. The application of such methods is likely to be influenced by the lateral spreading risk, importance of the structure and economics.

8.3 FUTURE WORK

There are many avenues to explore when investigating liquefaction induced lateral spreading. The following list includes work that relates to this study and may help with the greater understanding of this potentially damaging load mechanism on buried structures, and provide important information for designers to use in the future:

- Large scale shake table tests using liquefiable sand with an overlying non-liquefiable layer and structural models have been udertaken in the past but more information is needed about the distribution of lateral spreading soil stresses on the buried part of the structure and how they affect its behaviour. Passive soil failures around the structure and three dimensional effects affects of these failures on both small and large structural elements needs to be investigated.

- Liquefied soil drag forces on buried pipes and piles need to be investigated further in terms of estimating subsurface loads imposed by moving soil.

- The use of external methods to prevent possible structural damage caused by lateral spreading should be considered.

- Lateral spreading loads could be reduced by placing weak backfill around structures. The effects of this on dynamic foundation performance, durability and scouring resistance need to be examined.

References

1. Bartlett, S. F. and Youd, T. L. (1995), "Empirical Prediction of Liquefaction-Induced Lateral Spread", *Journal of Geotechnical Engineering*, ASCE, Vol. 121, No. 4, pp. 316-329.

2. Berrill, J. B., Christensen, S. A., Davis, R. O., Yiqiang, D. and Vreugdenhil, R. A. (1995), "The CPTU Test and Liquefaction: Some New Zealand Results", *Proceedings of the First International Conference on Earthquake Geotechnical Engineering*, Tokyo, pp 917-922.

3. Christensen, S. A. (1994), "Liquefaction of Cohesionless Soils in the March 2, 1987 Edgecumbe Earthquake, Bay of Plenty, New Zealand, and Other Earthquakes", *Master of Engineering Thesis*, University of Canterbury, Christchurch, New Zealand, 373 p.

4. Crook, C. N. and Hannah, J. (1989), "Regional Horizontal Deformation Associated with the 1987 Edgecumbe Earthquake, Bay of Plenty, New Zealand - an Introduction*", New Zealand Journal of Geology and Geophysics*, Vol. 32, No. 1, pp 93-98.

5. Davis, R. O. and Berrill, J. B. (1982), "Energy Dissipation and Seismic Liquefaction in Sands", *Journal of Earthquake Engineering and Structural Dynamics*, Vol. 10, No. 3, pp 111-119.

6. Downes, G. L. (1995), "Atlas of Isoseismal Maps of New Zealand Earthquakes", *Institute of Geological and Nuclear Sciences Monograph 11*, Lower Hutt, New Zealand, 304 p.

7. Elson, W. K. (1984), "Design of Laterally Loaded Piles", *CIRIA Report 103*, London, 86 p.

8. Fiegel, G. L. and Kutter, B. L. (1994a), "Liquefaction Mechanism for Layered Soils", *Journal of Geotechnical Engineering*, ASCE, Vol. 120, No. 4, pp. 737-755.

9. Fiegel, G. L. and Kutter, B. L. (1994b), "Liquefaction-Induced Lateral Spreading of Mildly Sloping Ground", *Journal of Geotechnical Engineering*, ASCE, Vol 120, No. 12, pp. 2236-2243.

10. GKN Reinforcements Ltd (1960), "Prestressing Steel (Strand) Catalogue", Somerset, England.

11. Miura, F., Stewart, H. E. and O'Rourke, T. D. (1991), "Effects of Liquefaction-Induced Lateral Spreading on Pile Foundations", *Soil Dynamics and Earthquake Engineering*, Vol. 10, No. 5, pp. 271-279.

12. Hamada, M. and O'Rourke, T. D. (1992), "Case Studies of Liquefaction and Lifeline Performance During Past Earthquakes", *Technical Report NCEER-92-0001*, Vol. 1, National Centre for Earthquake Engineering Research, New York.

13. Hamada, M. Yasuda, S. and Isoyama R. (1987), "Liquefaction-Induced Permanent Ground Displacement During Earthquakes", *Proceedings of the Pacific Conference on Earthquake Engineering*, 5-8 August, NZNSEE, pp 37-47.

14. Iwasaki, T. (1986). "Soil Liquefaction Studies in Japan: State of the Art", *Soil Dynamics and Earthquake Engineering*, Vol. 5, pp 2-68.

15. Law, K., Cao, Y. and He, G. (1990), "An Energy Approach for Assessing Seiamic Liquefaction Potential", *Canadian Geotechnical Journal*, Vol. 27, No. 3, pp 320-329.

16. Lin T. Y. and Burns, N. H. (1982), "Design of Prestressed Concrete Structures", Wiley, New York, 646 p.

17. O'Rourke, T. D. and Hamada, M. (1992), "Case Studies of Liquefaction and Lifeline Performance During Past Earthquakes", *Technical Report NCEER-92-0002*, Vol. 2, National Centre for Earthquake Engineering Research, New York.

18. Pender, M. (1993), "Aseismic Pile Foundation Design Analysis", *Bulletin of the New Zealand National Society for Earthquake Engineering*, Vol. 26, No. 1, March, pp 49-160.

19. Poulos, H. G. and Davis, E. H. (1980), "Pile Foundation Analysis and Design", Wiley, Brisbane, 397 p.

20. Rouse, H. (1938), "Fluid Mechanics for Hydraulic Engineers", First Edition, McGraw-Hill, New York, 422 p.

21. Sasaki, Y., Tokida, K., Matsumoto, M. and Saya, S. (1991), "Experimental Study on Lateral Flow of Ground Due to Soil Liquefaction", *Proceedings of the Second International Conference on Recent Advances in Geotechnical Earthquake Engineering and Soil Dynamics*, March 11-15, St. Louis, Missouri, pp 263-270.

22. Sasaki, Y., Towhata, I., Tokida, K., Yamada, K., Matsumoto, M., Tamari, Y.and Saya, S. (1991), "Mechanism of Permanent Displacement of Ground Caused by Seismic Liquefaction", *Soils and Foundations*, Vol. 32, No. 3, pp 79-96.

23. Shibata, T. and Teparaksa, W. (1988), "Evaluation of Liquefaction Potential of Soils Using Cone Penetration Tests", *Soils and Foundations*, Vol. 28, pp 49-60.

24. Standards Association of New Zealand, NZS3101:1995, Part 1, "Code of Practice for the Design of Concrete Structures", 256 p, Part 2, "Commentary on the Design of Concrete Structures", 264 p.

25. Standards Association of New Zealand, NZS4203:1992, Part 1, "Code of Practice for General Structural Design and Design Loadings for Buildings", 134 p, Part 2, "Commentary on General Structural Design and Design Loadings for Buildings", 96 p.

26. Streeter, V. L. and Wylie, B. E. (1985), "Fluid Mechanics", Eighth Edition, McGraw-Hill, New York, 586 p.

27. Taiping, Q., Chenchun, W., Lunian, W. and Huishan, L. (1984), "Liquefaction Risk Evaluation During Eartquakes", *Proceedings of International Conference on Case Histories in Engineering, St Louis*, Vol. 1, pp 445-454.

28. Tokida, K., Iwasaki, H., Matsumoto, H. and Hamada, T. (1993), "Liquefaction Potential and Drag Force Acting on Piles in Flowing Soils", *Soil Dynamics and Earthquake Engineering VI*, edited by Brebbia and Cakmak, Elsevier, pp 244-259.

29. Vargas, W. and Towhata, I. (1995), "Measurement of Drag Exerted by Liquefied Sand on Buried Pipe", *Proceedings of the First International Conference on Earthquake Geotechnical Engineering*, Tokyo, pp 975-980.

30. Youd T. L. and Perkins, D. M. (1987), "Mapping of Liquefaction Severity Index", *Journal of Geotechnical Engineering*, ASCE, Vol. 113, No. 11, pp 1374-1392.

31. Zhou, S. G. (1980), "Evaluation of the Liquefaction of Sand by Static Cone Penetration Test", *Proceedings of the Seventh World Conference on Earthquake Engineering*, Istanbul, Vol. 3. pp 156-162.

Appendix A

Calculations

Selected calculations are shown which include the following:

- Collapse load calculations for the bridge substructure with determination of plastic moments in the pier and piles.
- Moment-axial load interaction diagrams for the piles considering different conditions of anchorage and prestress.
- Cracking moments for different parts of the substructure are calculated with two elastic models of the foundations.
- Assumptions used in the passive wedge failure analysis are presented with some example calculations.

COLLAPSE LOAD CALCULATIONS

Using Works Consultancy Construction plans drawn in 1960 for Landing Road Bridge, the following was assumed.

All concrete $f'_c = 38$ MPa

$E_c = 3320\sqrt{f'_c} + 6900$ (NZS 3101: 1995)

$= 27.3$ GPa

Ordinary reinforcing

Normal Grade Steel eg D20 $f_y = 250$ MPa

High Grade Steel eg HD20 $f_y = 430$ MPa

$E_s = 200$ GPa

Prestressing Steel in Piles

$f_{pu} = 1810$ MPa

nominal diameter = 9.5 mm

cross sectional area = 51.6 mm^2

Dead Loads

All reinforcing was neglected in dead load calculations and $\gamma_{conc} = 24\ KN/m^3$. Dimensions from the plans were used. Ballustrades & Light stands were ignored

1 Pile Cap	370 KN
1 Pier	500 KN
Bridge Beams for one span	750 KN
Diaphragms for one span	200 KN
Decking for one span	720 KN
Dead Load on eight piles	2540 KN
Average Dead load per pile	315 KN

Ideal Plastic Moments

Dead Loads at the top and bottom of the pier are insignificant when considering interaction with plastic moments (< 2 % of maximum)

Top of Pier 8 25.4 mm HD bars each face

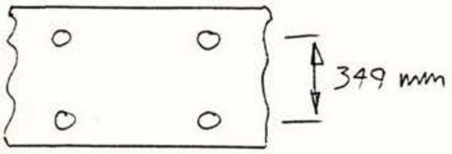

$$M_u = A_s f_y jd$$

$$= 8 \times \pi \times \frac{25.4^2}{4} mm^2 \times 430 \frac{N}{mm^2} \times 349 mm$$

$$= \underline{\underline{608\ KNm}}$$

Bottom of Pier

32 12·7 mm D bars each face

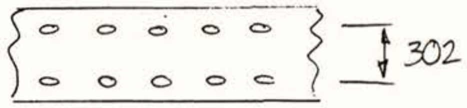

$$M_u = A_s f_y jd$$
$$= 32 \times \pi \times \frac{12.7^2}{4} mm^2 \times 250 \frac{N}{mm^2} \times 302\ mm$$
$$= \underline{\underline{306\ kNm}}$$

Piles

The anchorage of the pile prestressing strand governs the plastic moments in the piles.

1. Assuming the strand is straight in the pile cap with a maximum development length of 700 mm (NB pile cap is 762 mm high), no prestress at interface

   $$l_d \geq \left(f_{ps} - \frac{2}{3} f_{se}\right) \frac{d_b}{7} \qquad (NZS3101:1995)$$

   Prestress (f_{se}) = zero at top of piles. Let l_d = 700 mm and solve for f_{ps}

   $$f_{ps} \leq \frac{7}{9.5\,mm} \cdot 700\ mm$$
   $$\leq \underline{\underline{516\ MPa}}$$

2. Assuming strand was bent over to form hooks then the full development of strand is possible, but no prestress at interface.

3. Midheight of piles, have full development of strand and prestress after losses.

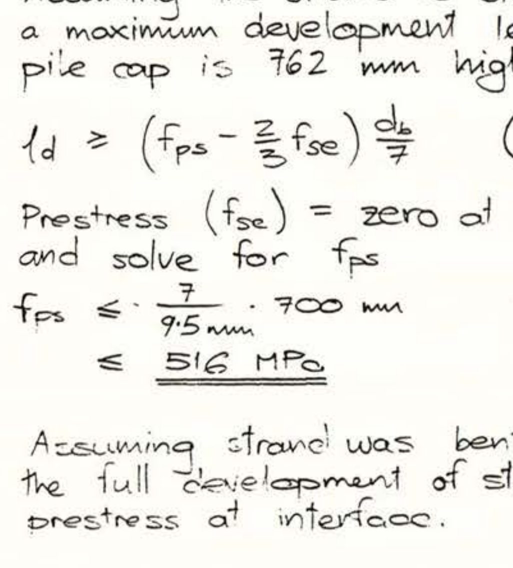

Using a method based on first principles, moment axial load charts were plotted for the piles for each of the three cases above.

The Ramberg-Osgood relationship was used to model the stress-strain behaviour of the prestressing strand

The stress in the strand for situation 1 was limited to 516 MPa in tension, and for 2 + 3 the stresses were up to three times greater at failure.

The three curves can be seen on page 101

Example Moment-Axial Load Calculations for Precast Prestressed Concrete Pile

Tendons

7 wire strand	E (GPa)	200
Area of one tendon (mm^2)		51.61
f_{pu} (MPa)		1810
Initial Prestress (% of f_{pu})		70%
Initial Force (one tendon, N)		65390
Losses in Initial Force (%)		20%
Force After Losses (one tendon, N)		52312
Maximum Strain at Fracture		0.06

Concrete

f_c' (MPa)	37.9
E (GPa)	27.3
β_1	0.7868
Maximum Compressive Strain	0.003

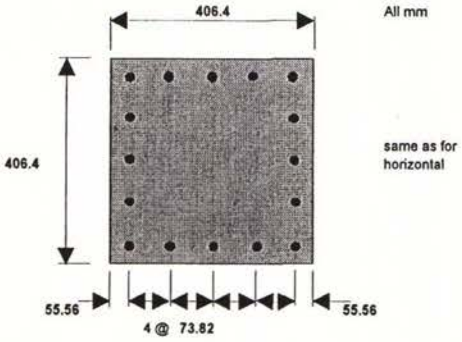

All mm

same as for horizontal

Changes in Strain At Ultimate Limit State

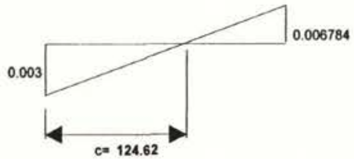

Stresses at Ultimate Limit State

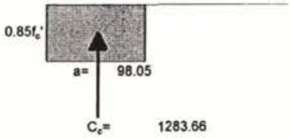

Concrete Compressive Force (C_c) at Ultimate Limit State

C_c (kN)	1283.7
Ultimate Axial Load P_u (kN)	315.0
Ultimate Moment M_u (kNm)	233.5

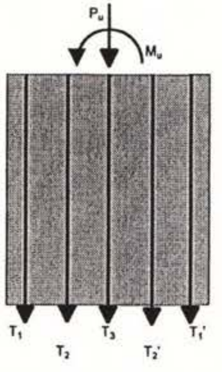

Initial Prestress Forces (after losses)

T_1, T_1' (N)	261559.5
T_2, T_2' (N)	104623.8
T_3 (N)	104623.8

Initial Strain in Tendons (after losses)

-0.00507

Tendons at Ultimate Limit State

	Change in Strain	Total Strain	Stress (MPa)	Force (kN)
T_1	0.001662	-0.00341	681.4	175.82
T_2	-0.00011	-0.00518	1034.8	106.81
T_3	-0.00189	-0.00696	1345.9	138.92
T_2'	-0.00367	-0.00874	1491.5	153.95
T_1'	-0.00545	-0.01051	1523.6	393.15
				968.66

Moment-Axial Load Interaction Chart for Precast Prestressed Concrete Piles at Landing Road Bridge

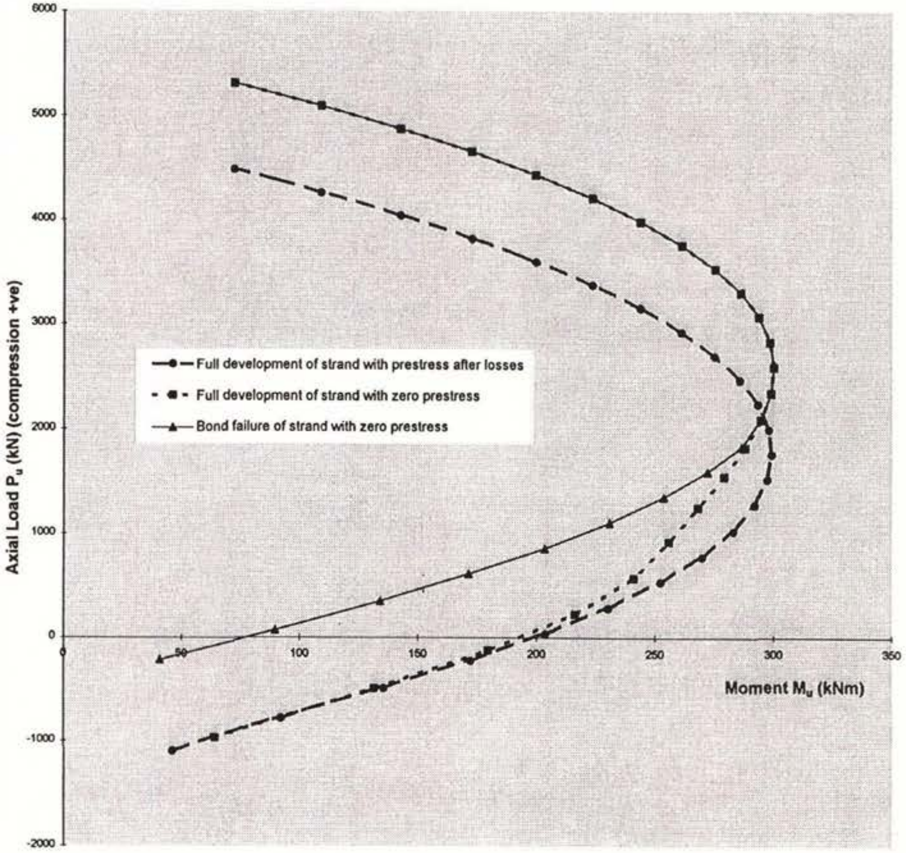

For a dead load of 315 KN per pile, the following plastic moments were determined.

1. Top of pile, bond failure, zero prestress $M_p = \underline{\underline{129 \text{ KNm}}}$
2. Top of pile, full development of strand, zero prestress $M_p = \underline{\underline{224 \text{ KNm}}}$
3. Midheight of pile, full development of strand, prestress after losses (20 %) $M_p = \underline{\underline{233 \text{ KNm}}}$

The axial load is small enough so that tensile failures would result ie, below balanced failure. In the collapse mechanism when lateral deformations occur, the riverward piles will increase in compressive load, and the landward piles will decrease by an equal amount. Thus the plastic moments will change similarly, and the lateral load calculations assume the changes in plastic moment to be equal, thus cancelling out. This allows the plastic moments calculated above to be used without any modification

Collapse loads

1. Assuming the bond failure mechanism occurs at the top of the piles we have

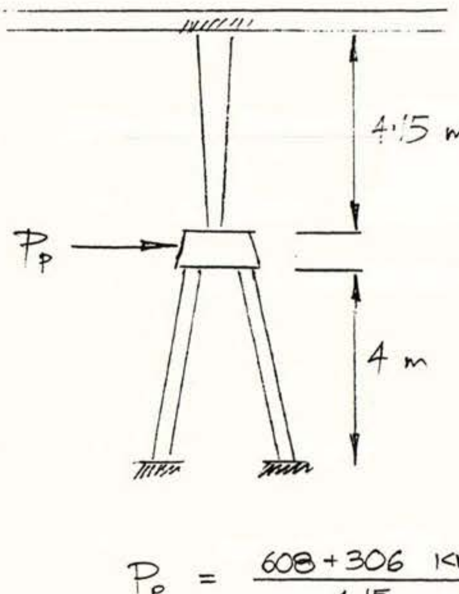

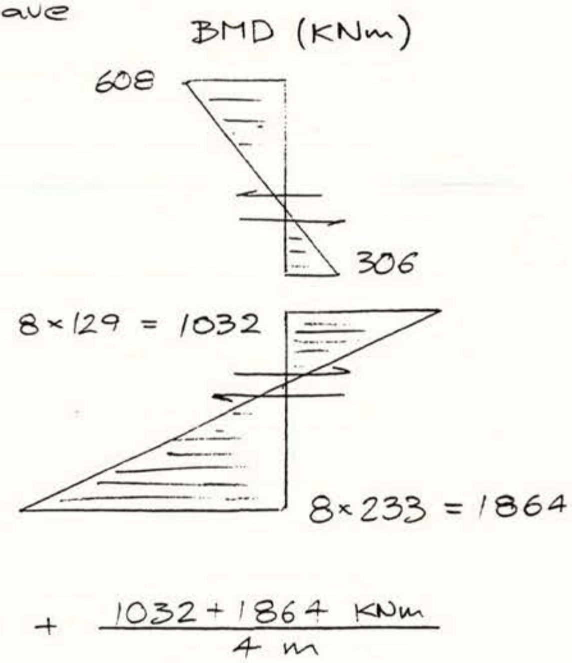

$$P_p = \frac{608 + 306 \text{ KNm}}{4{\cdot}15 \text{ m}} + \frac{1032 + 1864 \text{ KNm}}{4 \text{ m}}$$
$$= \underline{\underline{944 \text{ KN}}}$$

2. Assuming full development of the prestressing strand in the pile cap we have.

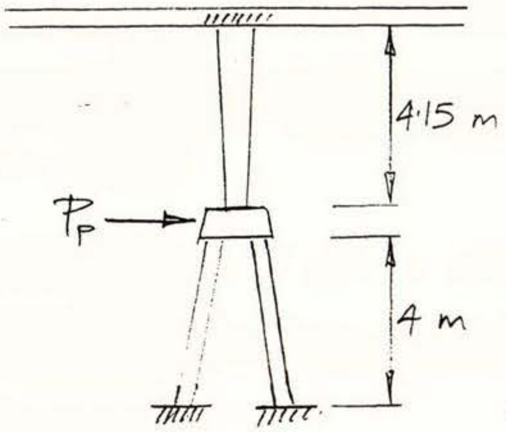

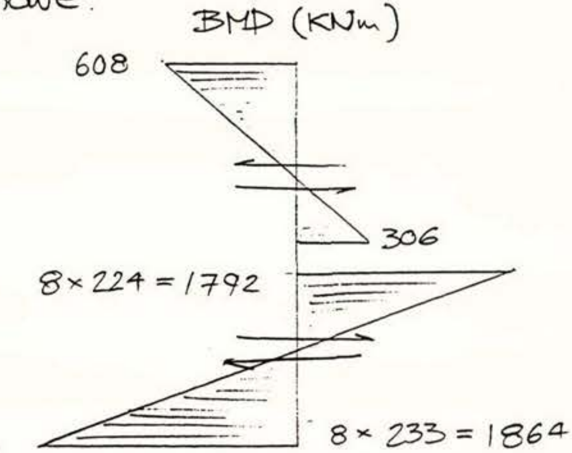

$$P_P = \frac{608 + 306 \text{ KNm}}{4{\cdot}15 \text{ m}} + \frac{1792 + 1864 \text{ KNm}}{4 \text{ m}}$$
$$= \underline{1134 \text{ KN}}$$

Thus the total collapse load of the substructure is between about 950 - 1130 KN.

CRACKING MOMENT CALCULATIONS

At the top and bottom of the pier, and top of the piles, we have construction joints, which are assumed to have no tensile cracking strength. But axial dead loads prevent cracks appearing until tensile stresses associated with flexure exceed the axial compressive stress at the extreme fibre.

At mid height of the piles, the modulus of rupture of the concrete is used because the member is continuous.

$$M_R = 0{\cdot}8\sqrt{f'_c} \qquad \text{(NZS 3101 : 1995)}$$
$$= \underline{\underline{4{\cdot}9 \text{ MPa}}}$$

The calculation of first cracking moments in the pier is relatively easy. But since the piles are raked, lateral deformations change the axial loads so that the piles in reduced compression (landward) will crack before the piles under increased compression (riverward). An iterative process is required to determine the first cracking moments.

An elastic analysis, using stiffness properties determined from plans, was used with the following two structural models:

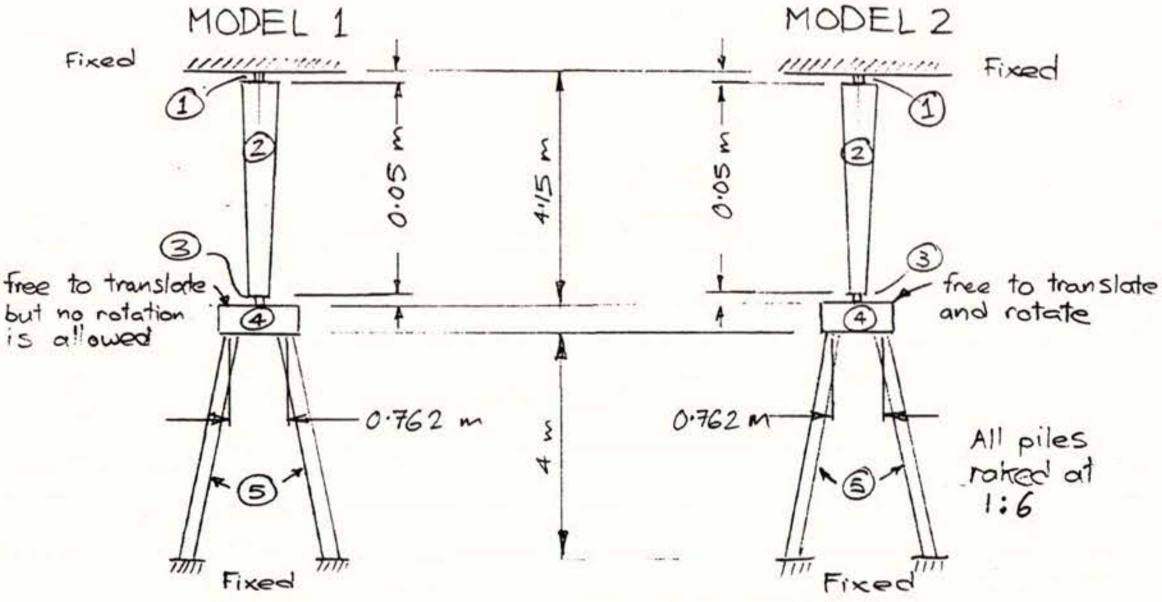

Because the tapered pier was much stiffer in comparison to the rest of the foundations, the top and bottom 0·05 m of it (members ① + ③) were modelled using the properties of the reinforcing only. This gave a more realistic distribution of bending moments in the substructure.

The pile cap is very stiff; in model 1 it is free to translate but rotation is prevented. In model 2, both translation and rotation were allowed.

All eight piles are represented by two groups of four piles (member ⑤). The properties of member ⑤ are 4 times the properties of one pile.

Member		A ($\times 10^3$ mm^2)	E (GPa)	I ($\times 10^6$ mm^4)
①		16·2	200	247·2
②	Top	7010·4	27·3	339212·2
	Bottom	3069·3	27·3	36934·3
③		8·1	200	197·4
④		6232·2	27·3	301560·0
⑤		655·6	27·3	9092·0

The deflected shape (exaggerated) and bending moment diagram at first cracking for models 1 + 2 are shown on pages 105 and 106

MODEL 1

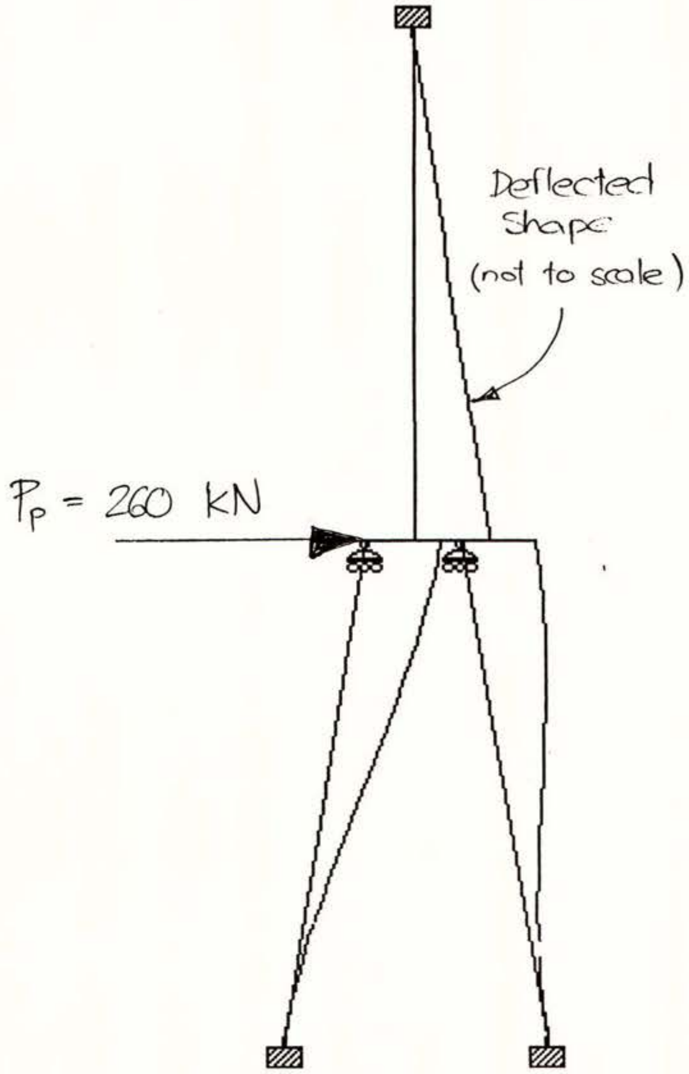
Deflected Shape (not to scale)
P_p = 260 kN

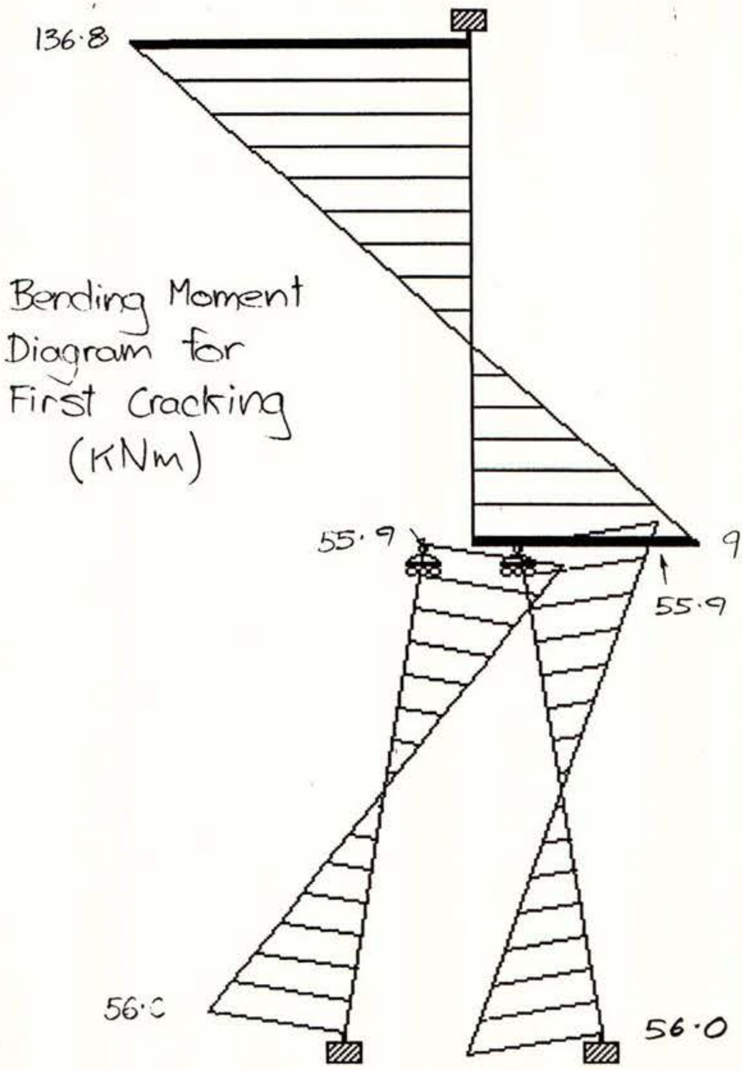
136·8
Bending Moment Diagram for First Cracking (kNm)
55·9
91·1
55·9
56·0
56·0

MODEL 2

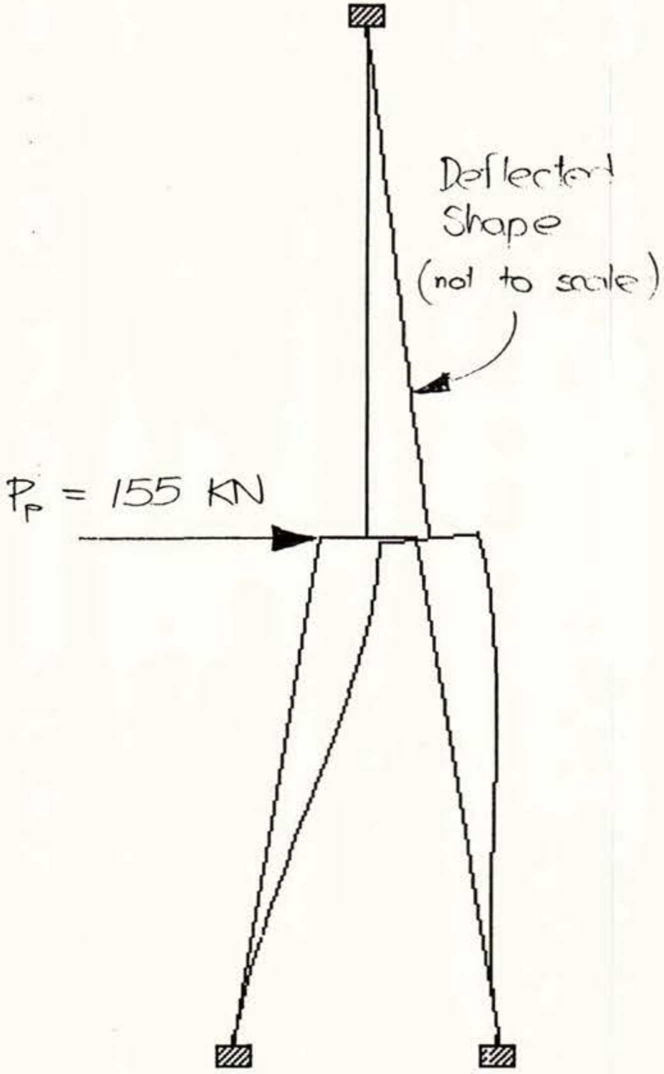
Deflected Shape (not to scale)
P_p = 155 KN

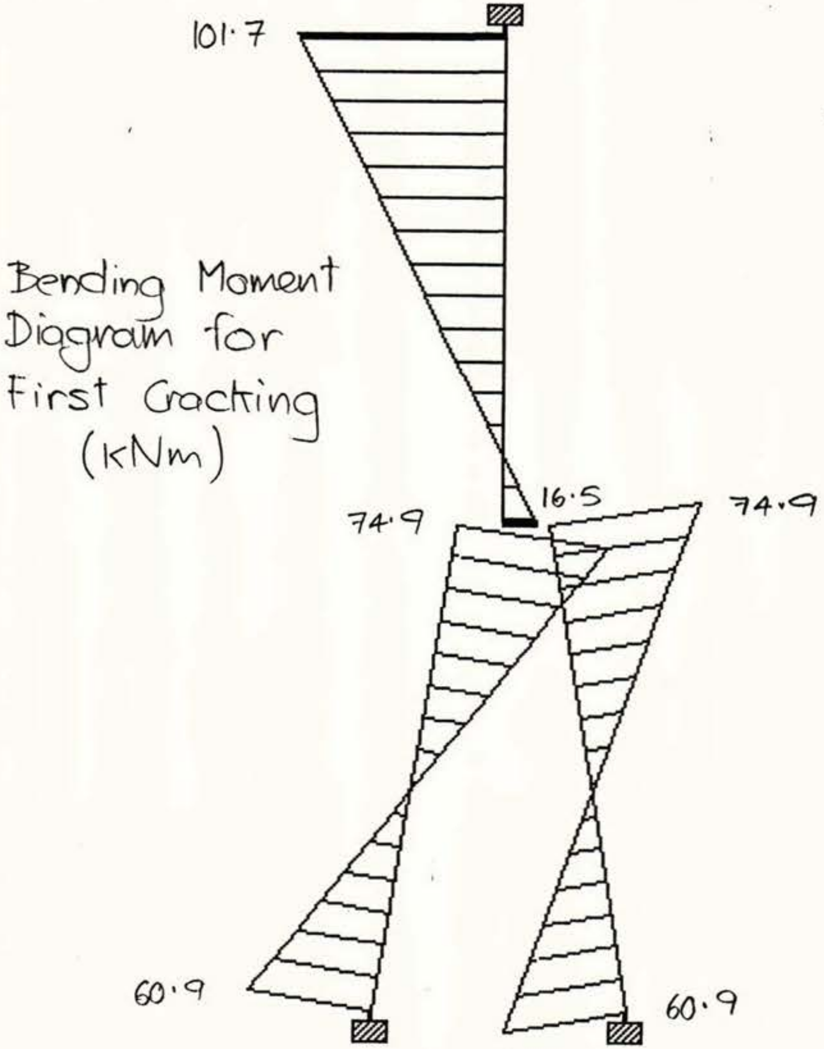
Bending Moment Diagram for First Cracking (kNm)
101·7
16·5
74·9
74·9
60·9
60·9

The transformed section approach was used in the calculations

Top of Pier

$$\text{Axial Dead Load} = 750 + 200 + 720$$
$$= 1670 \text{ KN}$$

$$n = \frac{E_s}{E_c} = 7{\cdot}32$$

$$A_t = bh + (n-1)A_s$$
$$= 9200 \times 762 + (7{\cdot}32-1) \times 16 \times \pi \times \frac{25{\cdot}4^2}{4} \text{ mm}^2$$
$$= 7{\cdot}06 \times 10^6 \text{ mm}^2$$

$$I_t = \frac{bh^3}{12} + (n-1)A_s(y-d)^2$$
$$= \frac{9200 \times 762^3}{12} + (7{\cdot}32-1) \times 16 \times \pi \times \frac{25{\cdot}4^2}{4} \times 349^2 \text{ mm}^4$$
$$= 345{\cdot}5 \times 10^9 \text{ mm}^4$$

$$f_c = \frac{1670 \times 10^3 \text{ N}}{7{\cdot}06 \times 10^6 \text{ mm}^2} = 0{\cdot}23 \text{ MPa}$$

$$\frac{M_c \frac{h}{2}}{I_t} = f_c$$
$$M_c = \frac{0{\cdot}23 \frac{\text{N}}{\text{mm}^2} \times 345{\cdot}5 \times 10^9 \text{ mm}^4}{762/2 \text{ mm}}$$
$$= \underline{\underline{216 \text{ KNm}}}$$

Bottom of Pier

$$\text{Axial Dead Load} = 1670 + 500$$
$$= 2170 \text{ KN}$$

$$A_t = 8080 \times 380 + (7{\cdot}32-1) \times 64 \times \pi \times \frac{12{\cdot}7^2}{4}$$
$$= 3{\cdot}12 \times 10^6 \text{ mm}^2$$

$$I_t = \frac{8080 \times 380^3}{12} + (7{\cdot}32-1) \times 64 \times \pi \times \frac{12{\cdot}7^2}{4} \times 151^2$$
$$= 38{\cdot}1 \times 10^9 \text{ mm}^4$$

$$f_c = \frac{2170 \times 10^3 \text{ N}}{3{\cdot}12 \times 10^6 \text{ mm}^2} = 0{\cdot}70 \text{ MPa}$$

$$M_c = \frac{0{\cdot}70 \frac{\text{N}}{\text{mm}^2} \times 38{\cdot}1 \times 10^9 \text{ mm}^4}{380/2 \text{ mm}}$$
$$= \underline{\underline{139 \text{ KNm}}}$$

Piles

Using the structural models on the previous page, an iterative process was used to determine first cracking in different parts of the model, following similar calculations to those above. The following tables show the sequence of cracking up to first yield for each model.

MODEL 1

Position	P_p (KN)	M_c (KNm)
Landward Pile Top	260	14
Bottom of Pier	405	140
Top of Pier	410	215
Bottom of Pier	870	Yield
Riverward Pile Top	>870	>50

MODEL 2

Position	P_p (KN)	M_c (KNm)
Landward Pile Top	155	19
Riverward Pile Top	220	27
Top of Pier	330	215
Landward Pile Top	770	Yield
Top of Pier	>770	Yield.

Model 1 shows that yield occurs first at the bottom of the pier with cracking of the riverward piles at very high passive loads. Model 2 shows yielding to first occur in the landward piles, with much lower first cracking moments in the riverward piles. The true behaviour of the substructure is expected to be somewhere between models 1 & 2.

PASSIVE WEDGE FAILURE ANALYSIS

The following parameters, determined from strength tests in the laboratory, were used for the analysis

		Direct Shear Tests	Triaxial Tests
Unit Weight	γ (KN/m^3)	12-14	12-14
Cohesion	c (KPa)	8-12	12-15
Angle of Internal Friction	ϕ (°)	40-45	8-13

Rankines Analysis

Passive failures in the fill were assumed to start at the level of the pile cap. The pier wall was assumed to be vertical, and the ground surface horizontal. Based on the trench logs, the average soil depth at Pier C was 1·2 m and Pier E, 1·1 m.

Example Calculation.

The total passive thrust per unit length is given by:

$$P_p = \frac{1}{2} K_p \gamma H^2 + 2c\sqrt{K_p}\,H \qquad K_p = \frac{1+\sin\phi}{1-\sin\phi}$$

Using the data for the triaxial tests take

$$\gamma = 12 \text{ KN/m}^3 ; \; c = 12 \text{ KPa} ; \; \phi = 10°$$

$$K_p = \frac{1+\sin 10}{1-\sin 10}$$

$$= 1{\cdot}42$$

Let $H = 1{\cdot}2$ m (at Pier C)

$$P_p = \frac{1}{2} \times 1{\cdot}42 \times 12 \frac{\text{KN}}{\text{m}^3} \times 1{\cdot}2^2 \text{ m}^2 + 2 \times 12 \frac{\text{KN}}{\text{m}^2} \times \sqrt{1{\cdot}42} \times 1{\cdot}2 \text{ m}$$

$$= 46{\cdot}6 \text{ KN/m}$$

Take the Pier width as 8·1 m then

$$P_p = 8 \text{ m} \times 46{\cdot}6 \frac{\text{KN}}{\text{m}}$$

$$= \underline{\underline{377 \text{ KN}}}$$

Coulombs Analysis

The same range of parameters was used, with the inclusion of wall friction, δ, and the angle of the failure surface with respect to the horizontal, θ.

From the trench logs, at Pier C θ was 25-30° and at Pier E, θ was 30°-35°. The solution of the total passive force is found graphically. The relationship $\delta = \frac{2}{3}\phi$ was used for the direct shear parameters and $\delta = 0°$, $\delta = 10°$ was used for the triaxial test parameters.

The following diagrams show the shape of the wedges used in calculations at both piers.

Pier C.

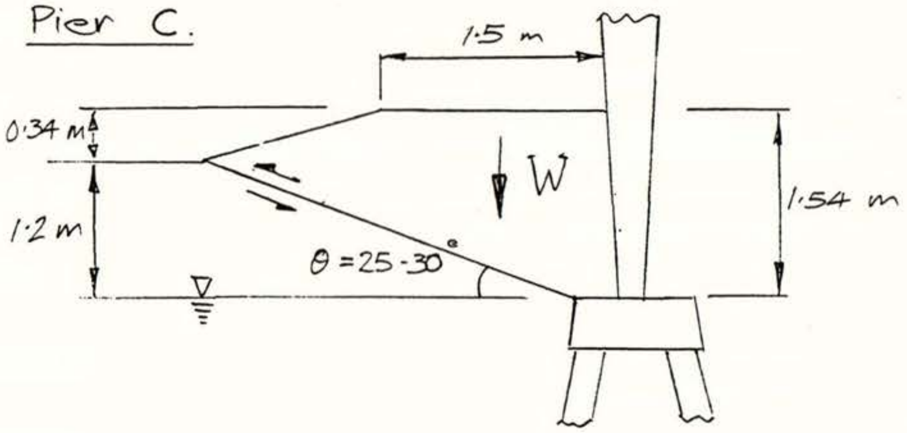

Pier E

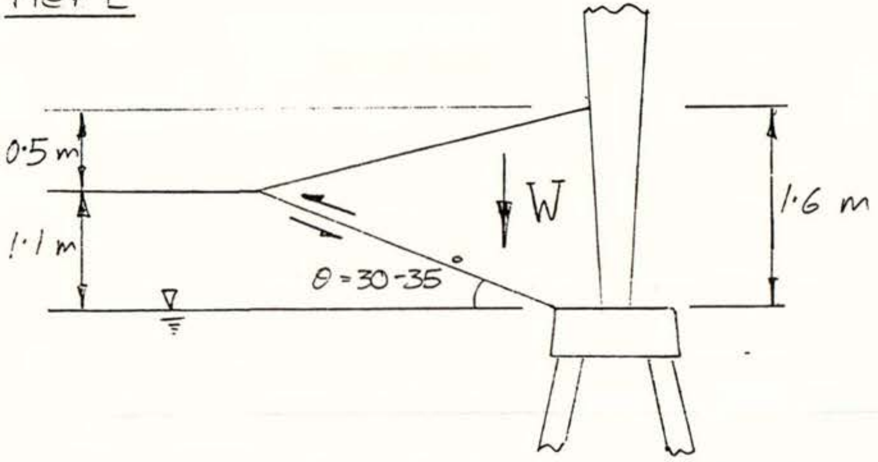

Schematic of Graphical Solution for P_P

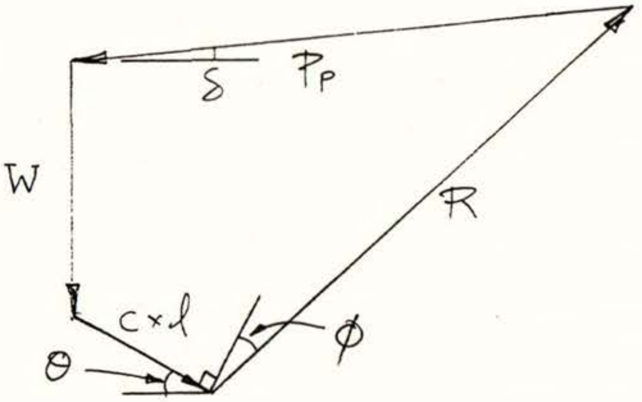

Appendix B

Laboratory Results

A summary of the laboratory test results is given which includes:

- Hand auger borehole logs from the preliminary site investigation

- Particle size distributions and dry density values for samples retrieved during hand augering

- Particle size distributions of sand samples from Trench 2

- Raw laboratory testing curves for direct shear and triaxial specimens

Dept. of Civil Engineering
University of Canterbury
Christchurch, NZ

Landing Road Bridge
Whakatane
NZ

By RK/JB
Date 30/3/95

BOREHOLE LOG

TYPE HAND AUGER
ELEVATION
BORING HA 1

STRIKE / DIP	RELATIVE COMPACTION	DRY DENSITY (t/m^3)	MOISTURE (%)	BLOWS/FOOT	SAMPLE SIZE	SAMPLE No	DEPTH IN m	MATERIAL SYMBOL	UNIFIED SOIL CLASS.	
										TOP SOIL
		2·61			BAG	1				LIGHT TAN SILT WITH GRAVELS
		2·56			BAG	2	0·5			TAN SILT WITH FINE ANGULAR GRAVELS
		2·19			BAG	3	1·0			GREYISH BLUE SANDY SILT WITH GRAVELS, WOODCHIPS, ORGANICS
		2·31			BAG	4	1·5			GREY SAND WITH WOODCHIPS
							2·0			GREY MEDIUM SAND WITH ANGULAR GRAVELS, WOODCHIPS
		2·54			BAG	5				DARK GREY SANDY COARSE SILT WITH SOME ORGANICS
		2·46			BAG	6	2·5			GREY MEDIUM SAND WITH COARSE SILT
										CAVING IN – BORING ABANDONED

WATER TABLE DEPTH @ 2·20 PM WAS 1·8 M.
TWO HOURS LATER 1·6 M

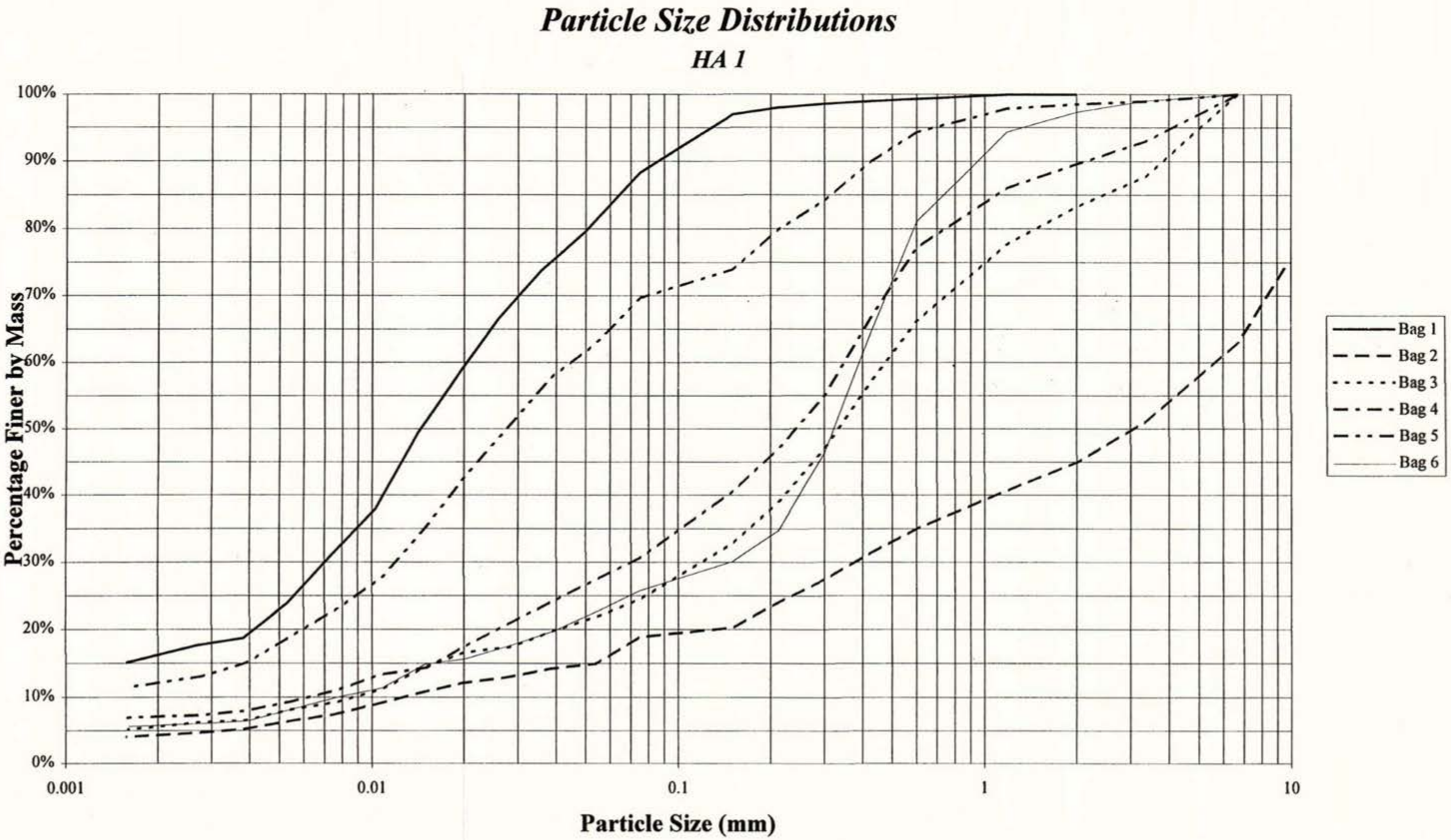
Particle Size Distributions
HA 1
Percentage Finer by Mass
100%
90%
80%
70%
60%
50%
40%
30%
20%
10%
0%
0.001
0.01
0.1
1
10
Particle Size (mm)
Bag 1
Bag 2
Bag 3
Bag 4
Bag 5
Bag 6

Dept. of Civil Engineering
University of Canterbury
Christchurch, NZ

Landing Road Bridge
Whakatane
NZ

By RK / JB
Date 30/3/95

BOREHOLE LOG

TYPE HAND AUGER

ELEVATION

BORING HA 2

DEPTH IN m	DESCRIPTION
	TOP SOIL
	LIGHT TAN SILT WITH WOODCHIPS
0·5	
	CAN NOT PENETRATE GRAVELS BORING ABANDONED
1·0	

STRIKE / DIP | RELATIVE COMPACTION | DRY DENSITY (t/m^3) | MOISTURE (%) | BLOWS/FOOT | SAMPLE SIZE | SAMPLE Nº | DEPTH IN m | MATERIAL SYMBOL | UNIFIED SOIL CLASS.

Dept. of Civil Engineering
University of Canterbury
Christchurch, NZ

Landing Road Bridge
Whakatane
NZ

By RK/JB
Date 30/3/95

BOREHOLE LOG

TYPE HAND AUGER **ELEVATION** **BORING** HA 3

STRIKE / DIP	RELATIVE COMPACTION	DRY DENSITY	MOISTURE (%)	BLOWS/FOOT	SAMPLE SIZE	SAMPLE No	DEPTH IN m	MATERIAL SYMBOL	UNIFIED SOIL CLASS.	
										TOP SOIL
		2·61			BAG	1				LIGHT TAN SILT WITH ANGULAR GRAVELS
							0·5			
		2·47			BAG	2				
							1·0			
										GREYISH BLUE SANDY SILT WITH WOODCHIPS, ANGULAR GRAVELS, PEAT
		2·33			BAG	3	1·5			MORE SAND IN MATERIAL
							2·0			
		2·47			BAG	4				GREY MEDIUM SAND
										DARK GREY MEDIUM SILT
										CAVING IN - BORING ABANDONED
							2·5			

WATER TABLE DEPTH @ 4·15 PM
WAS 1·65 M

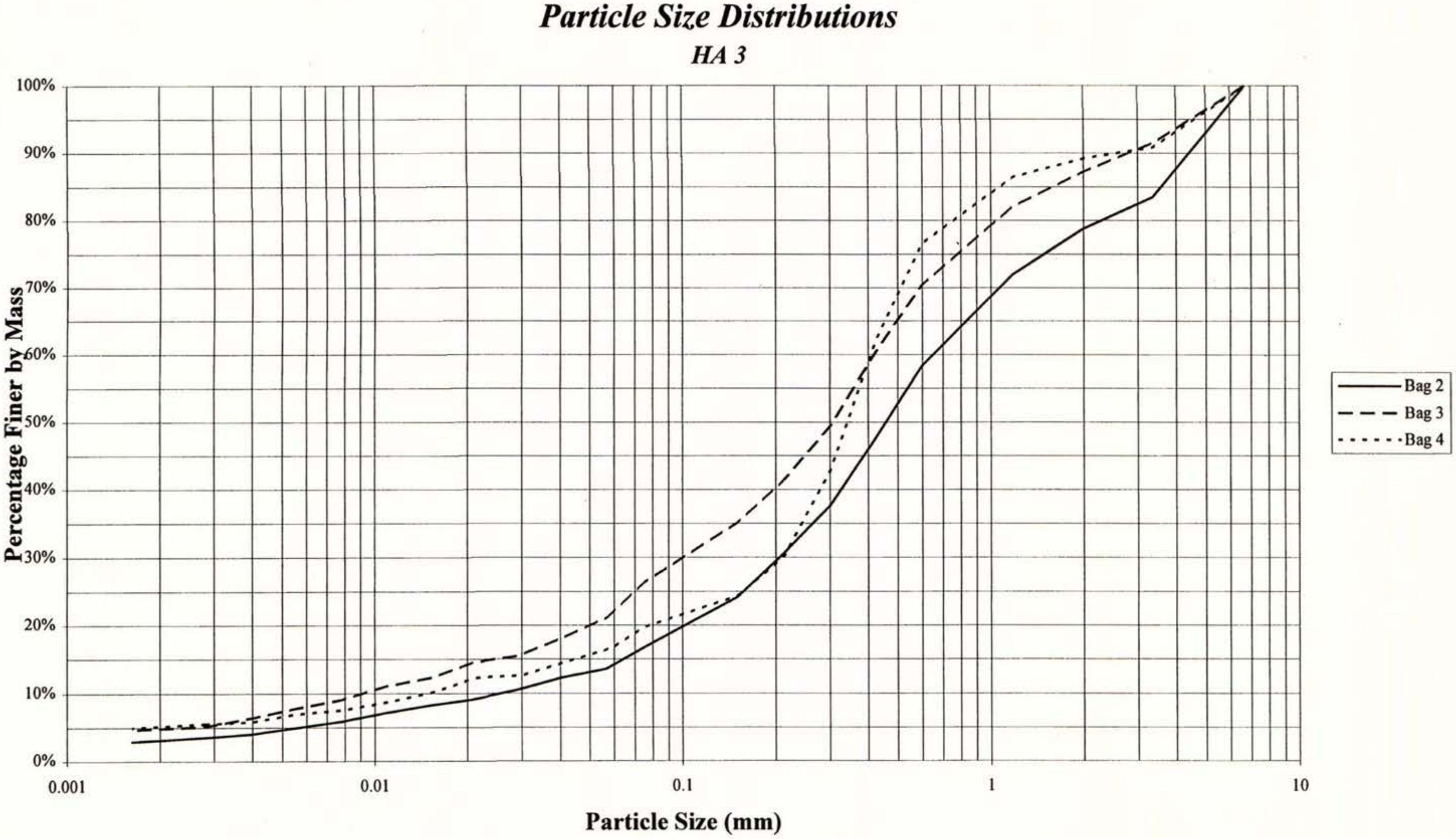
Particle Size Distributions
HA 3
100%
90%
80%
70%
60%
50%
40%
30%
20%
10%
0%
Percentage Finer by Mass
0.001
0.01
0.1
1
10
Particle Size (mm)
Bag 2
Bag 3
Bag 4

Dept. of Civil Engineering
University of Canterbury
Christchurch, NZ

Landing Road Bridge
Whakatane
NZ

By RK/JB
Date 31/3/95

BOREHOLE LOG

TYPE HAND AUGER

ELEVATION

BORING HA 4

STRIKE / DIP	RELATIVE COMPACTION	DRY DENSITY (t/m^3)	MOISTURE (%)	BLOWS/FOOT	SAMPLE SIZE	SAMPLE Nº	DEPTH IN m	MATERIAL SYMBOL	UNIFIED SOIL CLASS	
										TOP SOIL
										LIGHT TAN SILT WITH GRAVELS
										CAN NOT PENETRATE GRAVELS BORING ABANDONED
							0·5			

Dept. of Civil Engineering
University of Canterbury
Christchurch, NZ

Landing Road Bridge
Whakatane
NZ

By RK/JB
Date 31/3/95

BOREHOLE LOG

TYPE HAND AUGER

ELEVATION

BORING HA 5

STRIKE / DIP	RELATIVE COMPACTION	DRY DENSITY	MOISTURE (%)	BLOWS/FOOT	SAMPLE SIZE	SAMPLE No	DEPTH IN m	MATERIAL SYMBOL	UNIFIED SOIL CLASS.	
										TOP SOIL
		2·61			BAG	1				
										TAN SILT WITH ANGULAR GRAVELS, WOODCHIPS, MEDIUM SANDS
							0·5			
		2·59			BAG	2				GREY FINE SAND
							1·0			
		2·58			BAG	3				
										CAVING IN - BORING ABANDONED
							1·5			
							2·0			
							2·5			

WATER TABLE DEPTH @ 10·15 AM
WAS 0·95 M

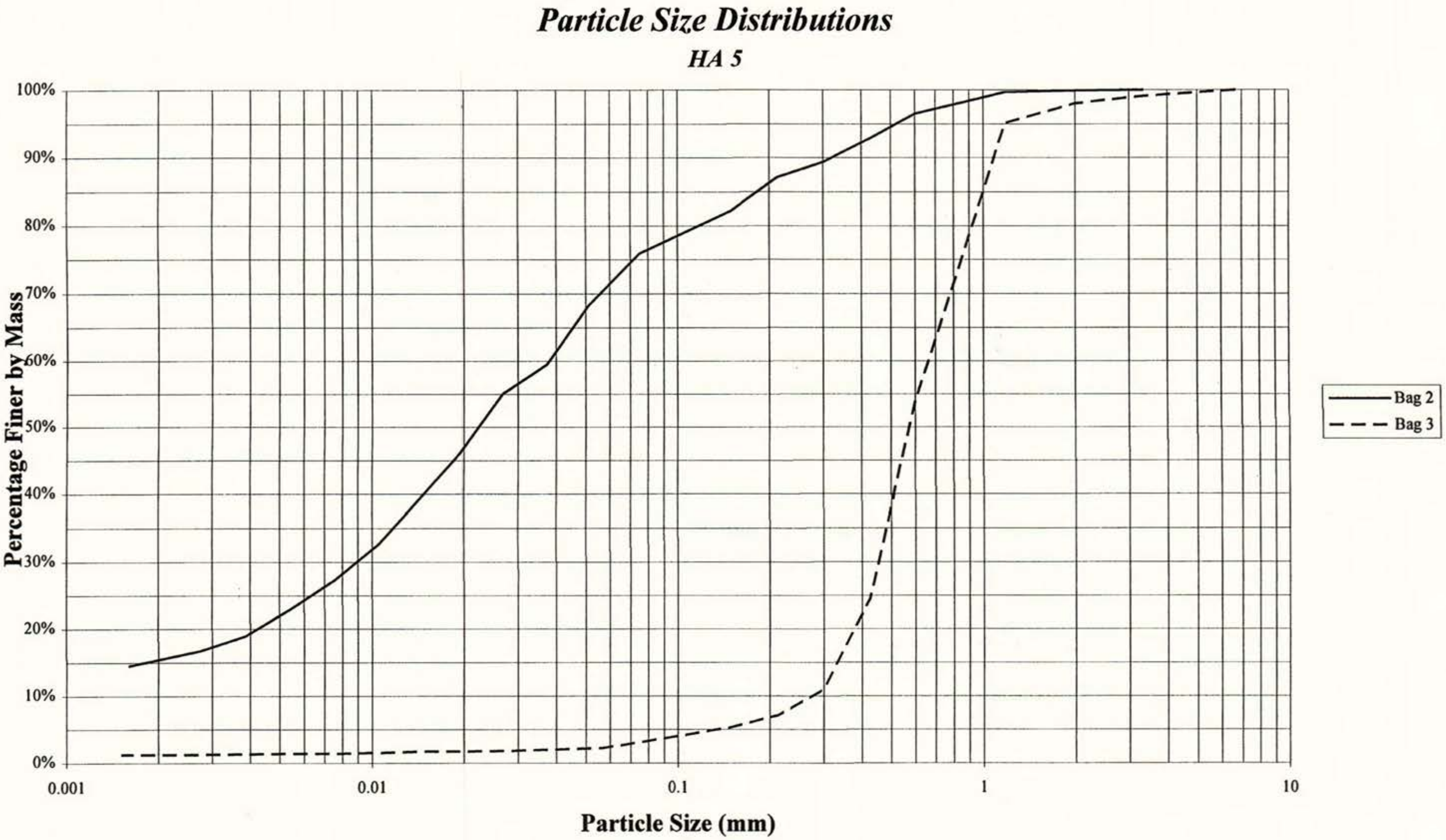
Particle Size Distributions
HA 5
Percentage Finer by Mass
100%
90%
80%
70%
60%
50%
40%
30%
20%
10%
0%
0.001
0.01
0.1
1
10
Particle Size (mm)
Bag 2
Bag 3

Dept. of Civil Engineering
University of Canterbury
Christchurch, NZ

Landing Road Bridge
Whakatane
NZ

By RK/JB
Date 31/3/95

BOREHOLE LOG

TYPE HAND AUGER

ELEVATION

BORING HA 6

STRIKE / DIP	RELATIVE COMPACTION	DRY DENSITY	MOISTURE (%)	BLOWS/FOOT	SAMPLE SIZE	SAMPLE No	DEPTH IN m	MATERIAL SYMBOL	UNIFIED SOIL CLASS.	
										TOP SOIL
		2·54			BAG	1				TAN SILT WITH FINE SAND, FINE GRAVELS
							0·5			
		2·61			BAG	2				LIGHT TAN CLEAN FINE SAND
							1·0			
		2·59			BAG	3				GREY FINE SAND WITH COARSE SILT
		2·54			BAG	4				GREY MEDIUM SAND WITH COARSE SILT
					BAG	5	1·5			RUST STAINING OF SAND
		2·07			BAG	6				
										CAVING IN - BORING ABANDONED
							2·0			
							2·5			

WATER TABLE DEPTH @ 11:00 AM
WAS 1·0 M

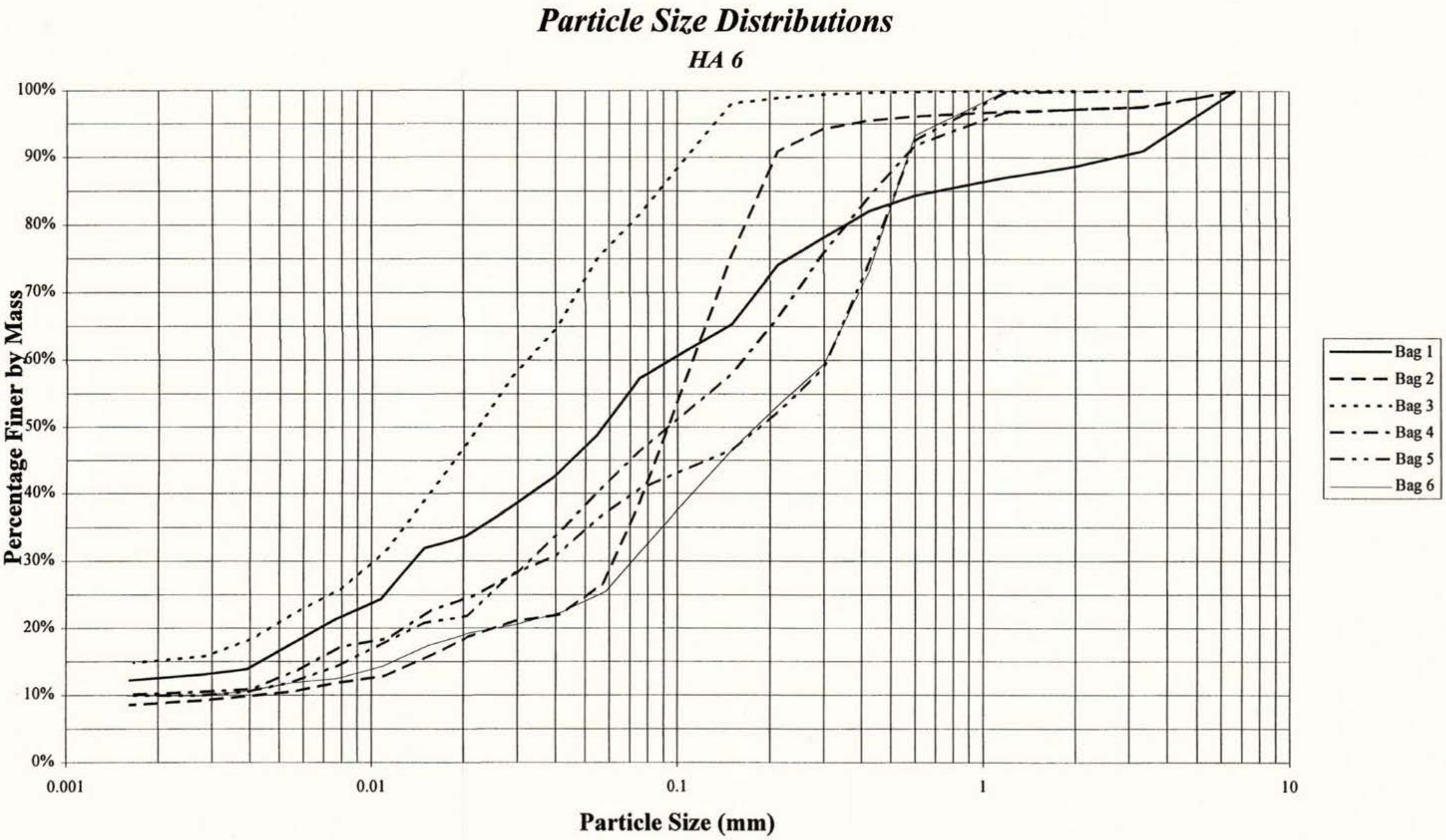
Particle Size Distributions
HA 6
Percentage Finer by Mass
100%
90%
80%
70%
60%
50%
40%
30%
20%
10%
0%
0.001
0.01
0.1
1
10
Particle Size (mm)
Bag 1
Bag 2
Bag 3
Bag 4
Bag 5
Bag 6

Particle Size Distributions

Trench 2

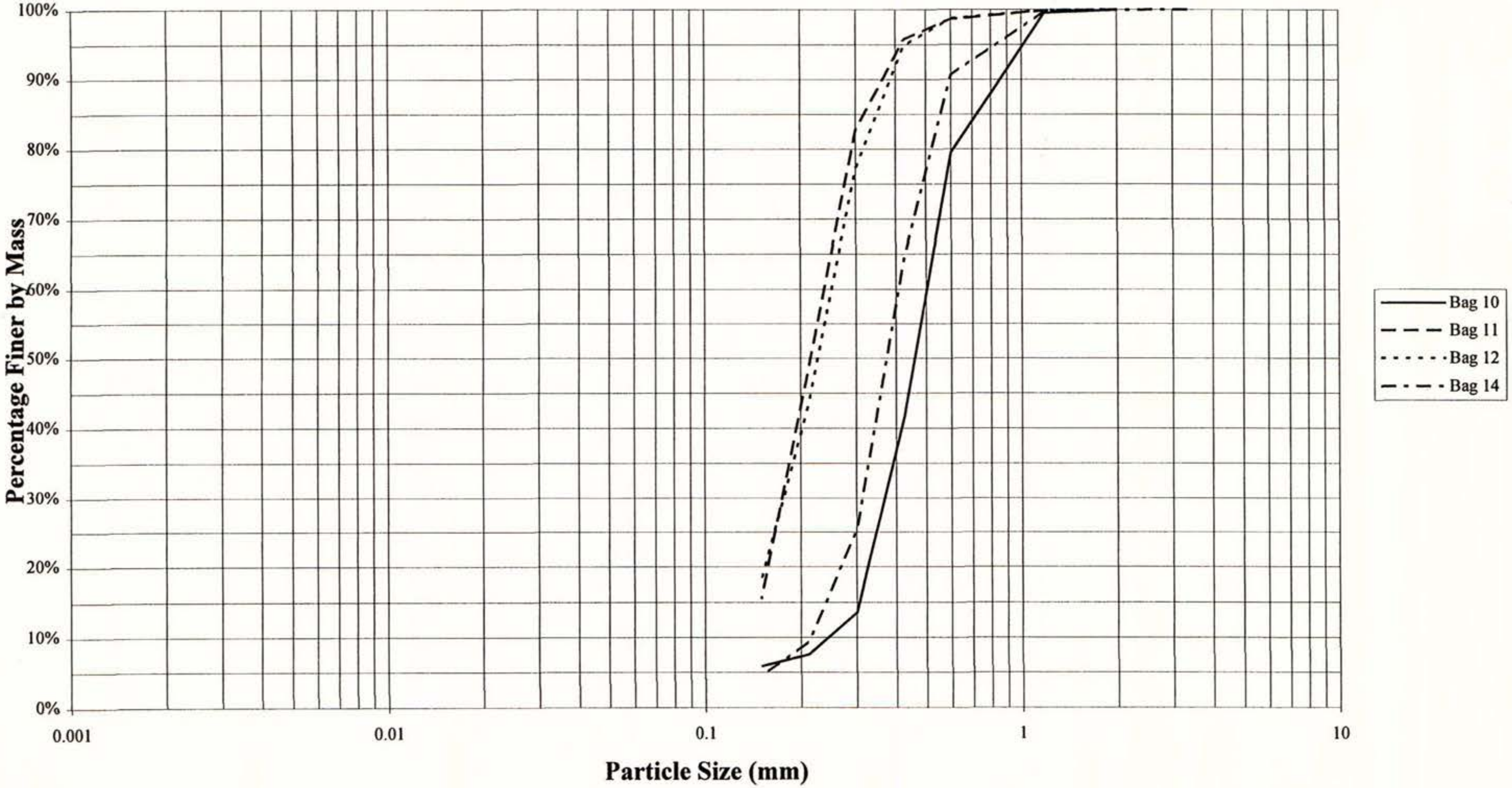

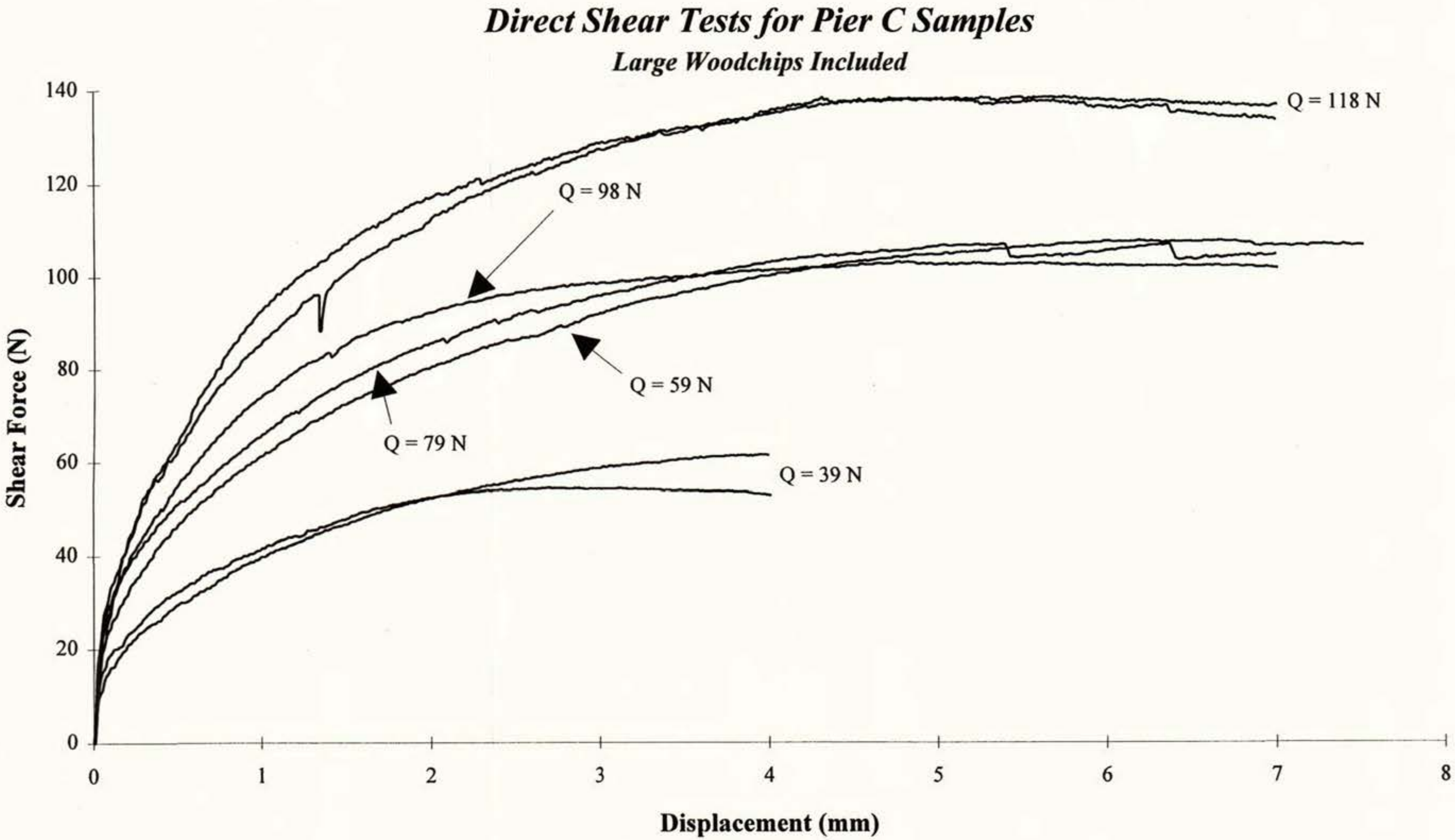

Direct Shear Tests for Pier C Samples

Large Woodchips Included

Direct Shear Tests for Pier C Samples

Large Woodchips Removed

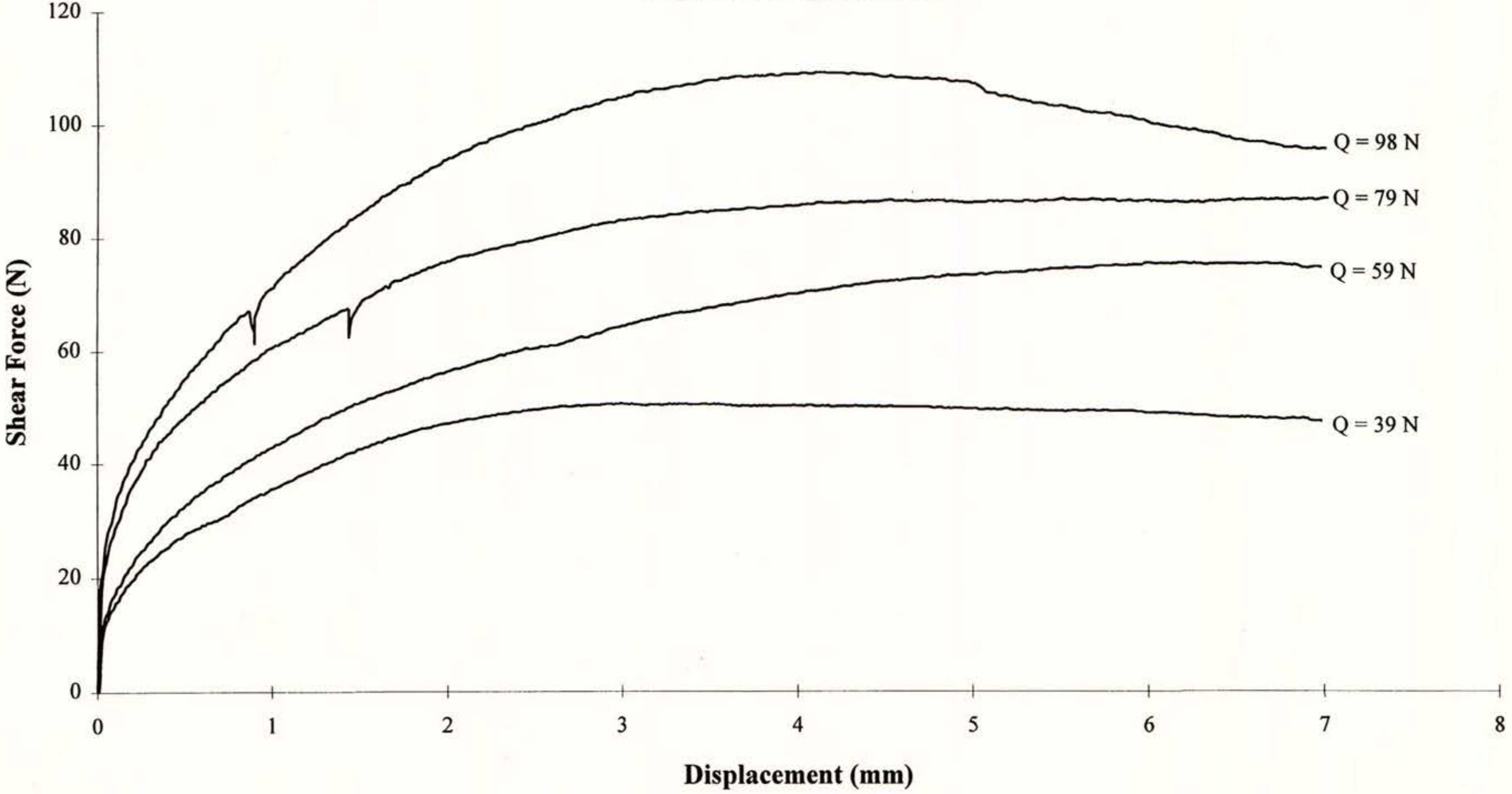

Direct Shear Tests for Pier E Samples

Large Woodchips Included

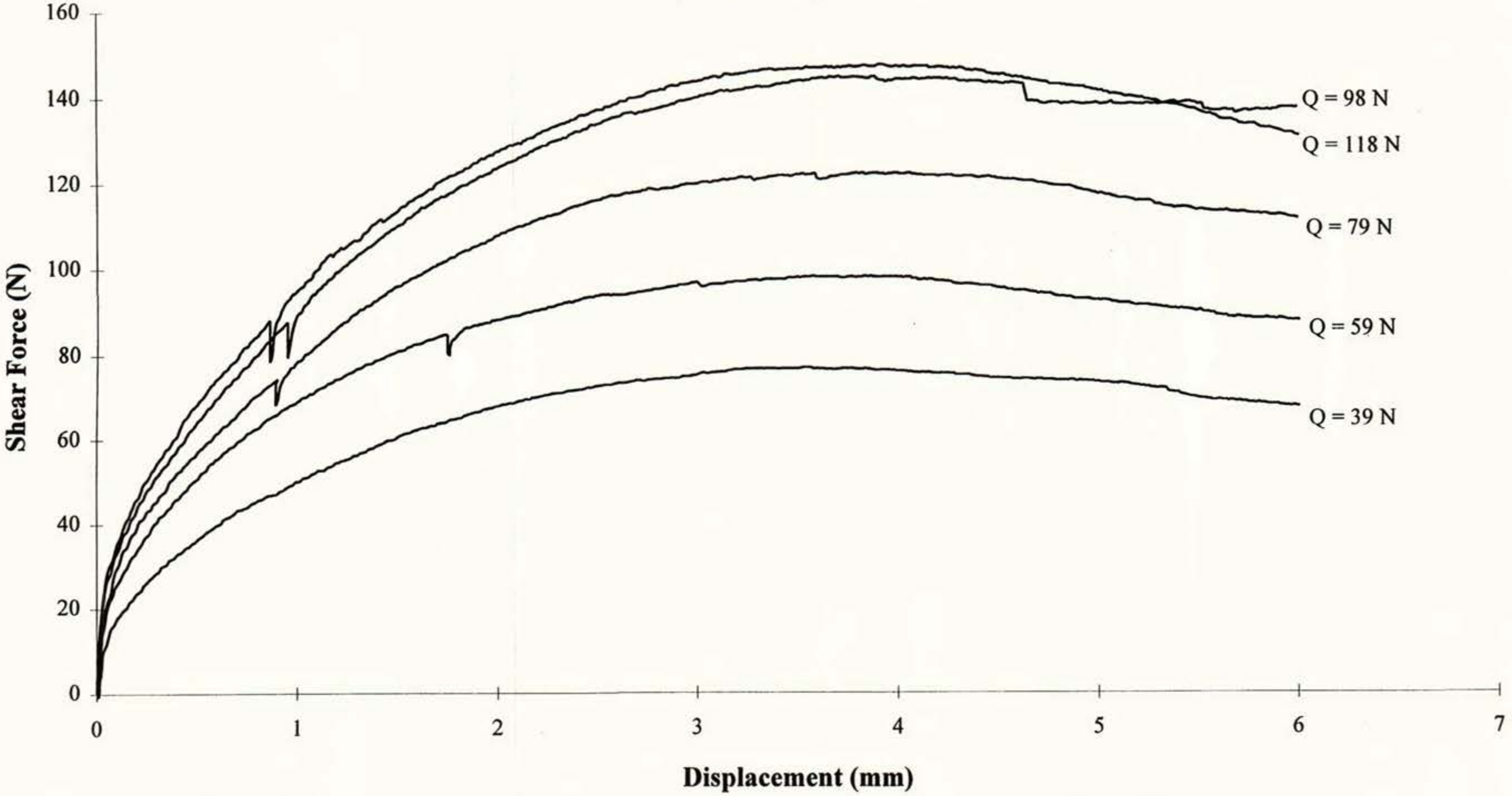

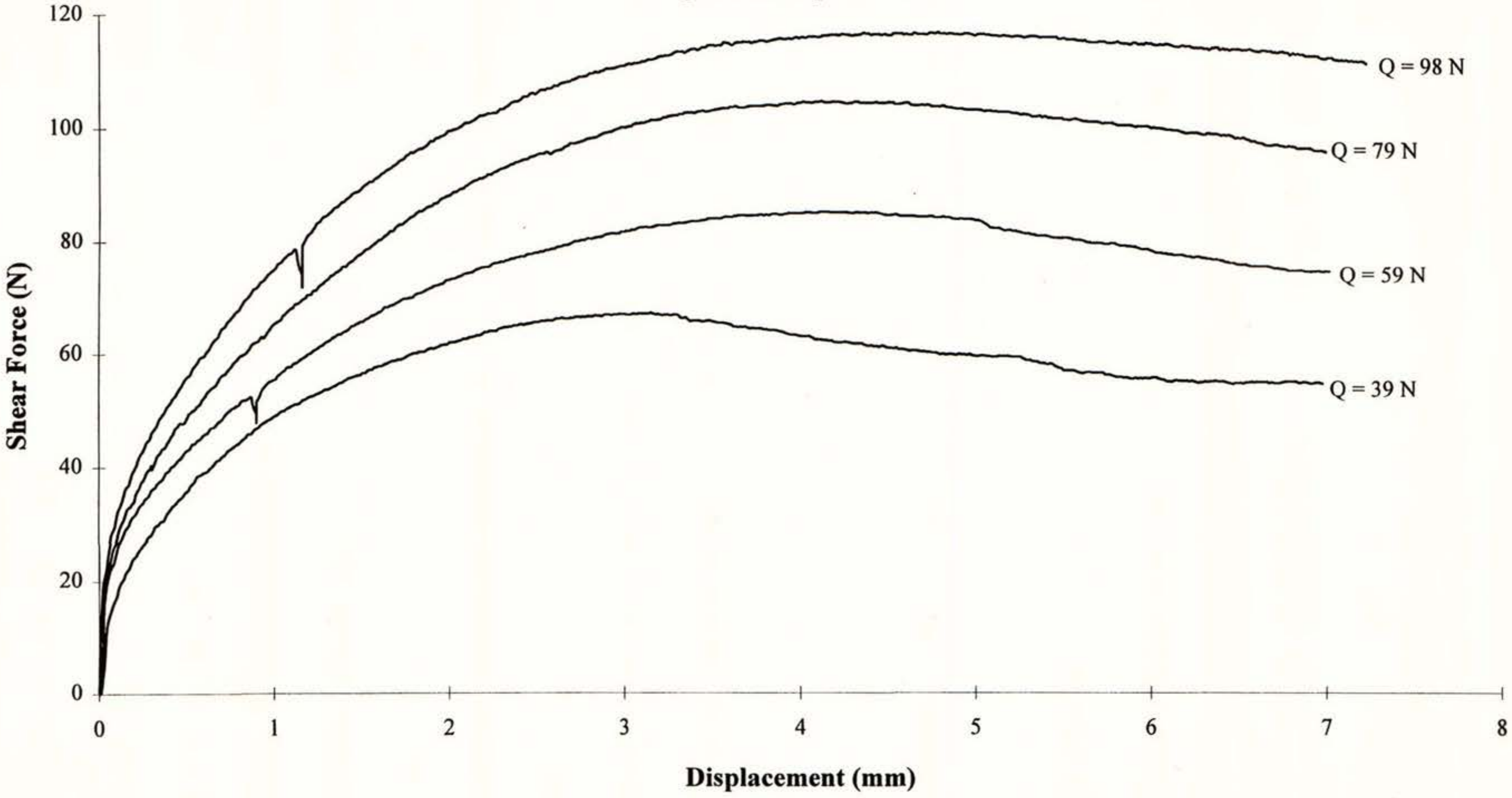

Direct Shear Tests for Pier E Samples

Large Woodchips Removed

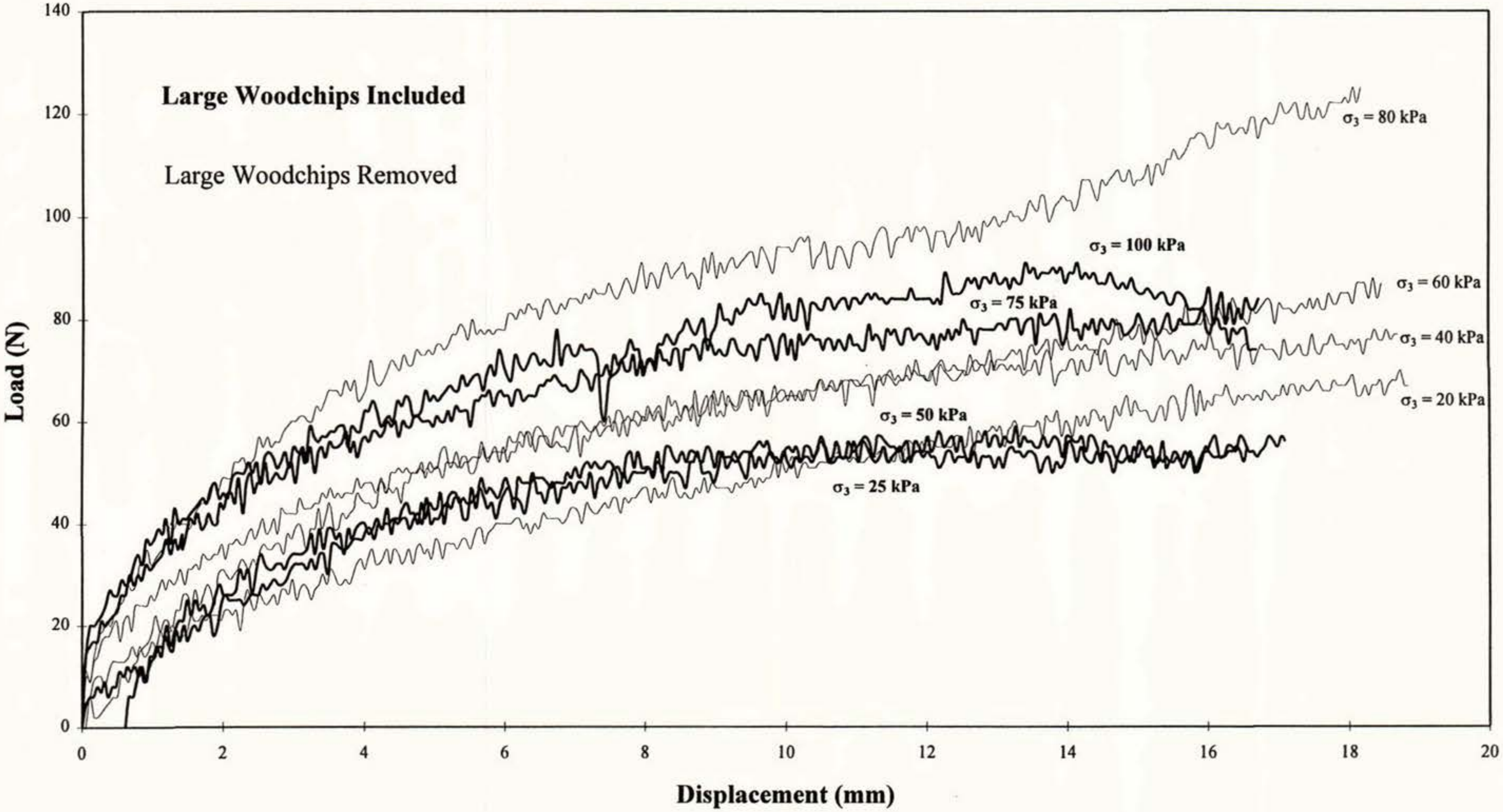

Triaxial Test Results for Pier C Samples

Appendix C

Trench Logs

Final trench logs for Trench 1, Trench 2, Pier C and Pier E are presented.

Trench 1

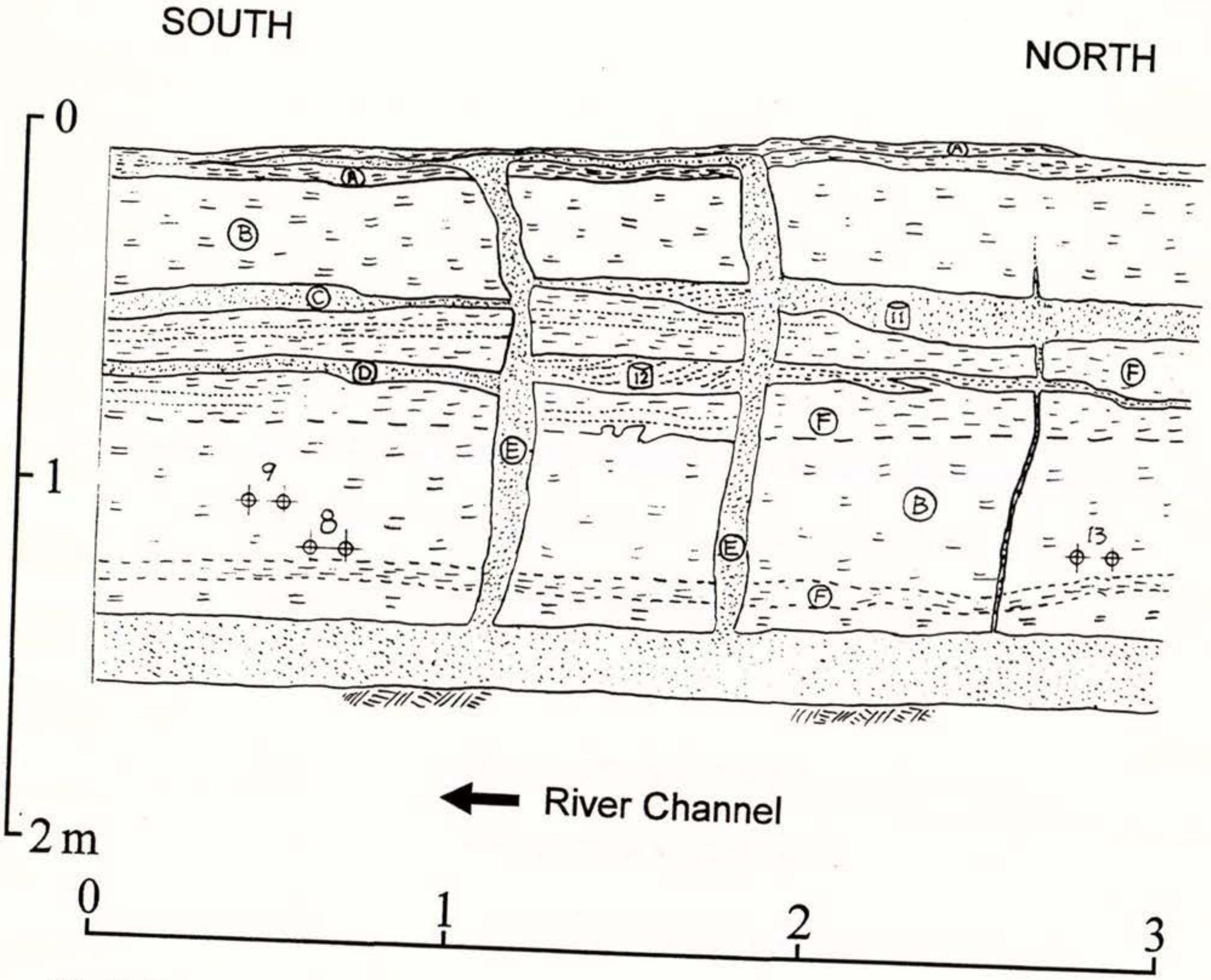

Soil Description

A	topsoil
B	greenish-grey clayey silt
C	light grey-tan medium fine sand
D	grey-tan medium fine sand
E	tan medium coarse sand
F	tan coarse silt, fine sand

Soil Samples

8	Drive Tubes (2)
9	Drive Tubes (2)
10	Bag Sample
11	Bag Sample
12	Bag Sample
13	Drive Tubes (2)
14	Bag Sample

Drawn Scale 1 : 20

J. Berrill
S. Pasa
R. Keenan

Trench 2

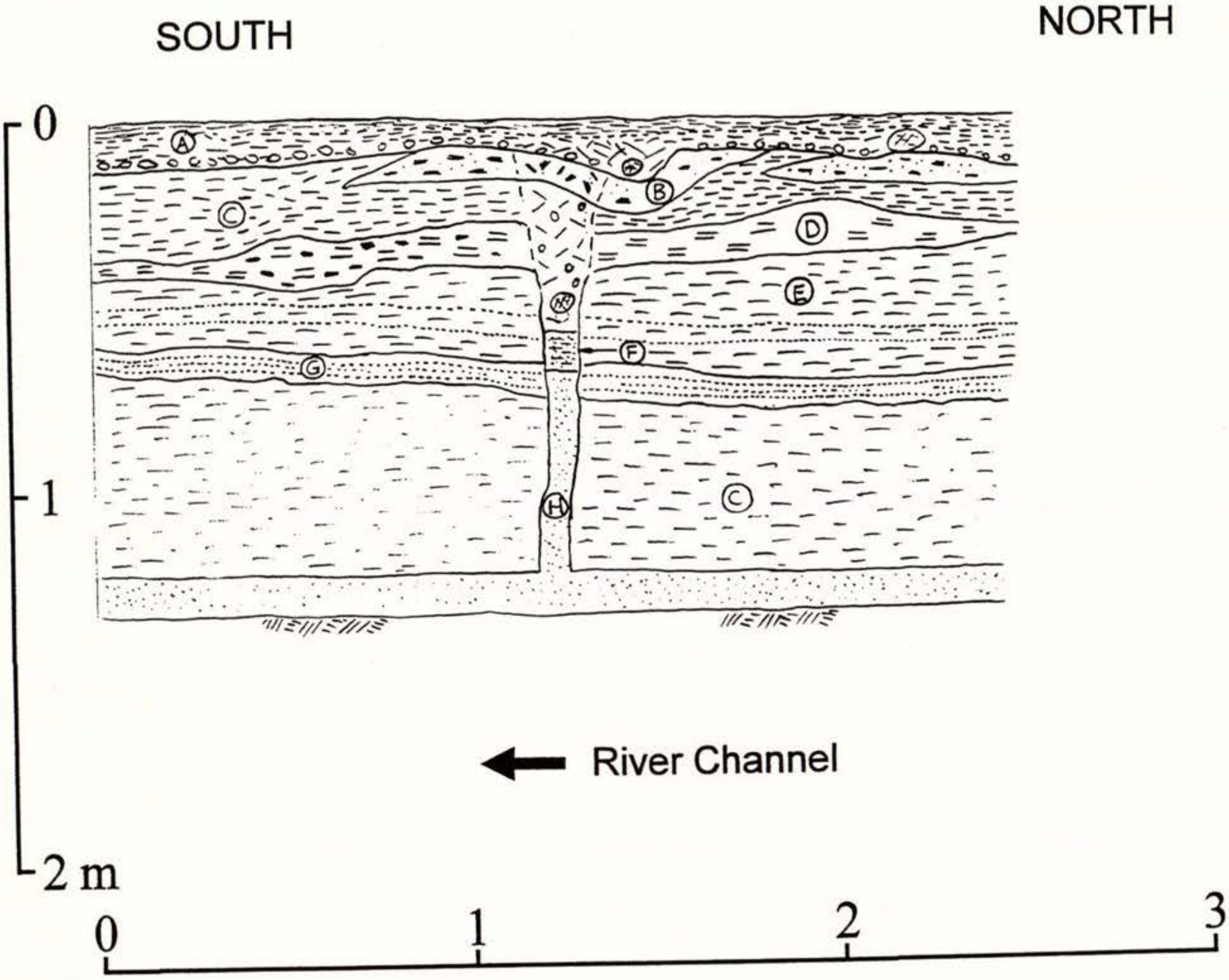

Soil Description

A	topsoil, round gravels
B	brown sandy silt, woodchips, organics
C	tan medium silt, fine sand
D	light grey-tan fine silt, wood chips, medium sand
E	tan sandy silt, sand lenses
F	light brown fine silt, fine sand
G	tan sandy silt, laminated fine sand
H	grey-tan medium sand

Drawn Scale 1 : 20

S. Pasa
R. Keenan

Pier C

Drawn Scale 1 : 20

J. Pettinga
S. Pasa
R. Keenan

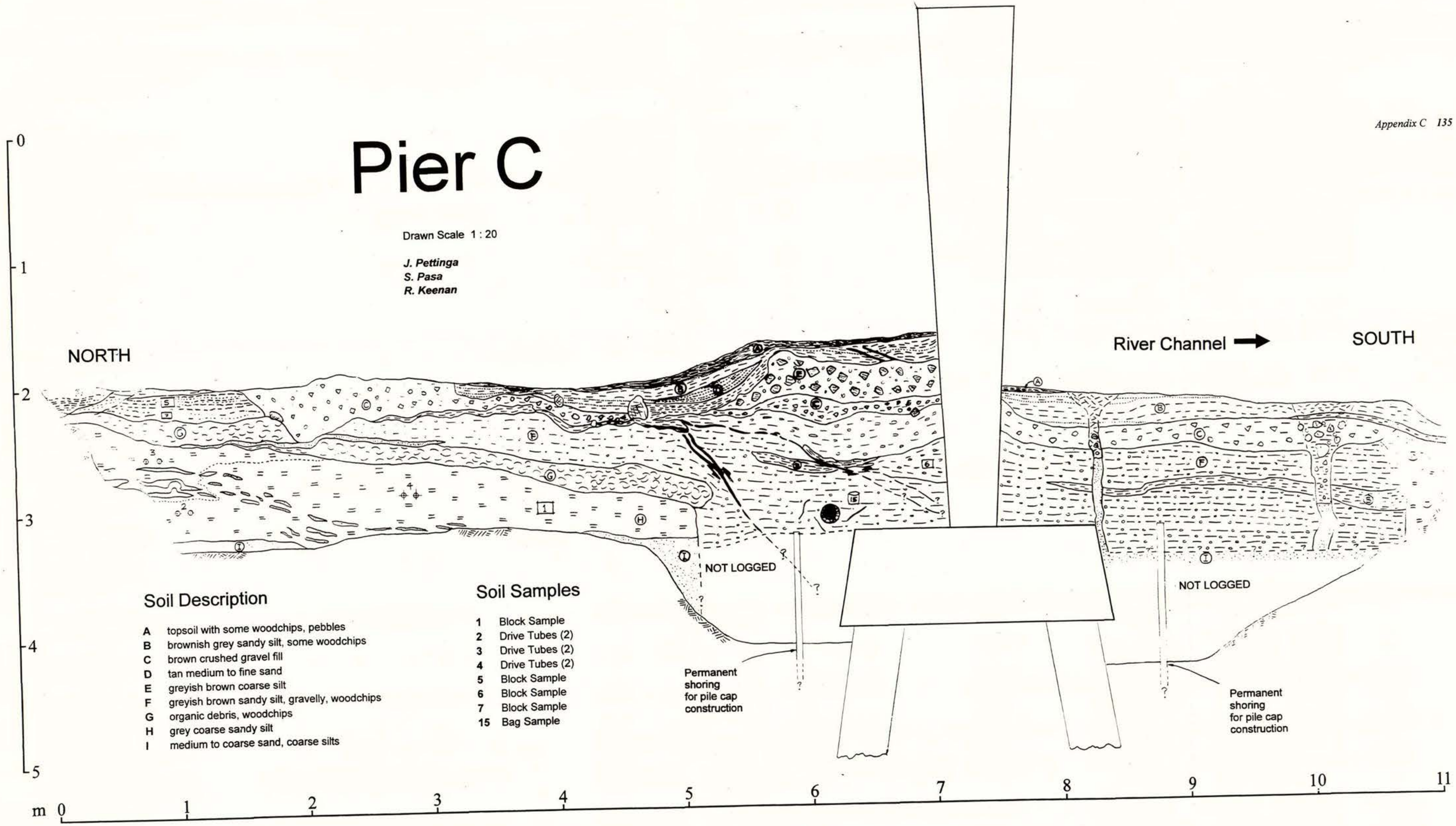

Soil Description

A	topsoil with some woodchips, pebbles
B	brownish grey sandy silt, some woodchips
C	brown crushed gravel fill
D	tan medium to fine sand
E	greyish brown coarse silt
F	greyish brown sandy silt, gravelly, woodchips
G	organic debris, woodchips
H	grey coarse sandy silt
I	medium to coarse sand, coarse silts

Soil Samples

1	Block Sample
2	Drive Tubes (2)
3	Drive Tubes (2)
4	Drive Tubes (2)
5	Block Sample
6	Block Sample
7	Block Sample
15	Bag Sample

Pier E

Drawn Scale 1 : 20

J. Pettinga
R. Keenan

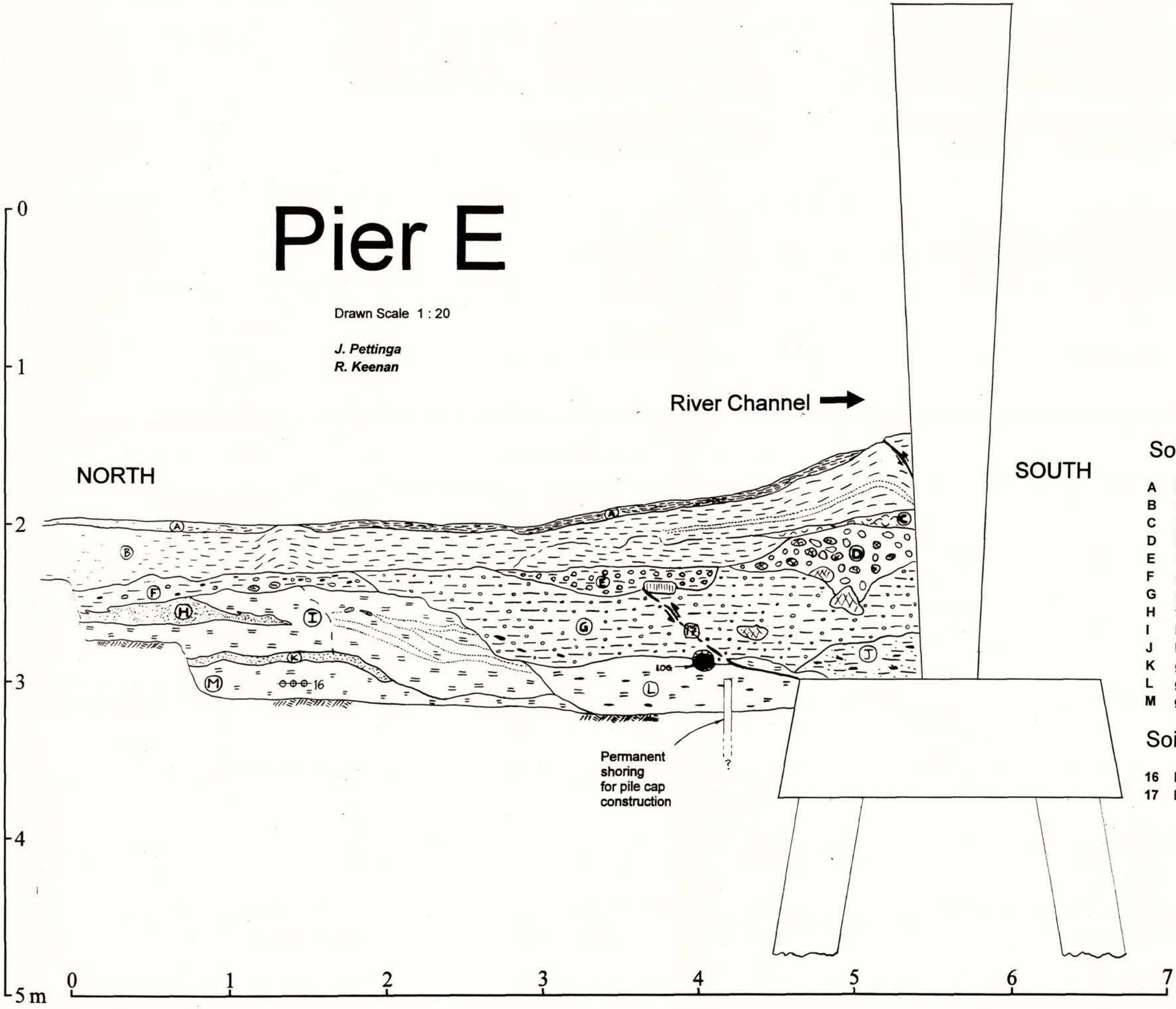

Soil Description

A	topsoil
B	tan silt, some sand laminates
C	grey sand, organics, woodchips
D	brown crushed gravel fill
E	brownish purple organics, woodchips, sand
F	dark tan coarse sandy silt, gravels, woodchips
G	greyish brown sandy silt, gravelly, woodchips
H	tan medium sand
I	blue-grey clayey silt, disturbed medium sand lenses
J	brownish grey sandy silt, woodchips
K	grey medium fine sand
L	grey clay,organics, woodchips
M	greenish-grey silty clay

Soil Samples

16	Drive Tubes (3)
17	Bag Sample